Photocatalytic oxidation of nitrogenous fertilizers using cyclodextrin and reduced graphene oxide modified metal-TiO_2 nanocomposites

Thesis submitted for the award of degree of

Doctor of Philosophy

Submitted by:

Palak Soni

(Regn. No. 902009016)

Under the supervision of

Dr. Bonamali Pal (Professor)

Dr. Raj Kumar Das (Assistant Professor)

DEPARTMENT OF CHEMISTRY AND BIOCHEMISTRY

THAPAR INSTITUTE OF ENGINEERING AND TECHNOLOGY

PATIALA-147004

Certificate

This is to certify that the work embodied in this thesis entitled " **Photocatalytic oxidation of nitrogenous fertilizers using cyclodextrin and reduced graphene oxide modified metal-TiO_2 nanocomposites**" has been carried out by Ms. Palak Soni under my supervision and guidance in the Department of Chemistry and Biochemistry, Thapar Institute of Engineering and Technology, Patiala. The candidate completed all the conditions required for the fulfillment of the award of the Degree of Philosophy.

I also certified that the work represented in this thesis is original and has not been submitted in part or full for the award of any degree in any other University or Institute.

Dr. Bonamali Pal
Professor and Supervisor
Dept. of Chemistry and Biochemistry
Thapar Institute of Engineering and Technology
Patiala-147004

Dr. Manmohan Chhibber
Professor and Head
Dept. of Chemistry and Biochemistry
Thapar Institute of Engineering and Technology
Patiala- 147004

Dr. Raj Kumar Das
Assistant Professor and Supervisor
Dept. of Chemistry and Biochemistry
Thapar Institute of Engineering and Technology
Patiala-147004

Candidate's Declaration

I, hereby declare that the work presented in the thesis entitled "**Photocatalytic oxidation of nitrogenous fertilizers using cyclodextrin and reduced graphene oxide modified metal-TiO_2 nanocomposites**", in fulfillment of the requirement for the award of the Degree of Doctor of Philosophy, Department of Chemistry and Biochemistry, Thapar Institute of Engineering and Technology, Patiala, is an authentic record of my own work carried out under the supervision of Dr. Bonamali Pal, Professor and Dr. Rajkumar Das, Assistant Professor, Department of Chemistry and Biochemistry, Thapar Institute of Engineering and Technology, Patiala, India. The matter embodied in this thesis has not been submitted in part or full to any other university or institute for the award of any degree in India or Abroad.

Palak

Palak Soni

Dr. Bonamali Pal
Professor and Supervisor
Dept. of Chemistry and Biochemistry
Thapar Institute of Engineering and Technology
Patiala-147004

Raj Kumar Das

Dr. Raj Kumar Das
Assistant Professor and Supervisor
Dept. of Chemistry and Biochemistry
Thapar Institute of Engineering and Technology
Patiala-147004

Dedicated

To

My Father

And

My Husband

Acknowledgement

The successful completion of thesis has been a challenging yet rewarding journey, and it would not have been possible without the support and encouragement of many individuals and institutions. I would like to express my gratitude to those who have supported and guided me throughout my Ph.D journey.

First and foremost, I extend my heartfelt thanks to my research supervisor, **Dr. Bonamali Pal, Professor** whose unwavering guidance, insightful feedback has been instrumental in shaping my research. His expertise and dedication to excellence have inspired me to push the boundaries of my work. Constant support has been a source of motivation throughout this journey. I am equally grateful to **Dr. Raj Kumar Das, Assistant Professor**. His invaluable advice and thoughtful critiques have significantly enhanced the quality of my research. His knowledge and ability to provide a different perspective have enriched my work. Continuous encouragement and willingness to help have made this journey more manageable and rewarding.

I would like to thank **Dr. Manmohan Chhibber**, Professor, and Head, Department of Chemistry and Biochemistry, Thapar Institute of Engineering and Technology, Patiala. I would like to acknowledge my doctoral committee members **Dr. Soumen Basu, Dr. Banibrata Maity,** and **Dr. B.N. Chudasama (SPMS)** for their constructive feedback, insightful suggestions, and ongoing support throughout this research. Their contributions have significantly shaped my work and have helped me to grow as a researcher.

I am grateful to **Department of Science and Technology (DST), Dean RDC and Thapar institute of engineering and technology (TIET), Patiala** for providing the financial and academic support necessary for my research. Special thanks to **Mr**. **Mayank**, office staff for their assistance and efficiency in handling various tasks and procedures.

I am thankful to my colleagues and fellow researchers **Dr. Piyush Sharma**, **Dr. Sakshi Bhardwaj**, **Dr. Pooja Bansal**, **Shreya Sharma**, **Jemini Dogra**, **Sukhan Sidhu**, **Mehak Bansal**, **Davinder Attan** and **Shikha Thakur**. Special thanks to my PG mates **Ashima Mahaja**n, **Preeti Rohilla, Shelly Singla,** and **Akanksha Katoch** for creating a collaborative and stimulating environment. Intellectual discussions, and moral support have made this journey more enjoyable and fulfilling.

My sincere appreciation goes to several institutions and laboratories Avantha Lab, SAI Lab TIET, IIT Roorkee, Punjab University Chandigarh, IIT Kanpur, IISER Mohali, Sprint testing solutions

Mumbai for their invaluable support, whether through access to facilities, technical assistance, or collaborative opportunities

I would like to express my deepest gratitude to my father **Mr. Vinod Soni**. His wisdom, guidance, and unshakeable confidence in my abilities have inspired me to reach for the stars. His support has been a driving force behind my determination to achieve my goals. Special thanks to my lovely mother **Mrs. Uma Soni**. Her endless patience, understanding, and care have provided me with the comfort and reassurance I needed to persevere. Herr sacrifices and dedication have been instrumental in my success.

I cannot find the right words to fully express how thankful I am for my loving husband **Mr. Rishav Kaushal.** He stood by me through every challenge, celebrated every success, and provided the emotional and practical support that made this achievement possible. Thank you for your sacrifices, understanding, and endless love. This accomplishment is as much yours as it is mine, and I am profoundly grateful to have you by my side.

I would like to thank my mother-in- law **Mrs. Suman Kaushal**, brother-in-law **Mr. Nihil Kaushal**, my brother **Saksham Soni**, my daughter **Prisha Kaushal** and all my family members for being my pillars of strength.

Thank you all for being a part of this journey and for helping me to achieve this significant milestone.

Table of Contents

CHAPTER- 2

Enhanced photocatalytic urea oxidation under neutral medium by reduced graphene oxide coated TiO_2 nanoparticles

CHAPTER-3

Influence of β-CD and Ag deposition over TiO_2 towards photocatalytic oxidation of urea under solar irradiation

CHAPTER- 4

β-CD and RGO loaded Ag-TiO_2 composites for enhanced photocatalytic oxidation of urea under sunlight

List of Abbreviations

RGO	Reduced graphene oxide
ABC	Ammonium bicarbonate
AN	Ammonium nitrate
AA	Anhydrous ammonia
CAN	Calcium ammonium nitrate
NO_3^-	Nitrate ion
NH_4^+	Ammonium ion
NUE	Nitrogen use efficiency
DRS	Diffuse reflectance spectroscopy
EDS	Energy dispersive X-ray spectroscopy
FESEM	Field emission scanning electron microscopy
β-CD	Beta-cyclodextrin
GO	Graphene oxide
DLS	Dynamic light scattering
PL	Photoluminescence spectroscopy
HRTEM	High resolution transmission electron microscopy
XRD	X-Ray diffraction
XPS	X-Ray photoelectron spectroscopy
IPA	Isopropyl alcohol
ICDD	International center for diffraction data
L	Length
M	Metal
mL	Milli-liter
mM	Milli molar
Mol	Mole
RM	Reaction mixture
NaF	Sodium fluoride
ROS	Reactive oxygen species

Mg	Milligram
Nm	Nanometer
NPs	Nanoparticles
wt.%	Weight percentage
LSPR	Localized surface plasmon resonance
CT3A1	β-CD_{25}/TiO_2@Ag_1
NCs	Nanocomposites
P25	Commercially available-TiO_2
eV	Electron volt
BE	Binding energy
SAED	Selected area electron diffraction
UV	Ultraviolet
µl	Micro-liter
µM	Micro molar
VB	Valance band
Vis	Visible
CT1	β-CD_{15}/TiO_2
CT2	β-CD_{20}/TiO_2
CT3	β-CD_{25}/TiO_2
ATR	Ag/TiO_2@RGO
CTAR	β-CD/TiO_2/Ag/RGO
CTR	β-CD/TiO_2/RGO

List of Symbols

e^-	Electron
h^+	Hole
$\cdot OH$	Hydroxyl radical
E_g	Band gap
Å	Angstrom
a	Absorption coefficient
A	Absorbance
°	Degree
Λ	Wavelength
%	Percentage
M	Micro
Θ	Theta
H	Hour
min^{-1}	Minute per second
cm^{-1}	Centimeter inverse
m	Meter
g	Gram
mg	Milligram
$O_2^{\bullet-}$	Superoxide radical
V	Volt
D	Distance
s	Second
Conc.	Concentration
V	Frequency
µmol	Micromol

Abstracts

Chapter-1

This comprehensive introduction provides a solid foundation for understanding the role of nitrogenous fertilizers, the challenges of nitrogen loss, and the potential of advanced nanocomposites in improving nitrogen utilization in agriculture is systematically explained in this chapter. However, significant nitrogen loss through volatilization, leaching, and emissions leads to environmental concerns and reduced crop efficiency. The research gap emphasizes the need for advanced nanocomposites like M-TiO_2, reduced graphene oxide (RGO), and cyclodextrin (CD) to enhance nitrate production and minimize nitrogen loss. The proposed approach suggests that combining these materials could lead to more efficient photocatalytic oxidation of urea, improving nitrate conversion and reducing nitrogen-related environmental issues.

Chapter-2

Nowadays, fertilizers are used to boost crop production. Nitrogenous fertilizers are assimilated as nitrate. Unfortunately, 60-70% of nitrogen is lost due to different leaching processes. Photocatalytic urea oxidation is now emerging as a new methodology. Nitrate conversion is favorable under alkaline ph. However, it can subsequently cause deprotonation of ammonium ions to result ammonia leaching. In this report, efficiencies of bare and RGO loaded TiO_2 were examined. In the presence of NaF, the nanocomposite possesses a 9.8(1) % nitrate yield, significantly greater than the other analogous reactions. Such observation will be helpful in developing new methodologies to afford sustainable agriculture.

Chapter-3

Photocatalytic oxidation of urea is an essential area of study for converting urea to nitrate. As crops absorb nitrogen in the form of NO_3^- but due to incomplete oxidation, a substantial fraction of it escapes into the atmosphere as N_2. Hence, an effective photocatalyst is urgently needed to improve nitrate conversion. This study focuses on the influence of β-cyclodextrin and Ag deposition on TiO_2 towards the photocatalytic oxidation of urea. β-cyclodextrin (15-25 wt.%) and Ag (1-3 wt.%) loaded binary and ternary nanocomposites have been prepared using hydrothermal and photo deposition

methods, respectively. The binary and ternary hybrids were characterized using FESEM, EDX, HR-TEM, XRD, XPS, DRS, PL, DLS, and FT-IR analysis. Photocatalytic urea degradation activity was evaluated under solar irradiation. The β-CD_{25}/TiO_2@Ag_1 ternary nanocomposites show 78% degradation efficiency with 17.8% nitrate yield after 180 minutes reaction time which is the highest. This observation can be ascribed to the higher affinity of β-CD towards N_2 due to the hydrophobic effect and the surface plasmon effect of Ag, which amplifies its visible light response. Such observations will attract much interest from a large section of material and agricultural chemists to design new catalysts for photochemical urea oxidation to afford sustainable agriculture.

Chapter-4

Urea oxidation is important to increase agricultural growth, which can meet the food requirements across the world. It is pivotal for converting nitrogen to nitrate that is usable by crops, thus preventing nitrogen loss to the atmosphere. This study focuses on improving the photodegradation efficiency of TiO_2 by incorporating β-CD (beta-cyclodextrin), RGO (reduced graphene oxide), and Ag to enhance nitrate conversion. FT-IR, DRS, PL, EDX, XRD, XPS, HR-TEM DLS, and FESEM were conducted to characterize these materials. Among all the catalysts, the quaternary composite, β- CD/ TiO_2/Ag/RGO, exhibited superior performance, achieving an 86.2% degradation efficiency with a 27.8% nitrate yield under sunlight irradiation within 150 minutes of reaction time. Several factors contribute to the enhanced photoactivity of β-CD/TiO_2/Ag/RGO, including the high surface area and absorptive power of β-CD, the high electron mobility of RGO, and the LSPR effect of Ag, extending the catalyst's response to visible light. An intriguing aspect of this study is the encapsulation of gaseous nitrogen into the hydrophobic interior cavity of β-CD, contributing to the enhancement of urea oxidation. These findings can be very substantial for both agriculturists and chemists, providing valuable insights into designing novel photocatalysts for improved urea oxidation, thereby enhancing agricultural,productivity.

CHAPTER- 1

Introduction and literature review

Section-A

1.1 Introduction

1.1.1 The Importance of Nitrogenous Fertilizers in Sustainable Agriculture

In agriculture, fertilizers are essential for supplementing the natural nutrients found in soil(1).Among these nutrients, nitrogen plays a vital role in processes like ammonification, nitrification, denitrification, and mineralization(2). However, due to its tendency to escape N from the soil through leaching, surface runoff, N_2O emissions and volatilization in soil, water, and air, an external supply of nitrogen is necessary for crop production(3). This practice has been widely adopted globally through the use of nitrogenous fertilizers. A lack of sufficient nitrogen available to plants can impede their growth and development(4). Common types include ammonium bicarbonate (ABC), ammonium nitrate (AN), urea, anhydrous ammonia (AA), and calcium-ammonium nitrate (CAN)(5). Urea, containing 46% nitrogen, is the most popular fertilizer due to its granular form, ease of storage and application, cost-effectiveness, and lower security risks compared to ammonium nitrate(6). These fertilizers are indispensable for sustainable agriculture, as they replenish soil nutrients, replace nutrients lost during harvest, and balance nutrients for improved product quality and higher yields(7).

1.1.2 Nitrogen Assimilation

Plants absorb nitrogen from the soil in the form of nitrate (NO_3^-) and ammonium (NH_4^+). So, to absorb nitrogen from urea it must first be broken down(8).

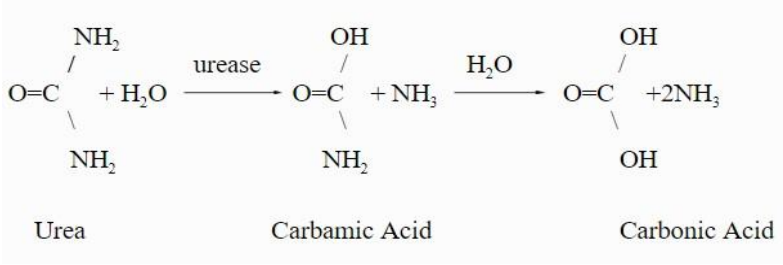

Scheme.1.1. Chemical pathway for the hydrolysis of urea to carbonic acid and NH_3.

Urease is an enzyme that naturally occurs and catalyzes the hydrolysis of urea into unstable carbamic acid (Scheme 1.1)(9). This carbamic acid rapidly decomposes without enzymatic catalysis, resulting in the formation of ammonia and carbondioxide(10). Ammonia is likely to escape into the atmosphere unless it reacts with water to form NH_4^+. The ammonia then converts to ammonium and hydroxide ions, initiating a nitrification process where nitrite and nitrate are produced (Scheme 1.2)(11). Ammonium ions are absorbed by plants through ammonia transporters, while nitrate is taken up by several nitrate transporters using a proton gradient for energy(12). Nitrogen is transported from the roots to the shoots via the xylem in the forms of nitrate, dissolved ammonia, and amino acids(13).

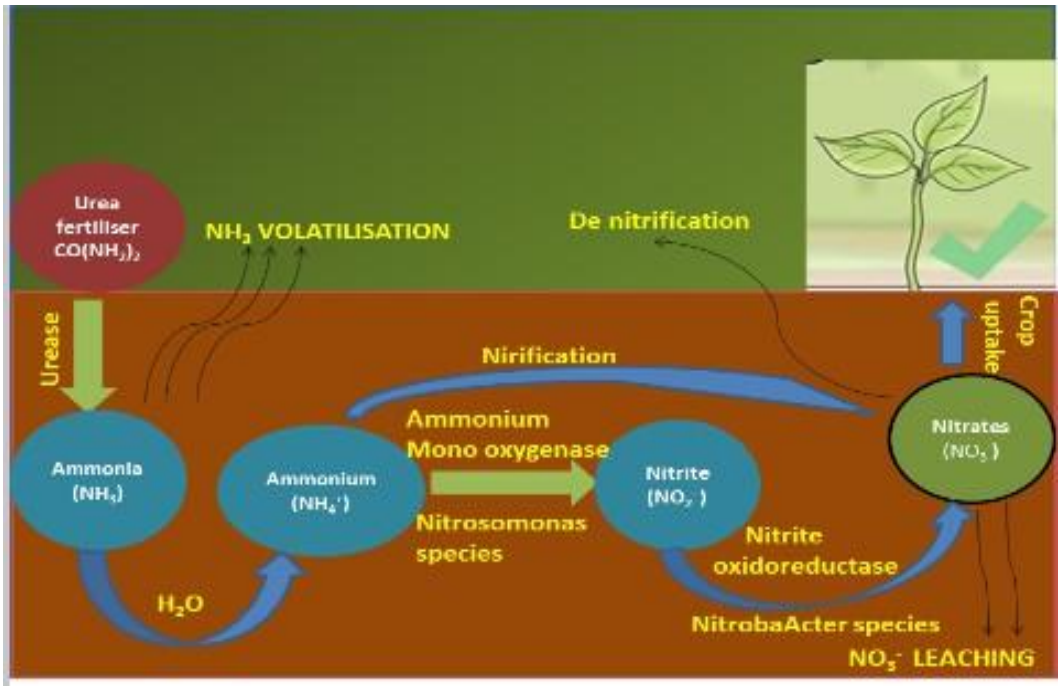

Scheme 1.2. Urea-based fertilizer transformation chain.

Urea fertilizer can lead to significant nitrogen losses (60-70%) through N_2 emissions, ammonia volatilization, nitrate leaching, and nitrous oxide emissions(14). These losses hurt plant growth and the environment, causing acidification and eutrophication. Additionally, high soil pH (around 9.0) from hydroxide ions increases ammonia volatilization, reducing economic efficiency and crop yields(15).

1.1.3 N-loss prevention methodologies

Improving Nitrogen Use Efficiency (NUE) is crucial for making agriculture more sustainable by reducing pollution, lowering production costs, and increasing yields. Various conventional methods have been employed to minimize the nitrogen loss and enhance nitrate

production(16).

Controlling Factors: -

- **Application method: -** Fertilizer spread over the soil surface or introduced under the soil reduces the N-loss(17).
- **Dose of fertilizer: -** Optimum dose of N-fertilizer allows for an increase in yield and reduces the N-loss.
- **Nature of soil: -**In no-till field, postharvest residues remain at the soil surface which make contact barrier between N-fertilizer and soil which reduces the N- loss(18).

Modification of fertilizers: -

- **Urease inhibitor: -**These inhibitors slow down the formation of ammonia due to which most of the ammonia undergo protonation, thus reduces the ammonia loss. e.g. NBPT (N-(n-Butyl) thiophosphorictriamide)(19).
- **Nitrifying Inhibitors: -**These inhibitors produce nitrate slowly which in turn reduces the chances of denitrification. DCD (dicyandiamide)

Photo-catalytic oxidation: -

- **Photocatalytic oxidation of M-TiO_2:** Loading metals like Au, Ag, Cu, or Pt onto TiO_2 enhances its photocatalytic oxidation of urea to nitrate. This process is simple, cost-effective, and efficient due to improved photon absorption and electron transfer. The "limited light response towards visible light" by the wide gap semiconductor nanoparticles can also be improved by coupling with another semiconductor with narrow band gap(20-21).Modifying TiO_2 with reduced graphene oxide, adding metals, or using supramolecules like cyclodextrin further boosts photocatalytic activity. Supramolecular structures, such as cyclodextrin, are increasingly used to mimic natural processes and improve visible-light-driven photocatalysis(22).

1.1.4 Selective oxidation of urea with different nanocomposites

To increase nitrate conversion and reduce 60-70% nitrogen losses from urea, various strategies are employed, including adding urease inhibitors, using controlled-release fertilizers, applying photocatalysts, and incorporating nano fertilizers. These losses contribute to global warming and eutrophication.

Siafu Ibahati Sempeho et al. developed a controlled-release fertilizer by intercalating urea into kaolinite followed by gum Arabic encapsulation, significantly reducing its volatility and improving utilization efficiency(23). Ruiling Wang et al. demonstrated that a graphene quan-

tum dot-modified g-C_3N_4 composite achieved a 90% total ammonia nitrogen (TAN) removal rate under light, outperforming pure g-C_3N_4 by three times.(24) Soona Parl et al. found that TiO_2 in urine oxidizes urea more efficiently than in water due to enhanced hydroxyl radical production, with surface platinization further improving this process.(25) Sachiko Haga et al. reported that a zeolite-TiO_2 composite effectively oxidizes ammonia under UV light, yielding high concentrations of NO_2^- and NO_3^-.(26) Shiying et al. showcased the Cu/ZnO/rGO nanocomposite's ability to degrade ammonia in water under visible light, primarily producing nitrogen gas with minimal nitrate and nitrite formation.(27) Biaopeng Li et al. studied urea oxidation using $NiCo_2S_4$ nanowires on a 3D carbon sponge, revealing enhanced charge transfer and kinetics.(28) Vincenzo Vaiano et al. optimized urea degradation using visible light and N-doped TiO_2 with LED dimming techniques, leading to improved ammonia and nitrate distribution.(29) Hsin-Hung et al. reported that titanate nanotubes, particularly in the rutile phase, enhanced photocatalytic ammonia oxidation.(30)orst Kisch et al. explored nitrogen fixation into ammonia and nitrate on $Fe_2Ti_2O_7$ films, highlighting dual catalysis in the presence of ethanol or humic acid.(31) Finally, Maria Vittoria Dozzi et al. examined aqueous ammonia abatement on Pt and Ru-modified TiO_2, finding that deposition methods significantly influence ammonia conversion and selectivity towards oxidized products like nitrate.(32)

Section-B

1.2 Research Gaps

Literature shows various photocatalysts have been studied for urea/ammonia oxidation to nitrate, with factors like metal deposition, amount, pH affecting conversion and product selectivity. As, 43% nitrate conversion has been achieved using Pt-deposited TiO_2 under UV light, but combining Pt (0.8 wt.%) with Ru NPs (0.1 wt.%) led to undesired N_2 as a product. Future research should focus on optimizing conditions to improve photocatalytic oxidation of urea.

- The main issue is the frequent formation of N_2 as a product, which reduces nitrate efficiency. To address this, we use M@TiO_2 (M=Ag/Cu/Au), reduced graphene oxide (RGO), and cyclodextrin (CD) where M@TiO_2 enhances photocatalytic oxidation by extending titania's response to the visible light region.

- RGO can enhance the surface area, improves photocatalytic oxidation, while CD can provide

catalytic and hydrophobic sites that can further boost photocatalytic oxidation. Additionally, CD can encapsulate N_2, leading to increased nitrate production and reduced nitrogen loss.

- It would be valuable to investigate the comparative activity of bare TiO_2, M-TiO_2, and M-TiO_2@RGO and M-TiO_2 @CD nanocomposites to improve nitrate efficiency.

- No investigation has been reported on fabricating multi-component composite such as M-TiO_2@RGO, M-TiO_2@CD for improving the photocatalytic activity of urea fertilizer under visible light.
- Few reports exist on M- TiO_2@RGO and M- TiO_2@CD nanocomposites for nitrate production from urea oxidation under visible light, indicating a need for further exploration.

Anatase TiO_2 has a large bandgap (3.2 eV) and high electron-hole recombination, limiting its photocatalytic efficiency under visible light. Introducing noble metals like Ag, Cu, and Au can improve performance via the LSPR effect but may lead to nanoparticle aggregation and undesired N_2 production during urea and ammonia photo-oxidation. Cyclodextrin (CD) stabilizes metal nanoparticles, preventing aggregation and promoting nitrate formation, while reduced graphene oxide (RGO) enhances electron transfer, improving photocatalytic efficiency shown in scheme 1.3.

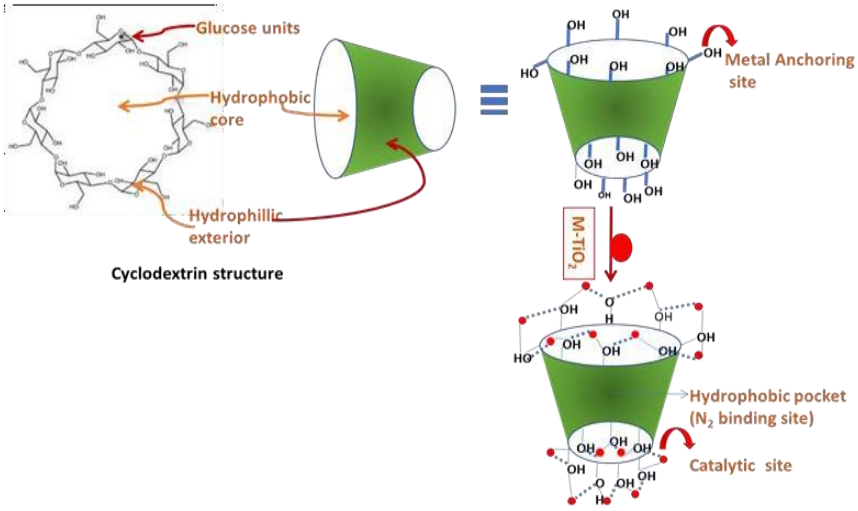

Scheme1.3. Proposed mechanism diagram illustrating the photocatalytic oxidation reaction with the photocatalyst CD@M-TiO_2 (M=Ag/Cu/Au) in the presence of visible light.

Efficient photocatalytic oxidation of urea requires high electron mobility, which can be achieved by combining TiO_2 with RGO. RGO provides high electron mobility, large surface area, and good conductivity, which can enhance the urea adsorption. The TiO_2/RGO composite can improve the photocatalytic activity by enhancing electron-hole separation, increasing active sites, and boosting light absorption for better overall performance.

The photocatalytic activity of TiO_2/RGO nanocomposites can be enhanced by loading metals

like Ag, Cu, or Au onto their surface. These plasmonic metals induce Surface Plasmon Resonance, increasing visible light absorption. When the metal's Fermi level is between the conduction and valence bands of TiO_2, electrons migrate to the metal nanoparticles due to Schottky barriers, facilitating electron capture by reactive species. This metal-loaded TiO_2/RGO composite is promising for applications such as photocatalytic urea oxidation. Keeping in view, the following objectives are proposed in this report.

1.3 Objectives

The main purpose of this work is to prepare various photocatalysts/adsorbents for the effective photocatalytic selective oxidation of urea. The specific objectives are as follows: -

- Preparation and characterization of different metal (Ag/Cu/Au) loaded TiO_2 nanostructures.
- Preparation and characterization of cyclodextrin and reduced graphene oxide modified metal-TiO_2 hybrid structures.
- To study the adsorption and photocatalytic oxidation of nitrogenous fertilizers by as prepared nanocomposites.

Section-C

1.4 Methodology

The chemicals will be purchased commercially. The preparation of photocatalyst will be done in the laboratory.

Chemicals and solvents: -Graphite powder (98% extra pure), Conc. H_2SO_4(98%). $KMnO_4$(99% extra pure), $NaNO_3$ (99%), HCl (35.4%), H_2O_2(30%w/v extra pure), deionized water, IPA solution, silver nitrate (99.9% purity), Titanium butoxide (≥97% purity), ethanol, cyclodextrin, ammonium chloride, distilled water.

1.4.1 Synthesis of Graphite Oxide (GO)

Graphite oxide was prepared using the Modified Hummers Method (Scheme 1.4). First, 2g of graphite powder was dissolved in conc. H_2SO_4 with constant stirring in an ice bath. Gradually, 6g of $KMnO_4$ and 1g of $NaNO_3$ was added, keeping the temperature below 20°C. The mixture was then be stirred at 35°C in a water bath for 18 hours, turning brown and pasty. After diluting with 240ml of distilled water below 50°C, 30% H_2O_2 was added, turning the mixture bright yellow. After 2 hours of stirring, the mixture was centrifuged, washed with 10% HCl, DI water, and ethanol, then dried under vacuum to obtain GO(31)(32).

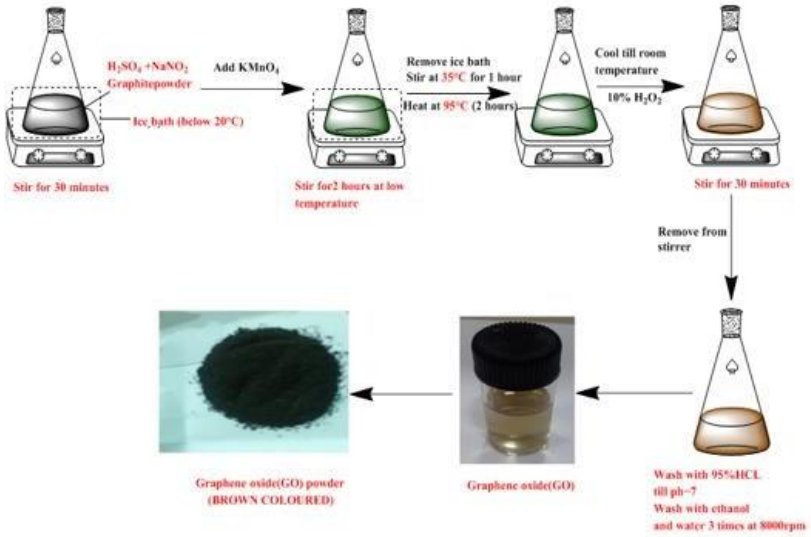

Scheme 1.4. Schematic representation for the synthesis of graphene oxide.

1.4.2 Synthesis of well-dispersed TiO_2/RGO nanocomposite

GO particles was dispersed in distilled water and ethanol. A titanium butoxide solution (1:9 molar ratio with ethanol) was added to the GO suspension and stirred for 12 hours at room temperature. The resulting solid was centrifuged, washed, and dried at 80°C for 3 hours, then ground and calcinated at 500°C for 2 hours to produce TiO_2/RGO nanocomposites(33).

1.4.3 Synthesis of TiO_2/RGO@M (M=Ag/Cu/Au) nanostructures

TiO_2/RGO@M (M=Ag/Cu/Au) was synthesized via the photo deposition method. For Ag loading, 100mg of TiO_2 was dissolved in 10ml of 50% aqueous IPA, then 934µL of 0.01M Ag solution was added for 1wt% deposition. The solution was purged with argon for 15 minutes to remove oxygen, sealed, and irradiated under UV light for 60 minutes with stirring. The mixture was centrifuged, washed with ethanol and DI water, and dried at 70°C for 2 hours to obtain 1 wt.% TiO_2/RGO@Ag. The same process applies for Cu and Au photo deposition(34).

1.4.4 Synthesis of RGO@M-TiO_2 (M-Ag/Cu/Au) hybrid structure

RGO@M-TiO_2 was synthesized by the self-assembly method (Scheme 1.5). Few amounts of RGO and M-TiO_2 powder was dispersed in DI water separately. Thereafter, the two col- loid solutions were mixed and agitated under vigorous stirring for 24 hours for a complete self-assembly reaction. The solid was centrifuged, washed, and dried at 60 ℃ for 12 hours. The process for the synthesis of the RGO@M-TiO_2 (M=Ag/Cu/Au) hybrid structure(35).

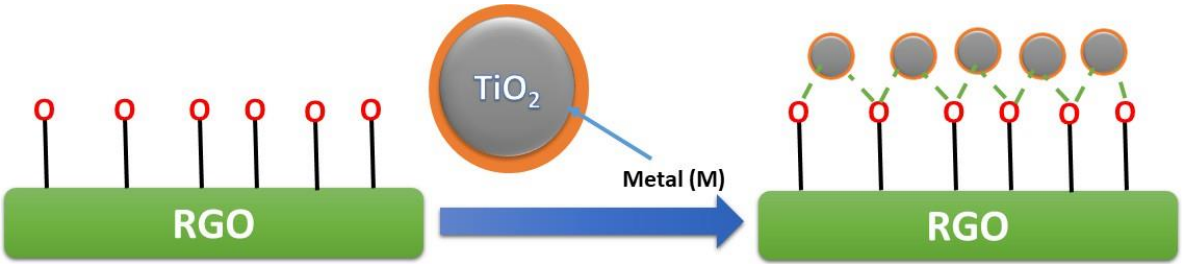

Scheme1.5. Schematic representation for the synthesis of RGO@M-TiO_2 nanocomposite.

1.4.5. Synthesis of CD@M-TiO_2 (M-Ag/Cu/Au) hybrid structure

CD@M-TiO_2 was synthesized by the self-assembly method. Few amounts of cyclodextrin and M-TiO_2 powder was dispersed in DI water separately. Thereafter, the two colloid solutions were mixed and agitated under vigorous stirring for 24 hours for a complete 16 self-assembly reaction. The solid was centrifuged, washed, and dried at 60℃for 12 hours.

The process for the synthesis of CD@M-TiO_2 (M=Ag/Cu/Au) hybrid structure(36).

Section-D

1.5 Characterization techniques

The desired nanocomposites were synthesized through a variety of self-devised and modified procedures, with experimental specifics outlined in the respective chapters. These newly created nano catalysts were then subjected to a comprehensive suite of characterization techniques to evaluate their optical, surface, and structural properties. Detailed descriptions of these different techniques are discussed below.

1.5.1 UV-Vis spectroscopy

The absorption properties of as-prepared 5ml liquid sample of nano catalysts were analyzed by UV-2450, Shimadzu within the wavelength range of 190-1100nm at a scanning speed of 200nm/min. The optical properties were measured using a diffuse reflectance spectrophotometer (DRS, Avantes) in the region 400–900 nm, with $BaSO_4$ bar as a reference by applying Tauc plot equation.

1.5.2 Dynamic light scattering (DLS)

DLS analysis was carried out to determine the average hydrodynamic size of prepared ternary/quaternary nanocomposites by dispersing 2 mg of the catalyst in 5 ml of deionized water using Malvern, Zetasizer with an acquisition time of 10-300sec, using a scattering angle of 173° and averaged over 3 to 10 runs to ensure accuracy.

1.5.3 Photoluminescence spectroscopy (PL)

The PL emission spectrum was carried out by dispersing 2 mg of the catalyst in 5 ml of deionized water on a PerkinElmer LS55 instrument at a scan speed of 50-200 nm/min to study the emission property and charge carrier separation at an excitation wavelength of 390 nm.

1.5.4 Raman analysis

Raman spectra were performed for the photocatalysts using a Labram HR confocal Micro-Ram spectrophotometer with an integration time of 10 sec per point at a step size of 0.5 cm^{-1} and averaged over 10 accumulations. The technique provided information about the structural defects, molecular composition, structure, and interactions within the sample.

1.5.5 X-ray powder diffraction (XRD)

The crystal structure, phase analysis, and diffraction pattern of the prepared samples were analyzed by X-ray powder diffraction using Smart Lab SE instrument equipped with HyPix-400: next generation 2D HPAD detector with diffraction angle (2θ) ranging from 10°-80° a scan rate of 5°/min.

1.5.6.X-ray photoelectron spectroscopy (XPS)

XPS analysis was conducted to study the oxidation state and chemical environment of the prepared nanocomposites. The data was recorded using PHI 5000 Versa Probe III instrument Al-Kα source (1486.6 eV).

1.5.7.Fourier transform infrared spectroscopy (FT-IR)

FT-IR spectra were recorded to explore the surface functional groups of prepared nano catalysts. This characterization was performed using Thermo Scientific Nicolet iS10within the frequency range of 400-4000cm^{-1}.

1.5.8Morphological analysis

Morphological studies of as -prepared samples were analyzed by Field Emission Scanning Electron Microscope (FESEM) and High-Resolution Transmission electron microscopy (HRTEM) using JEOL JSM-7600F operated at 30 kV and HRTEM-TALOS F200S G2 model operating at 200 kV voltage. EDS (Energy dispersive X-ray spectrometer) mapping was used to determine the elemental composition attached to another scanning electron microscope of the same model as mentioned above.

1.5.9 Total organic carbon and nitrate yield analysis

TOC (Total Organic Carbon) measurements were conducted with a Thermo Scientific HiPer TOC-TN-CLD module to evaluate the demineralization efficiency of CTA, ATR, CTR, and CTAR. The aliquots were mixed with H_3PO_4 (5% w/v) and $Na_2S_2O_8$ (10% w/v). Then the

reaction mixture was heated in a glass vessel to oxidize all the organic carbons to CO_2 which was detected using a non-dispersive infrared (NDIR) detector. The nitrate yield was further estimated using the ultraviolet spectrophotometer screening method (VARIAN-UV0910M156) by measuring the absorbance at 220 nm.

Nitrate yield analysis

Reagents: Stock nitrate solution, intermediate nitrate solution, HCl(~1M), Reagent water.

Procedure: 1. **Treatment of Sample**: A 50 mL clear sample was treated by adding 1mL HCl solution and mixed thoroughly.

2.Standards: NO_3^- calibration standards in the range of 0 to 7mg NO_3^--N/L were prepared by diluting the specified volumes of intermediate NO_3^- solution to 50ml. Other standard concentrations were also used. The NO_3^--N standards were treated in the same manner as the samples.

3.Spectrophotometric measurements: Absorbance or transmittance was spectrophotometrically measured against reagent water set at zero absorbance or 100% transmittance. A wavelength of 220nm was used to obtain the NO_3^--N reading, and a wavelength of 275nm was used to determine any interference from dissolved organic matter.

Calculations: NO_3^--N concentration was calculated from the following equation.

$$\mathbf{C=\frac{A-I}{S}}$$

Where,C= concentration, A= Absorbance, I- Intercept of the regression line, and S=slope of the regression line

1.6. Adsorption and photocatalytic activity

To examine the adsorption and photodegradation studies of the prepared samples TiO_2/RGO@M and Cyclodextrin and RGO modified M-TiO_2 (Scheme 1.6)). Urea will be used as a probe molecule. The photocatalytic reaction will be conducted at room temperature in a test tube under a sunlight irradiation. For carrying out the degradation process required amount of catalyst will be added to the test tube containing an aqueous solution of urea and magnetically stirred in the dark for 30 minutes to achieve adsorption-desorption equilibrium between urea and photocatalyst surface. After establishing the equilibrium, the solution will be irradiated for the required period under the light sources. A particular amount of solution will be taken at regular time intervals, centrifuge to remove the catalyst. After separation, the

absorbance spectra of urea formed was monitored.

$$ln\,\frac{C_0}{} = k_t$$

Where, C_0 denotes the initial concentration of urea before irradiation at time '0' and C_t is the concentration of urea after light irradiation at time

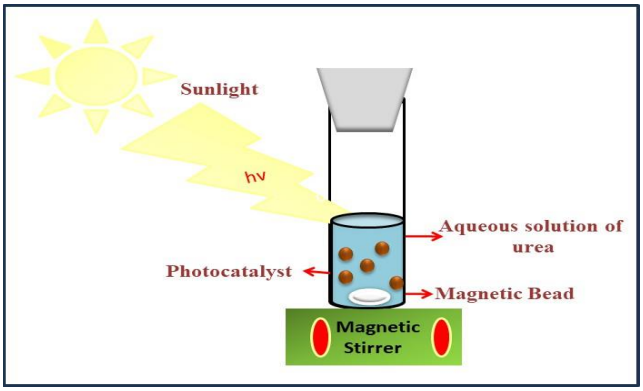

Scheme 1.6. Reaction setup for photocatalytic reaction.

1.7 Determination of urea

1.7.1. UV-Visible Spectroscopy:

Urea determination**:** -The determination of urea was carried out by using p-N, N Dimethylaminobenzaldehyde (DMAB), method (37).

1.8 Kinetic studies

Different kinetic models like pseudo-first order and pseudo-second-order models was analyzed to investigate urea's adsorption/photocatalysis process of different adsorbents/photocatalysts.

1. The Pseudo-first-order model is commonly used for initial rate and assumes that the rate of adsorption is directly related to the number of adsorption sites that are occupied.

2. The Pseudo-second order kinetic model depicts that the rate of solute uptake is directly proportional to the square of the difference of the concentration of the solute at a different time interval from the equilibrium concentration of the adsorbent.

The importance of urea chosen for study

Urea (Carbamide), with the formula $CO(NH_2)_2$, is a widely used fertilizer due to its high nitrogen content (46%). It boosts crop production by providing essential nutrients. However,60-70% of applied nitrogen can be lost to the atmosphere through ammonia volatilization, nitrate leaching, and nitrous oxide emissions, negatively impacting plant

growth and the environment. To address this, there is potential in developing TiO_2/RGO@M and M-TiO_2 nanocomposites modified with CD and RGO to enhance efficiency and reduce losses. The report proposes objectives to explore these innovations.

References

1) P. M. Glibert, J. Harrison, C. A. Heil, S. Seitzinger. Escalating Worldwide Use of Urea- A Global Change Contributing to Coastal Eutrophication. *Biogeochemistry*. **2006**, *77*, 441–463.
2) D. E. Kissel., H. L. Brewer, G. F. Arkin. Design and Test of a Field Sampler for Ammonia Volatilization. *Soil Sci. Soc. Am. J.* **1977**, *41*, 1133–1138.
3) D. Heuermann., H. Hahn., N. von Wirén. Seed Yield and Nitrogen Efficiency in Oilseed Rape After Ammonium Nitrate or Urea Fertilization. *Front. Plant Sci.* **2021**, 11, *1*–14.
4) J. Shade., L. Cattell Noll, V. Seufert, J. N. Galloway, J. W. Erisman. Decreasing Reactive Nitrogen Losses in Organic Agricultural Systems. *Org. Agric.* **2020**, *11*, 217-223,
5) R. Gil-Ortiz., M. A. Naranjo., A. R. Navarro., M. Caballero-Molada., S. Atares, C. García., O. Vicente. New Eco-Friendly Polymeric-Coated Urea Fertilizers Enhanced Crop Yield in Wheat. *Agronomy*. **2020**, *10, 1-17*.
6) N. F. da Silva, E. C. da Silva, T. Muraoka.; M.B. Teixeira, F.A.L Soares, F.N. Cunha,J. Adu-Gyamfi, W. S. da. S. Cavalcante. Nitrogen Utilization from Ammonium Nitrate and Urea Fertilizer by Irrigated Sugarcane in Brazilian Cerrado Oxisol. *Agric.* **2020**, *10*, 1–17.
7) J. Zhao., N. Li., R. Yu., Z. Zhao, J. Nan. Magnetic Field Enhanced Denitrification in Nitrate and Ammonia Contaminated Water under 3D/2D Mn_2O_3/g-C_3N_4 Photocatalysis. *Chem. Eng. J.* **2018**, *349*, 530–538.
8) G. Xu, X. Fan, A.J. Miller. Plant Nitrogen Assimilation and Use Efficiency. *Annu. Rev. Plant Biol.* **2012**, *63*, 153–182.
9) G. J. D. Kirk, H.J. Kronzucker. The Potential for Nitrification and Nitrate Uptake in the Rhizosphere of Wetland Plants: A Modelling Study. *Ann. Bot.* **2005**, *96*, 639–646.
10) X. Fan, M. Naz, X. Fan, Xuan; W. Miller, A. J, G. Xu. Plant Nitrate Transporters: From Gene Function to Application. *J Exp. Bot.* **2017**, *68*, 2463–2475.
11) A. Pal, R. Adhikary, S. Barman, S. Maitra. Nitrogen Transformation and Losses in Soil: A Cost- Effective Review Study for Farmer. *Int. J Chem. Stud*. **2020**, *8*, 2623–2626.
12) Y. Li, L. Huang, H. Zhang, M. Wang. Z. Liang. Assessment of Ammonia Volatilization Losses and Nitrogen Utilization during the Rice Growing Season in Alkaline Salt- Affected Soils. *Sustain*. **2017**, 8, 2623-2626.

13) L.K. Sharma, S.K. Bali. A Review of Methods to Improve Nitrogen Use Efficiency in Agriculture. *Sustain.* **2017**, *10*, 1–23.

14) Y. Niu, H. Li. Controlled Release of Urea Encapsulated by Starch-g-Poly (Vinyl Acetate). *Ind. Eng. Chem. Res.* **2012**, *51*, 12173–12177.

15) P. Tan, Y. Hu. Improved Synthesis of Graphene/β-Cyclodextrin Composite for Highly Efficient Dye Adsorption and Removal. *J Mol. Liq.* **2017**, *242*, 181–189.

16) J. Ye, S.Q. Liu, W.X. Liu, Z. Da. Meng, l. Luo, f. Chen, f. Zhou. Photocatalytic Simultaneous Removal of Nitrite and Ammonia via a Zinc Ferrite/Activated Carbon Hybrid Catalyst under UV-Visible Irradiation. *ACS Omega.* **2019**, *4*, 6411–6420.

17) Q. Zhou, H. Yin, A. Wang, Y. Si. Preparation of Hollow B–SiO_2@TiO_2 Compo- sites and Their Photocatalytic Performances for Degradation of Ammonia-Nitrogen and Green Algae in Aqueous Solution. *Chinese J Chem. Eng.* **2019**, *27*, 2535–2543.

18) T. S. H. Pham, L. Fu, P. G. Mahon Lai, A. Yu. Fabrication of β-Cyclodextrin- Functionalized Reduced Graphene Oxide and Its Application for Electrocatalytic Detection of Carbendazim. *Electrocatalysis.* **2016**, *7*, 411–419.

19) K. C Cameron, H. J. Di, J. L, Moir. Nitrogen Losses from the Soil/Plant System: A Review. *Ann. Appl. Biol.* **2013**, *162*, 145–173.

20) K. Rafiq, M. Sabir, MZ Abid, M Jalil, MA Nadeem, S. Iqbal, et al Tuning of TiO_2/CdS Hybrid Semiconductor with Au Cocatalysts: State-of-the-Art Design for Sunlight-Driven H_2 Generation from Water Splitting. *Energ Fuels*. **2024,***38*,4625–36.

21) L. Shi, C. Li, H. Gu, D. Fang. Morphology and properties of ultra ® ne SnO_2 ± TiO_2 coupled semiconductor particles.*Mat. Chem Phy.* **2000**;*62*:62–7.

22) S. I. Sempeho, H. T. Kim, E. A. Mubofu Pogrebnoi, G. Shao, A. Hilonga. Encapsulated Urea-Kaolinite Nanocomposite for Controlled Release Fertilizer Formulations. *J Chem.* **2015**, *2015, 1-17*.

23) R. Wang, T. Xie, Z. Sun, T. Pu, W. Li, J. P. Ao. Graphene Quantum Dot Modified G- C_3N_4 for Enhanced Photocatalytic Oxidation of Ammonia Performance. *RSC Adv.* **2017**, *7*, 51687–51694.

24) S. Park, J. T. Lee, J. Kim. Photocatalytic Oxidation of Urea on TiO_2 in Water and Urine: Mechanism, Product Distribution, and Effect of Surface Platinization. *Environ. Sci. Pollut. Res.* **2019**, *26*, 1044–1053.

25) S. Haga, H. Nagakawa, T. Ochiai, M. Nagata. Photocatalytic Oxidation of Aqueous Ammonia to Nitrite and Nitrate Ions on Zeolite TiO_2. *Chem. Lett.* **2018**, *47*, 1542–1544.

26) S. He, P. Hou E. Petropoulos, Y. Feng, Y. Yu, L. Xue, L. Yang. Highly Efficient Visible-Light Photocatalytic Performance of Cu/ZnO/RGO Nanocomposite for Decomposing of Aqueous Ammonia and Treatment of Domestic Wastewater. *Front. Chem.* **2018**, *6*, 1–13.

27) B. Li, C. Song, J. Rong, J. Zhao, H. E. Wang, P. Yang, K. Ye, K. Cheng, K. Zhu, J. Yan, D. Cao, G. Wang, A New Catalyst for Urea Oxidation: $NiCo_2S_4$ Nanowires Modified 3D Carbon Sponge. *J Energy Chem.* **2020**, *50*, 195–205.

28) V. Vaiano, O. Sacco, G. Di Capua, N. Femia, D. Sannino. Use of Visible Light Modulation Techniques in Urea Photocatalytic Degradation. *Water.* **2019**, *11,1-14.*

29) H. H. Ou, C. H. Liao, Y. H. Liou, J. H. Hong, S. L. Lo. Photocatalytic Oxidation of Aqueous Ammonia over Microwave-Induced Titanate Nanotubes. *Environ. Sci. Technol.* **2008**, *42*, 4507–4512.

30) H. Kisch. In the Light and in the Dark: Photocatalytic Fixation of Nitrogen into Ammonia and Nitrate at Iron Titanate Semiconductor Thin Films. *Eur. J Inorg. Chem.* **2020**, *2020*, 1376–1382.

31) M. V. Dozzi, S. Brocato, G. Marra, G. Tozzola, L. Meda, Selli. Aqueous Ammonia Abatement on Pt- and Ru-Modified TiO_2: Selectivity Effects of the Metal Nanoparticles Deposition Method. *Catal. Today.* **2017**, *287*, 148–154.

32) V. B. Parambhath, R. Nagar, K. Sethupathi, S. Ramaprabhu. Investigation of Spill- over Mechanism in Palladium Decorated Hydrogen Exfoliated Functionalized Graphene. *J Phys. Chem. C.* **2011**, 15679–15685.

33) R. Ikram, B. M. Jan, W. Ahmad. An Overview of Industrial Scalable Production of Graphene Oxide and Analytical Approaches for Synthesis and Characterization. *J Mater. Res. Technol.* **2020**, *9*, 11587–11610.

34) M. Sohail, H. Xue, Q. Jiao, H. Li, K. Khan, Y. Zhao. Synthesis of Well-Dispersed TiO_2@reduced Graphene Oxide (RGO) Nanocomposites and Their Photocatalytic Properties. *Mater. Res. Bull.* **2017,** *90*, 125-130.

35) K. H. Leong, L. C. Sim, D. Bahnemann, M. Jang, S. Ibrahim, P. Saravanan. Reduced Graphene Oxide and Ag Wrapped TiO_2 Photocatalyst for Enhanced Visible Light Photocatalysis. *APL Mater.* **2015**, 3, 1-8.

36) R. Chalasani, S. Vasudevan. Cyclodextrin-Functionalized Fe_3O_4@TiO_2: Reusable, Magnetic Nanoparticles for Photocatalytic Degradation of Endocrine-Disrupting Chemicals in Water Supplies. *ACS Nano.* **2013**, 7, 4093–4104.

37) J. D. Giraldo, B. L. Rivas. Determination of Urea Using p-N, N- Dimethylaminoben-

zaldehyde: Solvent Effect and Interference of Chitosan. *J Chil. Chem. Soc.* **2017**, 62, 3538–3542.

CHAPTER-2

Enhanced photocatalytic urea oxidation under neutral medium by reduced graphene oxide coated TiO_2 nanoparticles

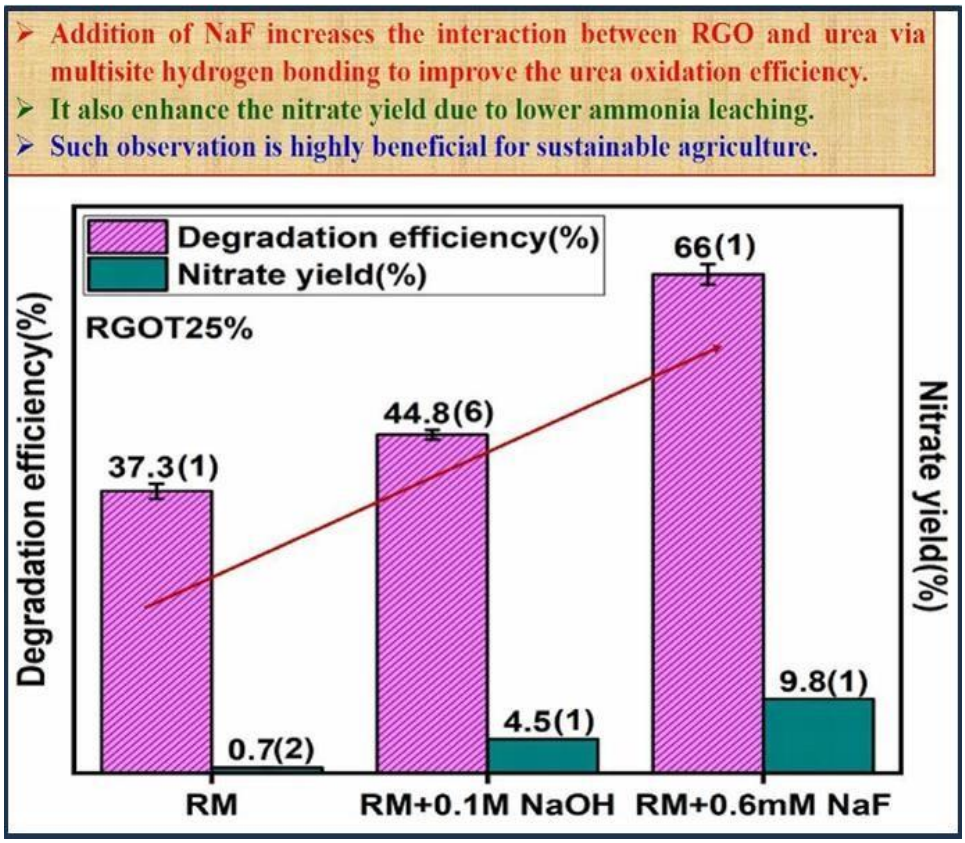

Schematic outline

This study reveals the photocatalytic oxidation of urea using bare TiO_2 and RGOT25% at different ambient conditions (RM), (RM+0.1M NaOH, pH~13), and (RM+0.6mM NaF) under sunlight irradiation. The RGOT25% composite demonstrates superior activity over bare TiO_2 due to a synergistic effect, enhanced interfacial surface area, and the high electron mobility of RGO. This results in reduced recombination rates and increased charge transfer efficiency. Additionally, NaF plays a dual role in boosting photocatalytic performance: it removes protons from the reaction medium without deprotonating ammonium ions, thereby minimizing ammonia leaching, and it enhances the binding of urea to the photocatalyst through multisite hydrogen bonding interactions.

2.1 Introduction

In the last few decades, due to enormous growth in population besides the depreciation of accessibility of land for agriculture, the whole world is facing the risk of food shortage. Consequently, crop production has to be increased manifold. Therefore, fertilizers have been applied to agricultural fields to enhance the growth and yield of crops. Urea is one of the most widely used nitrogenous fertilizers engaged in ammonification, nitrification, denitrification, and mineralization process (1,2). Urea accommodates 46% of nitrogen content and supplements essential nutriment to the plants, attributed to its effectiveness towards sustainable agriculture (3-5). Result of the inefficacious availability and easy leaching of nitrogen from the soil, the external supply of nitrogen is foremost essential to enhance crop yield, which has been executed globally for a long back by augmenting nitrogenous fertilizers like $CO(NH_2)_2$, NH_4NO_3, anhydrous NH_3, etc. (6,7) Generally, plants assimilate nitrogen through the soil in the form of nitrate and ammonium ions. Therefore, to absorb nitrogen from the soil, $CO(NH_2)_2$ must be hydrolyzed and the resultant NH_3 needs to be protonated to afford NH_4^+ ions (equation 1). Subsequently, the ammonium ions undergo a nitrification process to yield nitrate (equation 2). With the help of nitrate and ammonium transporters, these ions are taken up by plants, and the transport is powered by a proton gradient.

$$CO(NH_2)_2 + H_2O + 4H^+ = CO_2 + 2NH_4^+ \text{ ----------(1)}$$

$$NH_4^+ + 3H_2O = NO_3^- + 10H^+ + 8e^- \text{ ----------(2)}$$

A vital concern associated with it is that a significant fraction (60-70%) of urea gets vanished into the atmosphere through nitrate leaching, ammonia volatilization, and N_2O emissions which deteriorate plant growth and the environment through subsurface water acidification and global warming(8-10). Also, the nitrification process often produces nitrogen gas (N_2) as the major product due to incomplete oxidation, thus resulting in nitrogen leaching. Urea-contaminated water adversely affects not only human beings but also birds, wildlife, and livestock(11,12). Accordingly, it is essential to oxidize urea into beneficial and harmless products like NO_3^-, which is helpful in increasing overall crop production.

Several researchers attempted to oxidize urea in many different methodologies, such as the electrochemical method(13,14), photocatalytic method(15,16), chemical method(17), and biological method(18), to get beneficial products. However, in most cases, the principal issue is the formation of N_2 (gaseous product) due to incomplete oxidation of ammonia, which probably decreases the nitrate efficiency. As a result, more efficient oxidants are re-

quired to ensure the complete oxidation of urea.

TiO_2 has been regarded as one of the most widely used photocatalyst as it is non-toxic, economical, eco-friendly, and chemically stable (19). Once TiO_2 is exposed to energy equal to or greater than its band gap, it induces e^-/h^+ pairs. These e^- and h^+ react with water molecules to generate strong reactive oxygen species (ROS) (e.g., $H_2O_2^{\bullet}$, h_{vb}^+, $OH^{\bullet}$, $O_2^{\bullet-}$)(20), which causes urea oxidation. However, TiO_2 has several drawbacks owing to its wider bandgap that limits its visible light absorption capacity and rapid e^-/h^+ pair recombination rate, thereby reducing its photocatalytic activity (21-23). Moreover, photocatalytic oxidation of urea generally requires the transfer of $8e^-$ from NH_3 to NO_3^-, which enhances the probability of a complete electron transfer process leading to the formation of several byproducts.

To avert these complications, reduced graphene oxide (RGO) coated TiO_2 nanoparticles have been prepared, and their photocatalytic activity towards urea oxidation was monitored under different conditions. RGO has several excellent properties like a smaller band gap that shifts the adsorption edge towards the visible region, a large surface area that can increase the adsorption capacity, high electrical capacitance, and conductivity to afford maximum charge storage and transfer (24-25). Owing to such intriguing properties, RGO and other graphitic carbon based nanocomposites are emerging as new generation photocatalysts([26–31). Urea molecules can interact with RGO-TiO_2 nanocomposite effectively because RGO provides a large specific surface area which enhances the urea intake as well as promotes multiple electron transfer process (32).

Oxidation of ammonium ion to nitrate (equation 2) involves the removal of protons. As a result, urea oxidation becomes more favorable in an alkaline medium. Though under strongly alkaline conditions (in the presence of NaOH) the ammonium ions can get deprotonated to form ammonia, enhancing the risk of ammonia leaching. Moreover, alkalinity restricts crop growth by limiting the water supply to the roots(26). It also causes deficiencies of other micronutrients like phosphorous, iron, zinc etc.(26). To overcome these problems, we have also evaluated the photocatalytic urea oxidation efficiency under a near-neutral medium (pH ~6.5-7) in the presence of NaF. Fluoride is a much weaker base than hydroxide, through which it can remove the protons generated during the oxidation of ammonium ions but it will not undergo any acid-base reaction with the ammonium ions directly. As a result, the chances of ammonia leaching will be reduced. It can also enhance the interaction of urea with RGO via hydrogen bonding interactions **(Scheme 2.1)** to boost the photocatalytic activity further.

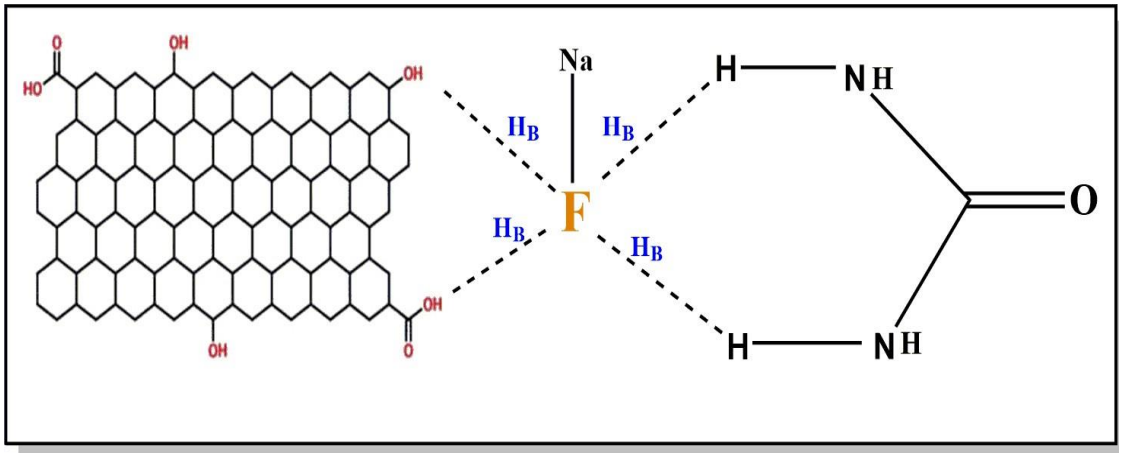

Scheme 2.1. Schematic representation of intermolecular hydrogen bonding between RGO, urea, and NaF.

2.2. Experimental section

2.2.1. Chemicals and reagents

Titanium dioxide (P25-TiO_2) was obtained from the Degussa Corporation in Germany. Graphite powder (98% extra pure), sodium nitrate ($NaNO_3$, 99%), concentrated sulfuric acid (H_2SO_4, 98%), hydrochloric acid (HCl, 35.4%), potassium permanganate ($KMnO_4$, 99% extra pure), Hydrogen peroxide (H_2O_2, 30%w/v extra pure), L-ascorbic acid (L-AA, 99.5%), ammonia (liq.NH_3, 28%) were purchased from LobaChemie Pvt. Ltd., India. Deionized (DI) water was prepared through (Milli-Q, Millipore) ultrafiltration system having a conductivity of (35 mho cm^{-1} at 25˚C) which was used during all the experiments. Analytical-grade chemicals were utilized without any additional purification.

2.2.2. Green synthesis of reduced graphene oxide (RGO)

0.24g GO and 100 DI water was sonicated for 30 minutes and marked as solution A. 2g L-AA was dissolved in 200 ml DI water and marked as solution B. Solution B was added dropwise to the solution A with continuous stirring, and the pH (9-10) of the mixture was adjusted with 28% aq.NH_3 solution(34). The resulting mixture was heated at 95˚C for 2 hours (avoid boiling) to reduce GO. The black fluffy solid was obtained that was washed several times with water and ethanol and then vacuum dried.

2.2.3. Synthesis of RGO-TiO_2 (25 wt.%) nanocomposite (Wet impregnation method)

An appropriate amount of RGO and TiO_2 (25 wt.%) was dispersed separately in DI water. The aqueous dispersion of TiO_2 was added dropwise to the RGO suspension and ultrasonicated for another 1 hour (35) and then stirred for 24 hours. The solid was isolated by centrifugation and dried at 60˚C to obtain the grayish-colored powder abbreviated as RGOT25%.

2.2.4. Characterizations and photocatalytic study

XRD patterns were recorded using (Smart Lab SE) instrument equipped with HyPix-400:

next-generation 2D HPAD detector with diffraction angle (2θ). PL emission spectrum was recorded using PerkinElmer LS55. Dynamic light scattering DLS analysis was done by Malvern, Zetasizer. The optical properties of the catalyst were analyzed using DRS. Avantes. FT-IR spectra was measured using Thermo Scientific Nicolet iS1. The Raman spectra were conducted using Labram HR confocal Micro-Raman spectrometer. The surface structural morphology of the materials was analyzed using field emission scanning electron microscopy (FESEM), EDS (SEM-EDS; JEOL JSM-7600F and high-resolution transmission electron. XPS were conducted through PHI 5000 Versa Probe III. The nitrate analysis was done using (APHA 5310D) and TOC was measured using a TOC analyzer (APHA-4500 NO_3 B). The urea concentration in the solution was measured using a UV-Visible spectrophotometer (SHIMADZU UV-2600) (λ_{max}=420nm)

The photocatalytic activities of the bare TiO_2, as well as the RGOT25% nanocomposite, were analyzed by monitoring urea degradation efficiencies under ambient conditions (Reaction mixture or RM), alkaline conditions (RM+0.1M NaOH, pH~13), and in the presence of NaF (RM+0.6mM NaF). All the photocatalytic reactions were performed under sunlight (in June 2021 at 10:00 am-4:00 pm when the intensity of sunlight was maximum) in different test tubes. In a typical photoreaction., 20mg of the catalyst was dispersed in aqueous urea (10ml of 0.6mM) solution in a test tube. Before sunlight irradiation, each suspension was stirred for 30 minutes under dark conditions to allow the adsorption-desorption equilibrium. Then, different test tubes containing the reaction mixture were irradiated with sunlight exposure. After every 1-hour interval, sample aliquots (1 ml) were taken out, centrifuged and the concentration of urea was measured upon the addition of DMAB (p-N, N-dimethylamino benzaldehyde) at absorbance value λ_{max} =420nm(36).

The percentage degradation (%D) was calculated by using this equation.

$$\%\boldsymbol{D} = \frac{\boldsymbol{C_O - C_t}}{\boldsymbol{C_O}} \times \mathbf{100}$$

Where C_O denotes the initial urea concentration, and Ct is the urea concentration after light irradiation at time t.

The rate of the photocatalytic reactions was fitted by using the pseudo-first-order kinetic equation.

$$\mathbf{2.303}\boldsymbol{log}\frac{\mathbf{C_0}}{\mathbf{C_t}} = \boldsymbol{kt}$$

Where C_o=Initial concentration, C_t = concentration at a different time interval, k= rate constant, t=time (min).

This nitrate efficiency was measured by the spectroscopic method (APHA-4500 NO_3^-B). Total organic carbon was determined using a TOC analyzer (APHA 5310 D) from which demineralization efficiency(37) was calculated from TOC data by using the following equation:

$$\boldsymbol{Demineralisation\ efficiency} = \frac{\boldsymbol{TOC_i - TOC_f}}{\boldsymbol{TOC_i}} \times \mathbf{100}$$

2.3. Results and discussion

X-Ray diffraction (XRD) measurements were carried out for the GO, RGO, bare TiO_2, and RGO25%, as seen in **Fig. 2.1 (a-d).** In **Fig.2.1 (a)**, GO displayed a diffraction peak (001) at 2θ=11.1˚ and 42.2˚ indicates the introduction of functional groups (-COOH, OH, CHO) within the carbon layers. After the GO reduction, the emergence of a broad characteristic diffraction peak (002) at 2θ=25.8˚ (ICDD card no.75-1621) in **Fig.2.1 (b)** designates that the L-AA acts as an effective reducing agent for the reduction of GO (38).

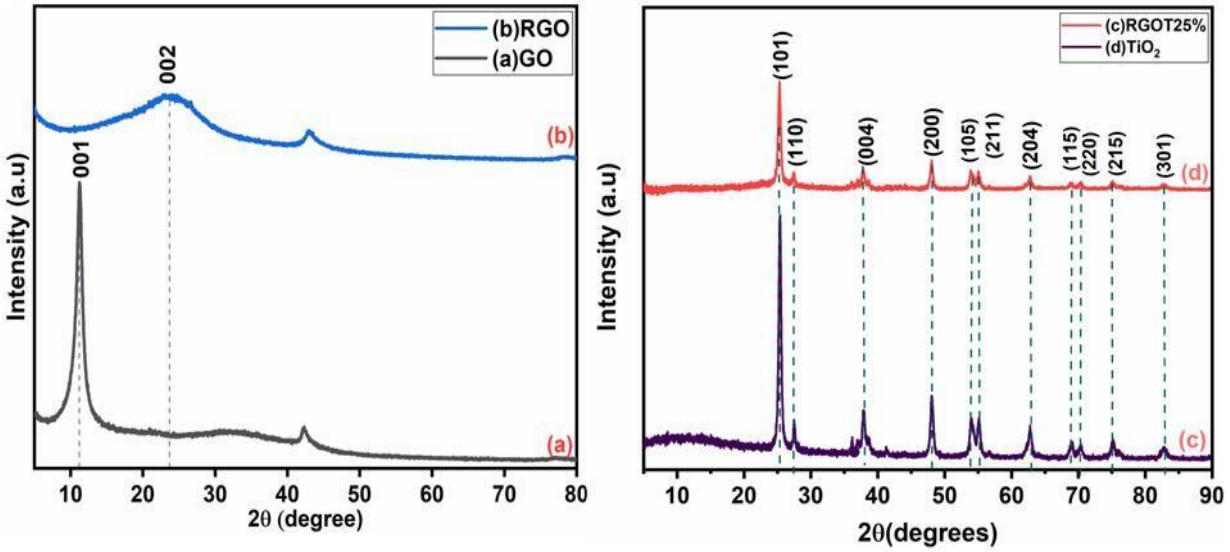

Fig 2.1: XRD patterns of (a) GO (b) RGO (c) RGOT25% nanocomposite, and (d) Bare TiO_2

XRD patterns of TiO_2 and RGOT25% exhibited **(Fig.2.1 (c-d))** several diffraction peaks at 2θ=25.2˚, 37.8˚, 48.2˚, 53.8˚, 55.8˚, 62.8˚, 68.8˚, 70.3˚, 75.1˚, and 82.7˚ which denotes the (101), (004), (200), (105), (211), (204), (115), (220), (215) and (301) crystallographic planes of anatase phase P25-TiO_2 (ICDD card no.21-1272) respectively(39).

In contrast, less intense peaks were detected on RGOT25% nanocomposite that decreases the e^- scattering of TiO_2 when dispersed upon the RGO surface. The peak of RGO was not observed in **Fig.2.1 (c)** due to its less crystalline nature and much lesser x-ray scattering coefficient compare to TiO_2. One characteristic peak was also detected at $2\theta=27.39^\circ$ for (110) planes in **Fig.2.1 (c-d)** confirming the formation of a rutile phase doped in the anatase phase.

DRS spectra and band gap values of bare TiO_2 and RGOT25% nanocomposite was shown in **Fig.2.2** and **Fig.2.3**. Bare TiO_2 and RGO showed an adsorption edge at a shorter wavelength of 329nm and 273nm and a band gap value of (E_g=3.14eV) in the UV region. In RGOT25%, the adsorption edge significantly shifted to a longer wavelength of 420 nm with a band gap value of (E_g=2.04 eV) due to the suppression in the recombination rate of photoexcited charge carriers. (40).

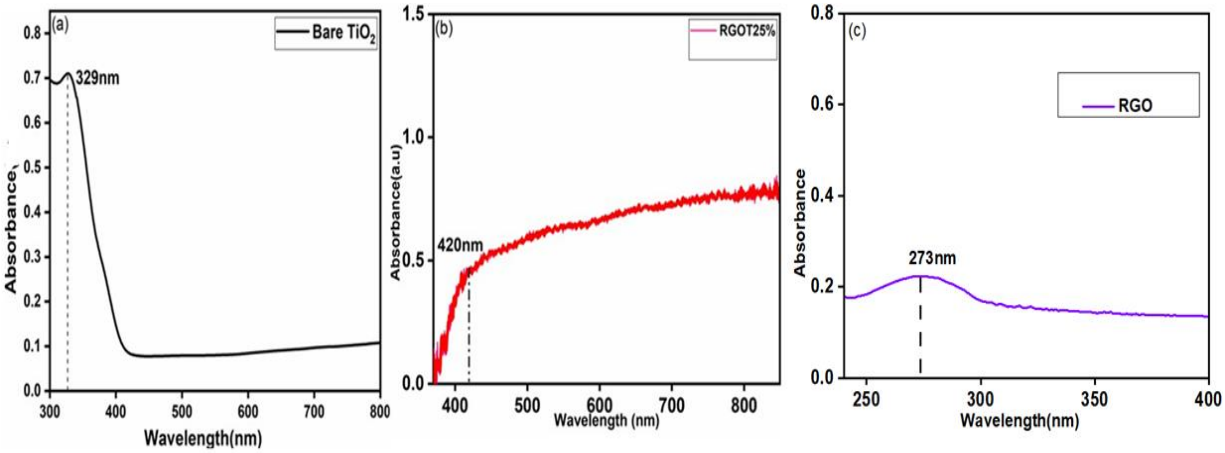

Fig.2.2. DRS (Diffuse reflectance spectroscopy) spectra of (a)Bare TiO_2 (b)RGOT25% nanocomposite and (c) RGO.

In RGOT25%, a red shift was observed that participates in the intermolecular interactions within TiO_2 and RGO that attributes to the formation of Ti–O–C bonds. The optical band gap of the bare TiO_2 and RGOT25% nanocomposite was calculated from the UV-DRS plot and Tauc's plot by using the Kubelka-Munk equation.

$$\boldsymbol{\alpha h\nu = A(h\nu - E_g)^n}$$

E_g= Band gap value of the sample, hν=energy of a photon, α=adsorption coefficient, A=constant n=exponential coefficient (n=1/2). Optical band gaps were estimated by plotting a graph between $(\alpha h\nu)^{1/2}$ v/s hν.

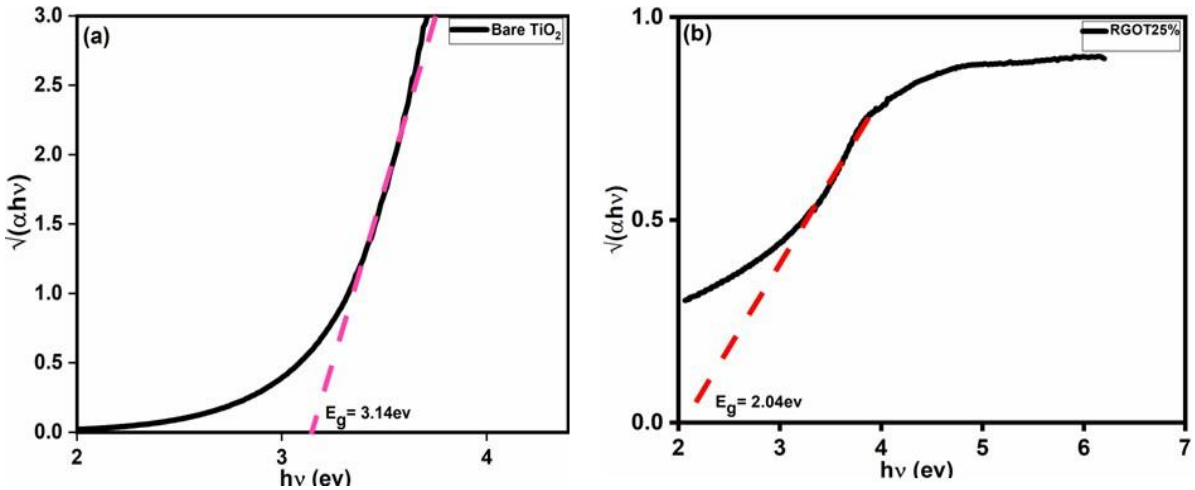

Fig.2.3. Tauc's plot (band gap values) of (a) Bare TiO_2 (b) RGOT25% nanocomposite.

Furthermore, photoluminescence (PL) spectra of bare TiO_2 and RGOT25% were used to analyze the rate of e^-/h^+ pair recombination. Both bare TiO_2 and RGOT25% exhibit only one characteristic peak at 533 nm upon excitation with 390 nm radiation **(Fig.2.4).** The PL intensity of RGOT25% nanocomposite was substantially lowered than that of bare TiO_2, probably owing to the rapid transfer of electrons from the conduction band of pristine TiO_2 (anatase) to the valence band of RGO and the rutile phase of bare TiO_2. As a result of this migration, the e^- and h^+ in RGOT25%, the recombination rate was decreased.

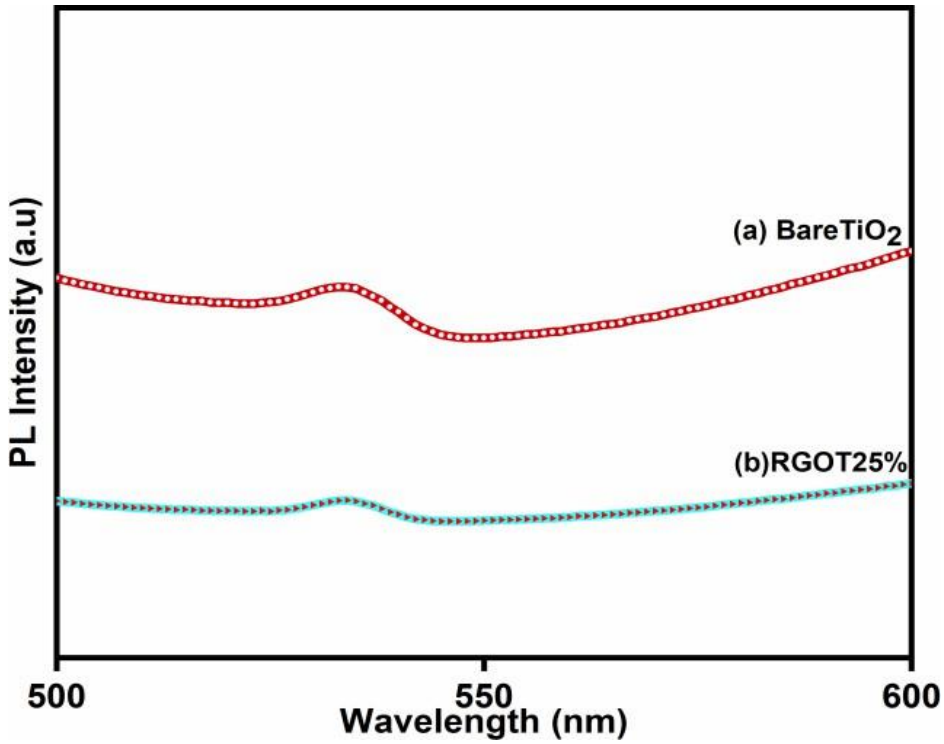

Fig. 2.4. PL spectra (a) Bare TiO_2 (b) RGOT25% nanocomposite.

The DLS particle size analysis was performed for bare TiO_2, RGO, and RGOT25% nano-

composites by dispersing each 2 mg catalyst in 5ml water. It revealed that the hydrodynamic size of bare TiO_2 **(Fig.2.5 (a))** was 129 nm. RGO (392 nm and 5556 nm) and RGOT25% (171nm and 5549nm) in **(Fig.2.5.(a,c))** showed two statistical modes(41). The hydrodynamic size of RGO was greater than that of RGOT25%, probably due to the deposition of TiO_2 particles over the RGO surface that passivates the surface functional groups of RGO.

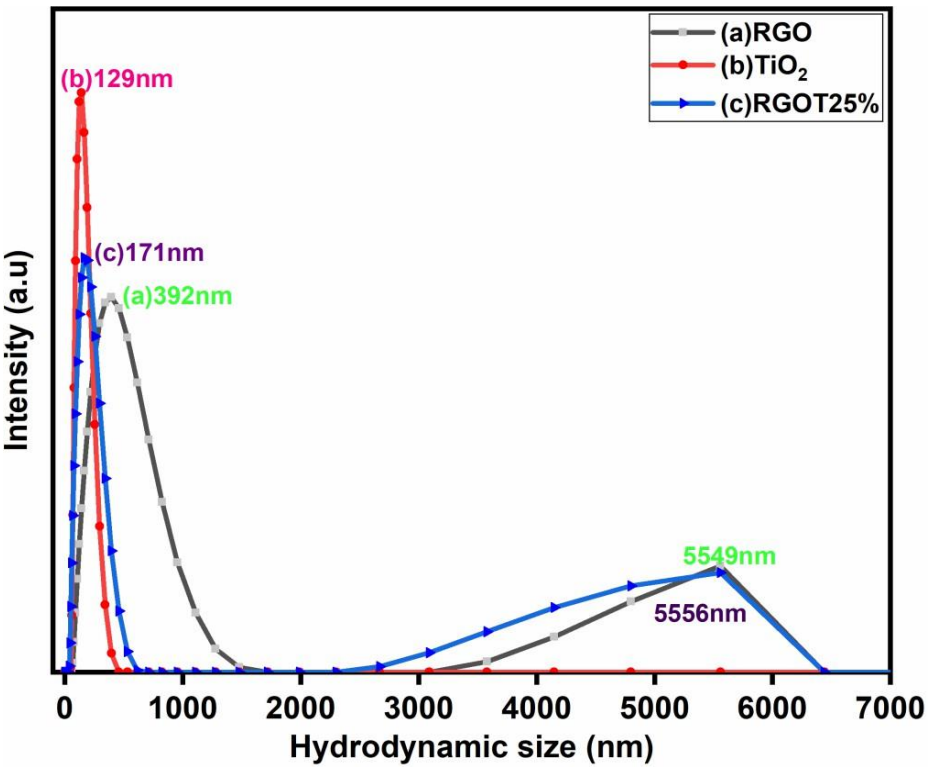

Fig.2.5. Particle size distribution (DLS) of (a) RGO (b) Bare TiO_2 and (c) RGOT25% nanocomposite.

Fourier transform infrared spectra (FT-IR) of graphene oxide (GO) **(Fig.2.6 (a))** shows several characteristic peaks. The signal at 3443 cm^{-1} is attributed to O–H stretching mode(42), the absorption peak at 1631 cm^{-1} belongs to C=C stretching mode[43]. While the peaks observed at 1724 cm^{-1}, 1380 cm^{-1} and 1073 cm^{-1} corresponds to the C=O [42], C–OH (42), and epoxy C–O[44] stretching modes respectively. Whereas the peak at 577 cm^{-1} corresponds to the out-of-plane O–H bending mode(43). In the FTIR spectra of RGO **(Fig. 2.6(b)),** all these signals correspond to all the oxygen-containing functional groups have either become much less intense or almost disappeared, confirming the successful reduction of GO to RGO with L-AA (42–44). **(Fig2.6 (c))** exhibits a broad peak at 1000 cm^{-1} ascribed to the Ti–O–Ti stretching and bending vibrational modes. In RGOT25%, a band was observed at 427 cm^{-1} which corresponds to a Ti–O–C bond and provides the evidence for the nanocomposite formation **(Fig2.6 (d))** (45).

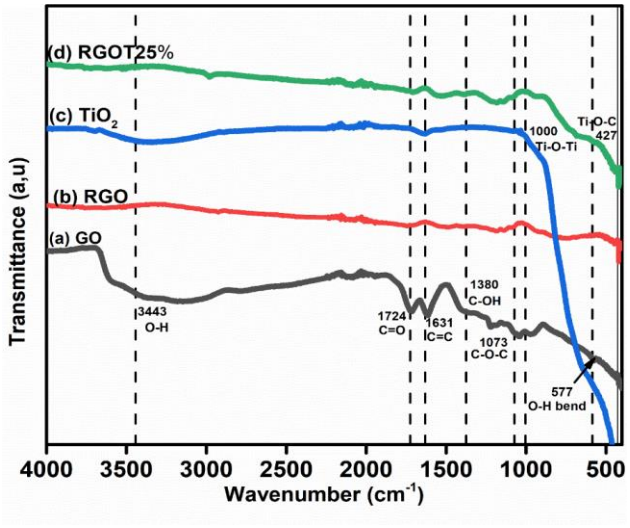

Fig.2.6. FT-IR spectra of (a)GO (b)RGO (c)Bare TiO_2 (d)RGOT25% nanocomposite.

The Raman spectra of parent TiO_2 are displayed in **Fig. 2.7(c)** where $E_{g(1)}$, $B_{1g(1)}$, A_{1g}+$B_{1g(2)}$, and $E_{g(2)}$ peaks of P25-TiO_2 (anatase) were observed at 147, 404, 520 and 642 cm^{-1}, respectively. The peak position of RGOT25% is somewhat shifted as compared to pristine TiO_2, confirming the nanocomposite formation. In **Fig, 2.7(a)**, the other two peaks were also observed at 1349 and 1595 cm^{-1} owing to the D and G bands (46). Similarly, the two peaks located at 1346 and 1584 cm^{-1} were also observed in **Fig. 2.7(b)**, resembling the D and G bands. The D band is attributed to sp^3 C-atoms out plane vibrations causing the imperfections and asymmetry in the structure, and the G band is linked to the sp^2 C-atom associated with the crystallization and the uniformity of the C-atom. The I_D/I_G ratio of RGO was 0.96 increased to 1.18 for RGOT25% indicating the absence of any defects in RGOT25% nanocomposite.

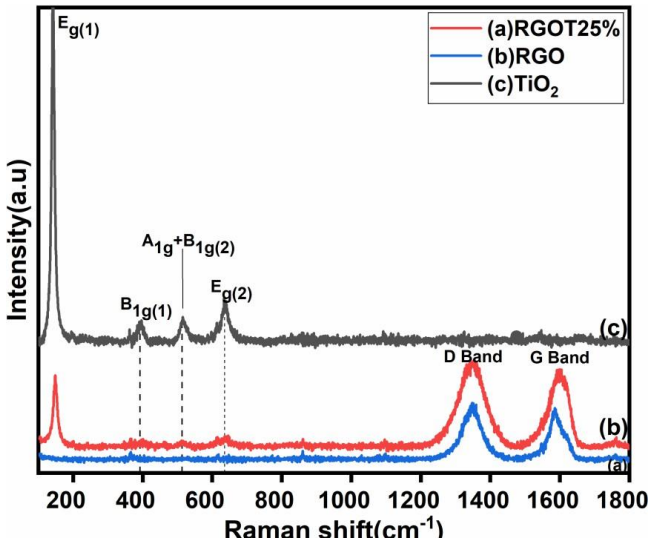

Fig.2.7. Raman spectra of (a) RGOT25% nanocomposite (b) RGO and (c) Bare TiO_2.

Fig 2.8(e) and (f) displays the SEM images of TiO_2 and RGO where TiO_2 shows spherical

and irregular surface morphology and RGO reveals a thin, wrinkled, and layered sheet like morphology, characteristic of exfoliated graphene structures.**Fig.2.8 (a-d)** shows the SEM images of RGOT25% nanocomposite revealed that TiO_2 particles are homogeneously spread on the surface of RGO sheets. **Fig.2.9** displays EDX pro- files and the table represents the percentage of the elements in RGO and TiO_2. This elemental mapping also confirms deposition of TiO_2 on the RGO surface. A signal of gold (Au) element was also observed due to the gold coating of samples during SEM analysis.

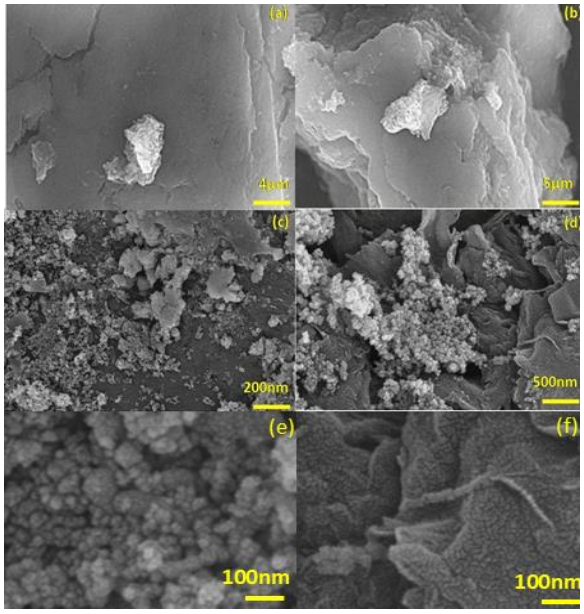

Fig. 2.8. Field electron Scanning electron microscopy (FE-SEM) images of (a-d) RGOT25% nanocomposite at different scales, (e) Bare TiO_2 and (f)RGO.

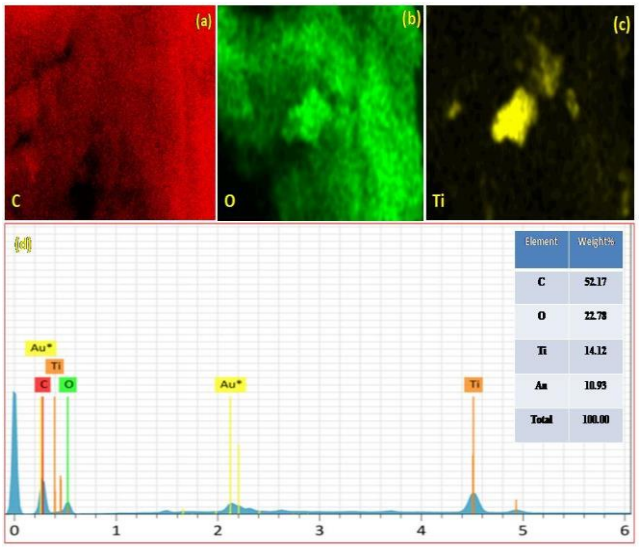

Fig. 2.9. Elemental dot mapping (a-c) and EDX analysis pattern and composition (d) of RGOT25% nanocomposite.

The HR-TEM images in **Fig.2.10(a-d)** displayed the surface morphology of RGOT25% nanocomposite. **Fig.2.10(a)** shows the homogeneous distribution of TiO_2 nanoparticles over the surface of RGO in RGOT25% nanocomposite. **Fig2.10(b)** showed that the TiO_2 and RGO nanoparticles facets are firmly attached, which was favorable for charge transfer and photocatalytic efficiency of the catalyst. **Fig, 2.10(c)** exhibited the crystal structure with lattice spacings of 0.35nm, which was well matched with the crystalline (101) plane of the anatase phase of TiO_2. In **Fig. 2.10(d)**, the SAED pattern showed that the RGOT25% was crystalline due to the presence of the (101) plane for the anatase phase of TiO_2.

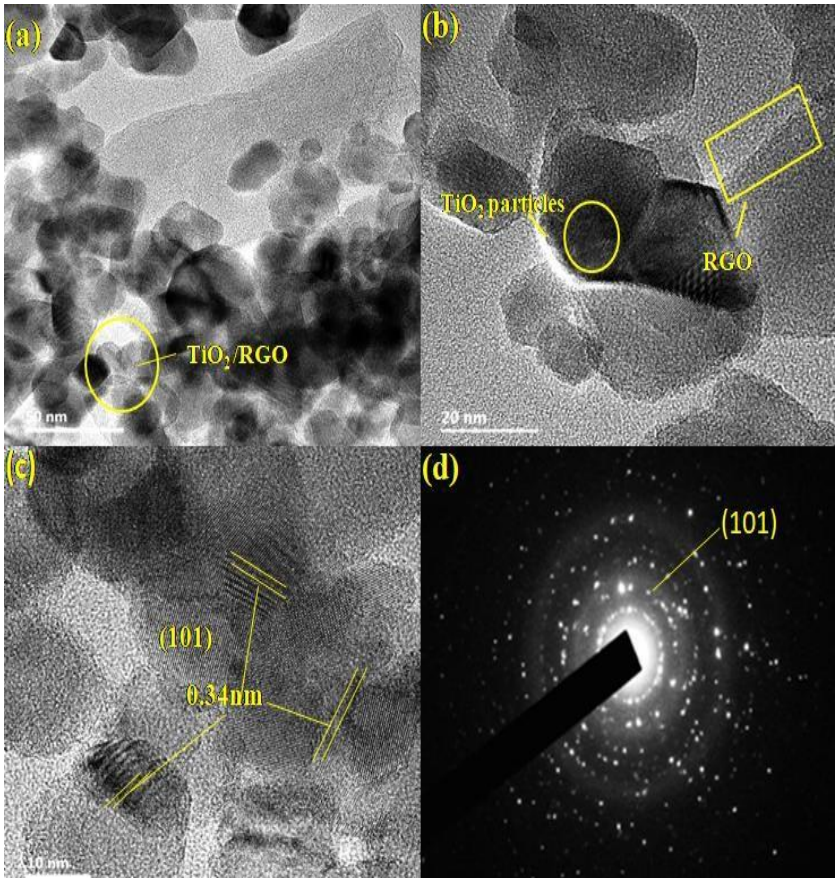

Fig.2.10 (a-c) HRTEM images and (d)SAED pattern of RGOT25% nanocomposite.

To analyze the oxidation state, the composition of elements, and the chemical environment in RGOT25%, XPS analysis was carried out. The XPS survey spectra **(Fig.2.11(a))** confirms the presence of all the individual elements in the sample. In C1s spectra **(Fig2.11(b)),** peaks were observed at different binding energies of 284.47ev and 285.5ev, which signifies the C=C/C–C, C–O bonds (47). **(Fig.2.11(c))** represents the O1s spectra which exhibit two peaks at 531ev and 532.4ev corresponding to the Ti–O and C–O bond in RGO composites. In **(Fig.2.11(d)** the spectra with two characteristic peaks at 459.67ev and

465.53ev could be correlated with the Ti $2p_{3/2}$ and Ti $2p_{1/2}$ peaks of P25-TiO_2. Ti 2p level can be deconvoluted to spin-orbit peaks (Ti $2p_{3/2}$ and Ti $2p_{1/2}$), and that accounts for binding energies difference of 5.9ev confirming the existence of Ti(IV) as reported in the literature (46).

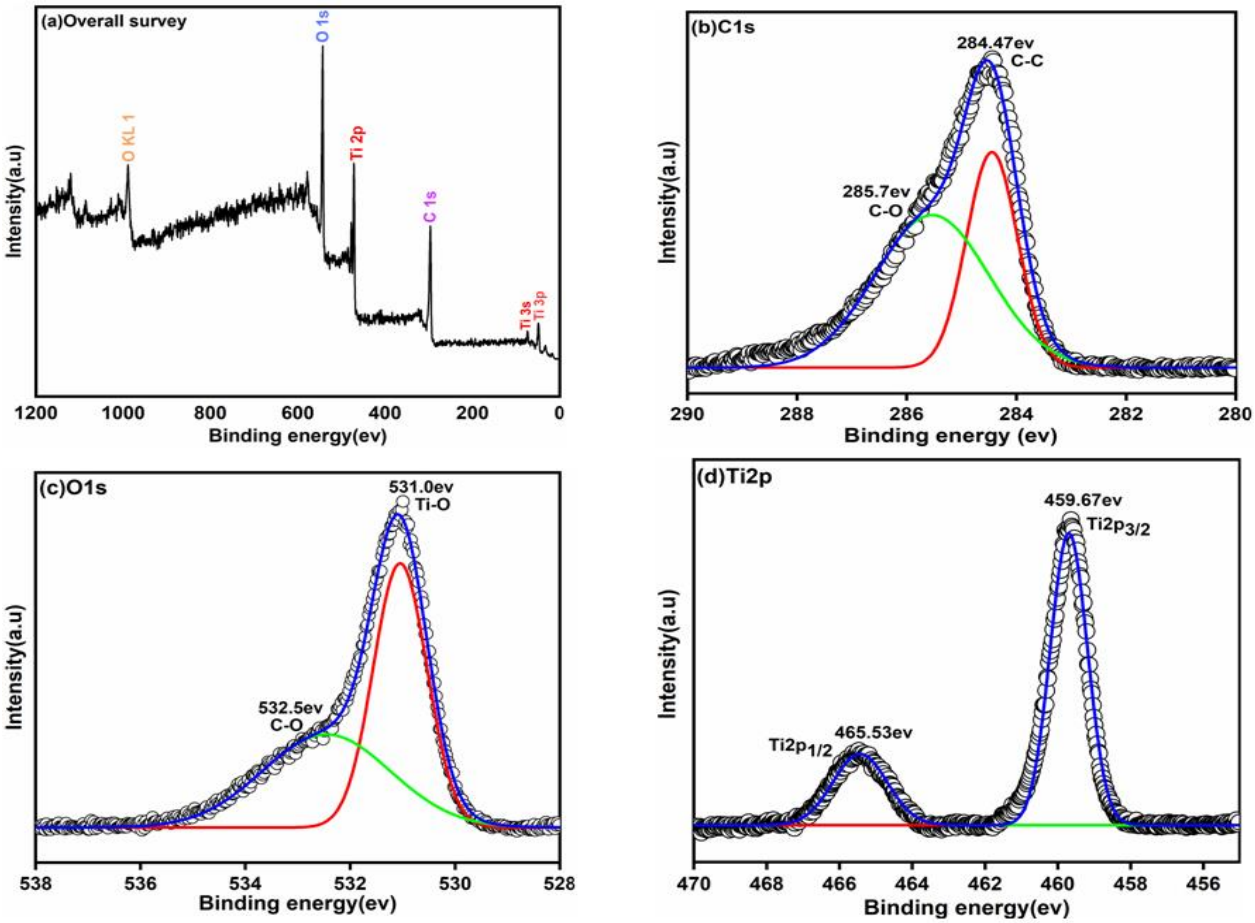

Fig 2.11: X-Ray photoelectron spectroscopy (XPS) (a) Overall survey spectra (b) C1s (c) O1s and (d)Ti2p spectra of RGOT25% nanocomposite.

2.4. Photocatalytic activity study

In this experiment, the photodegradation of urea under different reaction conditions (RM, RM+0.1M NaOH, and RM+0.6mM NaF mixture) by TiO_2 was carried out for 360 minutes under sunlight irradiation. **Fig.2.12(a**) and **2.13** represent the gradual decrease in UV-Visible absorption (λ_{max} =420nm) values. Improved photocatalytic activity of bare TiO_2 was observed in the presence of NaF (pH~6.5-7.6) as compared to urea in alkaline pH. The urea photooxidation reactions (RM, RM+0.1M NaOH, and RM+0.6mM NaF mixture) obey pseudo-first-order kinetics **(Fig.2.12(b**). **Fig.2.12(c-d)** depicts that NaF addition increases the rate constant ($0.18x10^{-2}$ min^{-1}) value and degradation (54.8%) efficiency of urea by TiO_2 under sunlight irradiation

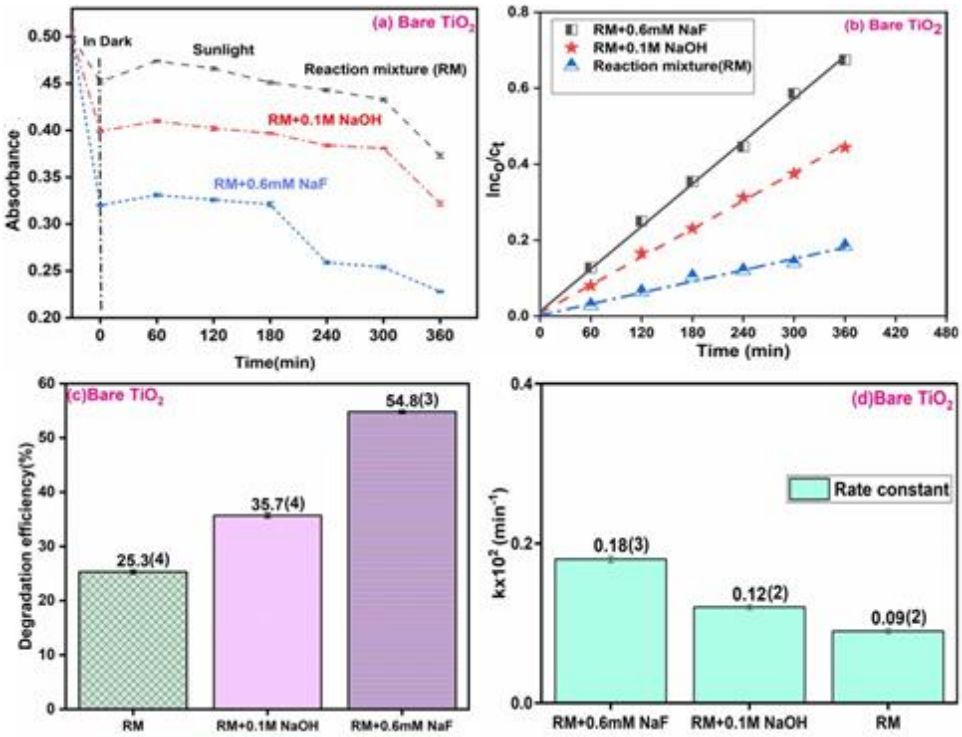

Fig 2.12: (a) Changes observed in absorbance vs time under solar light irradiation (b) pseudo-first-order kinetic fitting (c) Variation in photocatalytic urea oxidation efficiency (%) for bare TiO2 photocatalyst and (d) changes in the pseudo-first-order rate constant (RM RM+0.1M NaOH, and RM+0.6mM NaF) under different reaction conditions.

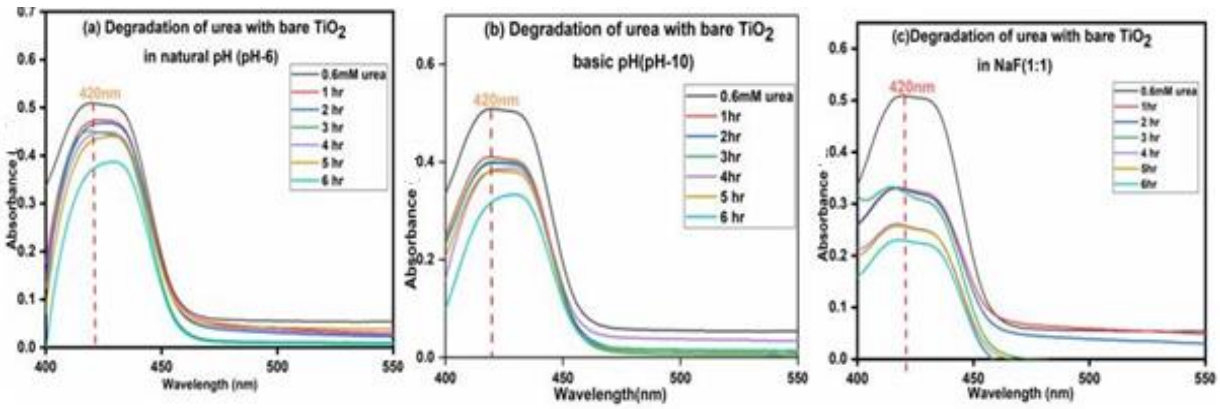

Fig.2.13. (a-c) Comparative changes observed in UV-visible absorption spectra of urea degradation with effect from bare TiO_2 in natural pH, basic pH, NaF (1:1).

Fig.2.14(a) and **2.15** also represent the absorption values of urea photodegradation with RGOT25% nanocomposite in the presence of 0.1M NaOH (pH~13) and 0.6mM NaF (pH~6.5-7.6). A maximum decrease in absorption value was observed in the case of NaF addition. **Fig.2.14(b**) represents the kinetics plot that follows the pseudo-first order kinetic law.**Fig.2.14(c-d)** shows the rate constant 1.54×10^{-2} min^{-1} and degradation efficiency 66(1) % in the presence of NaF, indicating the improved photocatalytic activity due to the presence of NaF during urea oxidation.

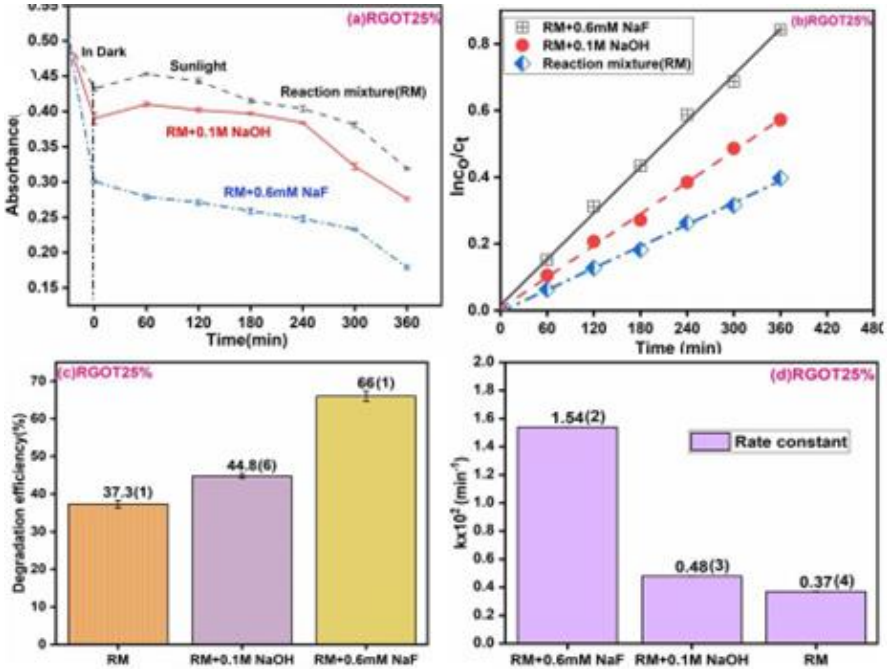

Fig 2.14: (a) Changes observed in absorbance vs time under solar light irradiation (b) pseudo-first-order kinetic fitting (c) Variation in photocatalytic urea oxidation efficiency (%) for RGOT25% photocatalyst and (d) changes in the pseudo-first-order rate constant under different reaction conditions (RM RM+0.1M NaOH, and RM+0.6mM NaF).

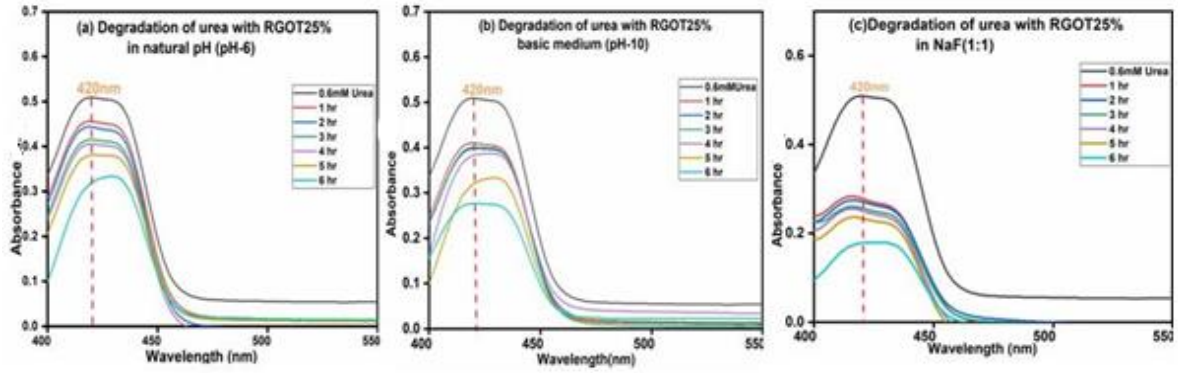

Fig.2.15. (a-c) Comparative changes observed in UV-visible absorption spectra of urea degradation with effect from RGOT25% nanocomposite in natural pH, basic pH, NaF (1:1).

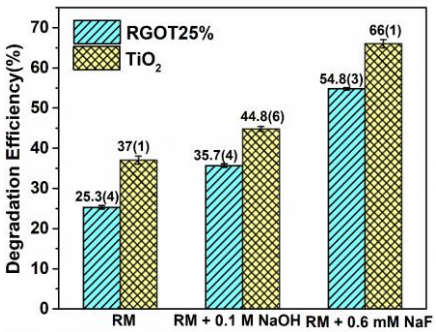

Fig 2.16. Comparison of degradation efficiencies for TiO_2 and for RGOT25% composite under different reaction conditions (RM RM+0.1M NaOH, and RM+0.6mM NaF).

The pH of the RM+0.6mM NaF reaction mixture remains nearly neutral (~6.5-7.6) throughout the reaction. The superior photocatalytic activity of the RGOT25% composite compared to bare TiO_2 **(Fig2.16)** can be attributed to a synergistic effect, increased interfacial surface area and the high electron mobility of RGO, which decreases the rate of recombination rate and thereby increases the charge transfer rate. NaF plays a dual role in enhancing photocatalytic activity. It not only removes protons from the reaction medium without causing deprotonation of ammonium ions thereby suppressing the probability of ammonia leaching. Moreover, it can also increase the binding of urea with the photocatalyst via multisite hydrogen bonding interactions**. (Scheme 2.1).**

To confirm the complete degradation of urea, the demineralization efficiencies of RGOT25% catalyst under different reaction conditions (RM, RM+0.1M NaOH, and RM+0.6mM) have been monitored **(Fig. 2.17, Table 1).** In most cases, the demineralization efficiency values are very close to the degradation efficiency. Such observation suggests the complete degradation of urea.

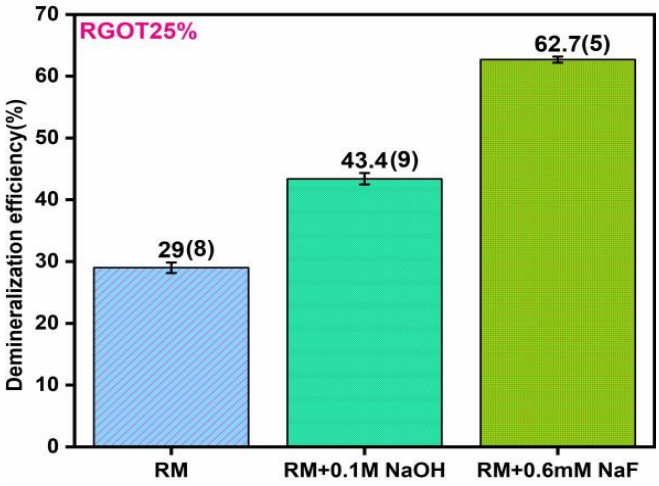

Fig 2.17: Variation in demineralization efficiency (%) for RGOT25% composite photocatalyst under different reaction conditions (RM RM+0.1M NaOH, and RM+0.6mM NaF).

Table1. TOC values and demineralization efficiency of RGOT25% photocatalyst under different reaction conditions (RM, RM+0.1M NaOH, and RM+0.6mM NaF).

Reaction Condition	Degradation efficiency (%)	Demineralization efficiency (%)
RM	37.3(1)	29.0(8)
RM+0.1M NaOH	44.8(6)	43.4(9)
RM+0.6mM NaF	66(1)	62.7(5)

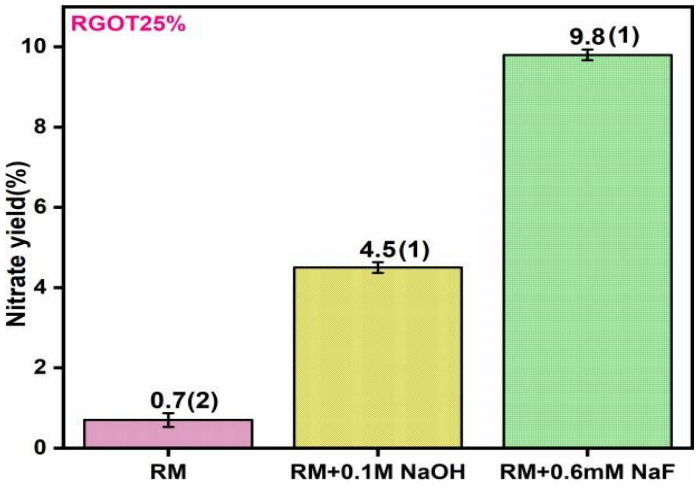

Fig 2.18: Variation in nitrate yield (%) for RGOT25% composite photocatalyst under different reaction conditions (RM RM+0.1M NaOH, and RM+0.6mM NaF).

To understand the extent of urea oxidation and nitrogen leaching, the nitrate yields were determined under different reaction conditions (RM, RM+0.1M NaOH. and RM+0.6mM NaF) in the presence of RGOT25% catalyst. After 6 hours of sunlight irradiation, there was practically no nitrate formation in the case of the reaction mixture under ambient conditions (0.7(2) %). Interestingly, the nitrate yield was higher in the presence of NaF (9.8(1) %) more than twice compared to the alkaline pH (4.5(1) %) **(Fig2.18, Table 2)**. Such observation confirms that due to the lesser basicity and hydrogen bonding ability of fluoride ions, the extent of ammonia leaching is significantly reduced.

2.5. Effect of TiO_2 loading

In order to understand the effect of TiO_2 loading on the catalytic activity, TiO_2 loading on RGO were varied from 10 to 25%. It has been observed that the catalytic activity in the presence of NaF increases upon increasing the TiO_2 loading **(Fig. 2.19)**. Such observation can be attributed to the enhancement in the number active sites due to an increase in TiO_2 loading.

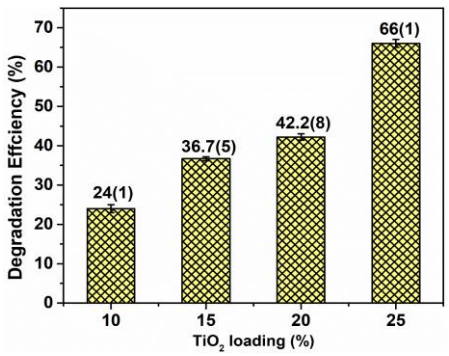

Fig.2.19. Changes in urea degradation efficiency with TiO_2 loading on RGO in presence of NaF.

2.6. Mechanistic Detailed study

The proposed reaction mechanism **(Scheme 2.2)** involves the electronic transition from the valence band of TiO_2 to its conduction band to afford e^-/h^+ pair. The transfer of an excited electron from the conduction band of TiO_2 to the RGO surface reduces the extent of electron-hole pair recombination. The electrons and holes undergo redox reactions with the water molecules and molecular oxygen, respectively, to generate hydroxyl radicals (·OH) and superoxide anions ($O_2^{\cdot -}$). These reactive oxygen species oxidize urea to cause urea degradation (49).

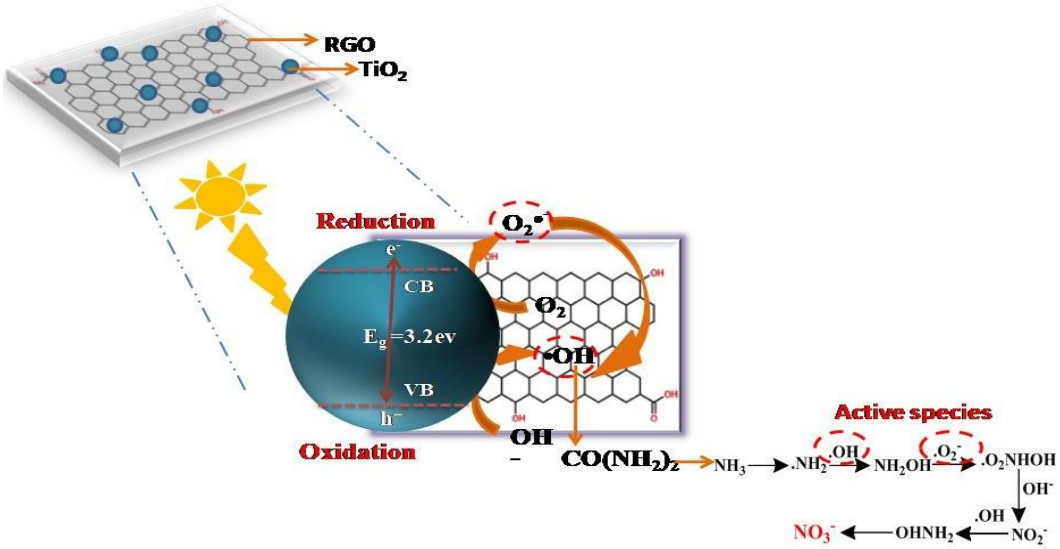

Scheme 2.2. Mechanistic approach for urea degradation by RGOT25% nanocomposite under sunlight.

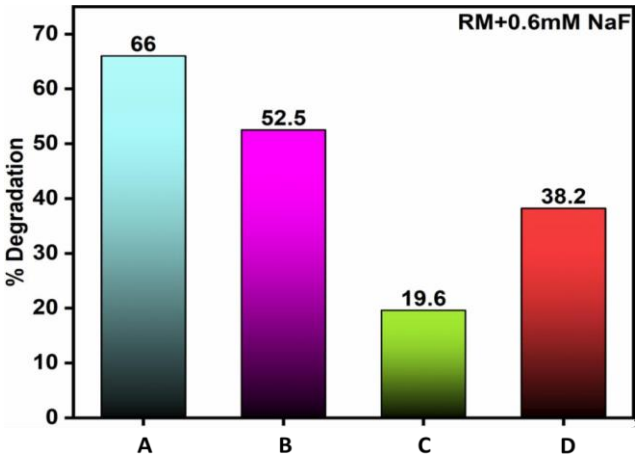

Fig.2.20 Changes in the photocatalytic urea oxidation efficiency of RGOT25% composite photocatalyst after 6 hours reaction time in the presence of NaF under different conditions (A) Original reaction mixture (B) Reaction mixture having 0.5mgNa_2EDTA (C)Reaction mixture containing 0.5ml iso-propanol(D) Reaction mixture upon purging of argon for 15 minutes

To determine the roles of the different reactive species, several control experiments were performed **(Fig. 2.20).** Addition of Na_2EDTA (0.5 mg) and iso-propanol (0.5 ml) to the reaction mixture reduces the urea degradation efficiency from 66% to 52.5% and 19.6% respectively. They act as efficient hole scavengers and suppress the formation of hydroxyl radicals resulting from the oxidation of water molecules by holes. Moreover, purging of Ar for 15 minutes decreases photocatalytic urea oxidation efficiency to 38.2%. This is because purging of Argon results removal of oxygen from the reaction mixture, thereby reducing the probability of superoxide radical formation. Such observation suggests that both hydroxide radicals and superoxide anions are responsible for photocatalytic oxidation reactions.

Table 2. Nitrate yields in presence of RGOT25% photocatalyst under different reaction conditions (RM, RM+0.1M NaOH, and RM+0.6mM NaF).

Catalyst	Nitrate yield (%)
RGOT25% (RM)	0.7(2)
RGOT25% (RM+0.1M NaOH)	4.5(1)
RGOT25% (RM+0.6mM NaF)	9.8(1)

To, the best of our knowledge there is only one report quantifying the nitrate yield in the photocatalytic urea oxidation process[48]. Despite of quite similar degradation efficiency (%) ration efficiency. maximum nitrate yield is reported to be around 0.37% (48) **(Table 3)** suggesting quite high amount of nitrogen loss during the urea oxidation process. This confirms our original assumption that the addition of NaF in the reaction mixture under neutral medium can enhance the nitrate production efficiency by manifold

Table 3. Nitrate yields in presence of RGOT25% photocatalyst under different reaction conditions (RM, RM+0.1M NaOH, and RM+0.6mM NaF).

Catalyst	Degradation Efficiency (%)	Nitrate yield (%)	Reference
N-doped TiO_2/polystyrene	70	0.37	(48)
RGOT25% (RM+0.6mM NaF)	66(1)	9.8(1)	This Work

References

1) F. J. Carmona, G Dal Sasso, G B Ramírez-Rodríguez, Y Pii, J . M . Delgado-López, A. Guagliardi. Urea-functionalized amorphous calcium phosphate nanofertilizers:

optimizing the synthetic strategy towards environmental sustainability and manufacturing costs. *Sci Rep*. **2021**; *11*, 1–14.

2) R. Pinton, N. Tomasi, L. Zanin. Molecular and physiological interactions of urea and nitrate uptake in plants. *Plant Signal Behav*. **2016**; *11*, 1-12.
3) G. Selvarajh, H. Y. Ch'Ng. Enhancing soil nitrogen availability and rice growth by using urea fertilizer amended with rice straw biochar. *Agronomy*. **2021**, *11*, 1–16.
4) N. Kottegoda, C. Sandaruwan, G. Priyadarshana, A. Siriwardhana, U. A. Rathnayake, D. M. Berugoda Arachchige. Urea-Hydroxyapatite Nanohybrids for Slow Release of Nitrogen. *ACS Nano*. **2017**, *11*, 1214–21.
5) J. Sun, W. Li, C. Li, W. Chang, S. Zhang, Y. Zeng. Effect of Different Rates of Nitrogen Fertilization on Crop Yield, Soil Properties and Leaf Physiological Attributes in Banana Under Subtropical Regions of China. *Front Plant Sci.* **2020**, *11*, 1–11.
6) Z. Ou Yang, X. Mei, F. Gao, Y. Li, J. Guo. Effect of Different Nitrogen Fertilizer Types and Application Measures on Temporal and Spatial Variation of Soil Nitrate-Nitrogen at Cucumber Field. *J Environ Prot (Irvine, Calif)*. **2013**, *04*, 129–35.
7) P. Jadon, R. Selladurai, S. S. Yadav, M. V. Coumar, M. L. Dotaniya, A. K. Singh. Volatilization and leaching losses of nitrogen from different coated urea fertilizers. *J Soil Sci Plant Nutr*. **2018**, *18*, 1036–47.
8) R. Hashimi, M. H. Hashimi. Effect of Losing Nitrogen Fertilizers on Living Organism and Ecosystem, and Prevention Approaches of their Harmful Effect. *Asian Soil Res J.* **2020**, *4*, 10–20.
9) K. Mahmud, D. Panday, A. Mergoum, A. Missaoui. Nitrogen losses and potential mitigation strategies for a sustainable agroecosystem. *Sustain*. **2021**, *13*, 1–23.
10) L. Ngatia, J. M. Grace III, D. Moriasi, R. Taylor. Nitrogen and Phosphorus Eutrophication in Marine Ecosystems. *Monit Mar Pollut*. **2019**, 1–17.
11) A. N. Laghari, Z. A. Siyal, M. A. Soomro, D. K. Bangwar, A. J. Khokhar, H. L. Soni. Quality Analysis of Urea Plant Wastewater and its Impact on Surface Water Bodies. *Eng Technol Appl Sci Res*. **2018**, *8*, 2699–703.
12) A. S. Dickerson, J. S. Lee, C. Keshava, A. Hotchkiss, A. S. Persad. Assessment of Health Effects of Exogenous Urea: Summary and Key Findings. *Curr Environ Heal reports.* **2018**, *5*, 205–12.
13) P. Mirzaei, S. Bastide, A. Dassy, R. Bensimon, J. Bourgon, A. Aghajani. Electrochemical oxidation of urea on nickel-rhodium nanoparticles/carbon composites. *Electrochim Acta*. **2019**, *297*, 715–24.

14) M. Cataldo Hernández, N. Russo, M. Panizza, P. Spinelli, D. Fino. Electrochemical oxidation of urea in aqueous solutions using a boron-doped thin-film diamond electrode. *Diam Relat Mater*. **2014**, *44*, 109–16.

15) S. Park, J. T. Lee, J. Kim. Photocatalytic oxidation of urea on TiO_2 in water and urine: mechanism, product distribution, and effect of surface platinization. *Environ Sci Pollut Res.* **2019,** *26*, 1044–53.

16) L. Madriz, M. Parra, F. S. García Einschlag, O. Núñez, F. M. Cabrerizo, R. Vargas. Photocatalytic Oxidation of Urea on Surface-Modified Bi_2WO_6 with trans-4-Stilbenecarboxaldehyde. *J Phys Chem C.* **2021**, *125*, 12682–9.

17) X. An, D. Stelter, T. Keyes, B. M. Reinhard. Plasmonic Photocatalysis of Urea Oxidation and Visible-Light Fuel Cells. *Chem*. **2019**, *5*, 2228–42.

18) X. Zhu, M. Burger, T. A. Doane, W. R. Horwath. Ammonia oxidation pathways and nitrifier denitrification are significant sources of N_2O and NO under low oxygen availability. *Proc Natl Acad Sci U S A*. **2013**, *110*, 6328–33.

19) A. Jawad. The Study of Commercial Titanium Dioxide (TiO_2) Degussa P25 for the Adsorption of Acidic Dye. *Sci Lett*. **2020**, *14*, 68–83.

20) M. Rejek, J. Grzechulska-Damszel, B. Schmidt. Synthesis, Characterization, and Evaluation of Degussa P25/Chitosan Composites for the Photocatalytic Removal of Sertraline and Acid Red 18 from Water. *J Polym Environ*. **2021**, *29*, 3660–7.

21) B. Boga, J. Székely, Z. Pap, L. Baia, M. Baia. Detailed Spectroscopic and Structural Analysis of TiO_2/WO_3 Composite Semiconductors. *J Spectrosc*. **2018**; *2018*, 1-7.

22) S. A. Khan, S. Ali, M. Sohail, M.A. Morsy, Z. H. Yamani. Fabrication of $TiO_2/Ag/Ag_2O$ Nanoparticles to Enhance the Photocatalytic Activity of Degussa P25 Titania. *Aust J Chem*. **2016**, *69*, 41–6.

23) P. Jadhav, E. S.S. Joshi, A. V. Shivapur, V.V. Karjinni. Study on Nano Material TiO_2 / P25 Degussa for the Characteristics of Dairy Wastewater. *IRJET*, **2020**, *7*, 963-967.

24) P. Ranjan, S. Agrawal, A. T. R. Sinha, Rao, J. Balakrishnan, Thakur . A Low-Cost Non-explosive Synthesis of Graphene Oxide for Scalable Applications. *Sci Rep*. **2018**, *8*, 1–13.

25) L. L. Tan, W. J. Ong, S. P. Chai, A. R. Moha. Reduced graphene oxide-TiO_2 nanocomposite as a promising visible-light-active photocatalyst for the conversion of carbon dioxide. *Nanoscale Res Lett*. **2013**, *8*, 1–9.

26) A. Dobermann, T . Fairhurst, Institute IRR. Rice: Nutrient Disorders & Nutrient Management. Potash \& Phosphate Institute, East \& Southeast Asia Programs; **2000**.

27) N. Zhang, M. Q. Yang, S. Liu, Y. Sun, Y. J. Xu. Waltzing with the Versatile Platform of Graphene to Synthesize Composite Photocatalysts. *Chem Rev*. **2015**, *115*, 10307–77.

28) F. Zhang, Y. H. Li, J. Y. Li, Z. R. Tang, Y. J. Xu. 3D graphene-based gel photocatalysts for environmental pollutants degradation. *Environ Pollut*. **2019**, *253*, 365–76.

29) M. Q. Yang, N. Zhang, M. Pagliaro, Y. J. Xu. Artificial photosynthesis over graphene–semiconductor composites. Are we getting better? *Chem Soc Rev*. **2014**, *43*, 8240–54.

30) Y. H. Li, Z. R. Tang, Y. J. Xu. Multifunctional graphene-based composite photocatalysts oriented by multifaced roles of graphene in photocatalysis. *Chinese J Catal*. **2022**, *43*, 708–30.

31) C. Han, Y. H. Li, M. Y. Qi, F. Zhang, Z. R. Tang, Y. J. Xu. Surface/Interface Engineering of Carbon-Based Materials for Constructing Multidimensional Functional Hybrids. *Sol RRL*. **2020**, *8*, 1-25.

32) N. I. Zaaba, K. L. Foo, U. Hashim, S. J. Tan, W. W. Liu, C. H. Voon. Synthesis of Graphene Oxide using Modified Hummers Method: Solvent Influence. *Procedia Eng*. **2017**, *184*, 469–77.

33) M. Sabzevari, D. Cree, L. Wilson. Preparation and Characterization of Graphene Oxide Cross-Linked Composites. *The Canadian Society for Mechanical Engineering International Congress*.**2018**,*2014*.

34) E. Andrijanto, S. Shoelarta, G. Subiyanto, S. Rifki. Facile synthesis of graphene from graphite using ascorbic acid as reducing agent. *AIP Conf Proc*. **2016**, *1725*, 1-4.

35) R. K. Nainani, P. Thakur. Facile synthesis of TiO_2-RGO composite with enhanced performance for the photocatalytic mineralization of organic pollutants. *Water Sci Technol*. **2016**, *73*, 1927–36.

36) J. D. Giraldo, B. L. Rivas. Determination of urea using p-N,N- dimethylaminobenzaldehyde: Solvent effect and interference of chitosan. *J Chil Chem Soc*. **2017**, *62*, 3538–42.

37) V. Vinesh, A. R. M. Shaheer, B. Neppolian. Reduced graphene oxide (RGO) supported electron deficient B-doped TiO_2 (Au/B-TiO_2/RGO) nanocomposite: An efficient visible light sonophotocatalyst for the degradation of Tetracycline (TC). *Ultrason Sonochem*. **2019**, *50*, 302–10.

38) H. V. Bao, N. M. Dat, N. T. H. Giang, B. Thinh D, L. T. Tai, D. N. Trinh. Behavior of ZnO-doped TiO_2/RGO nanocomposite for water treatment enhancement. *Surfaces and Interfaces*. **2021**, *23*, 1-9.

39) F. W. Low, C. W. Lai. Reduced Graphene Oxide Decorated Tio_2 for Improving Dye-Sensitized Solar Cells (DSSCs). *Curr Nanosci*. **2018**, 15, 631–6.

40) W. Wang, Z. Wang, J. Liu, Z. Luo, S. L. Suib, P. He. Single-step one-pot synthesis of TiO_2 nanosheets doped with sulfur on reduced graphene oxide with enhanced photocatalytic activity. *Sci Rep*. **2017,** *7*, 1–9.

41) L. Kuang, W. Zhang. Enhanced hydrogen production by carbon-doped TiO_2 decorated with reduced graphene oxide (RGO) under visible light irradiation. RSC Adv. **2016**, *6*, 1-25.

42) A. T. Habte, D. W. Ayele. Synthesis and Characterization of Reduced Graphene Oxide (RGO) Started from Graphene Oxide (GO) Using the Tour Method with Different Parameters. *Adv Mater Sci Eng*. **2019**, *2019*, 1-9.

43) I. O. Faniyi, O. Fasakin, B. Olofinjana, A. S. Adekunle, T. V. Oluwasusi, M. A. Eleruja. The comparative analyses of reduced graphene oxide (RGO) prepared via green, mild and chemical approaches. *SN Appl Sci*. **2019**, *1*, 1181.

44) N. Sharma, V. Sharma, Y. Jain, M. Kumari, R. Gupta, S. K. Sharma. Synthesis and Characterization of Graphene Oxide (GO) and Reduced Graphene Oxide (RGO) for Gas Sensing Application. *Macromol Symp*. **2017,** *376*, 1-5.

45) H. Zhang, X. Wang, N. Li, J. Xia, Q. Meng, J. Ding. Synthesis and characterization of TiO_2/graphene oxide nanocomposites for photoreduction of heavy metal ions in reverse osmosis concentrate. *RSC Adv*. **2018**, *8*, 34241–51.

46) G. T. S. How, A. Pandikumar, H. N. Ming, L. H. Ngee. Highly exposed {001} facets of titanium dioxide modified with reduced graphene oxide for dopamine sensing. *Sci* Rep. **2014**, *4*, 2–9.

47) X. Yan, Y. Li, F. Du, K. Zhu, Y. Zhang, A. Su. Synthesis and optimizable electrochemical performance of reduced graphene oxide wrapped mesoporous TiO_2 microspheres. *Nanoscale*. 2014, *6*, 4108–16.

48) V. Vaiano, O. Sacco, G. Di Capua, N. Femia, D. Sannino. Use of visible light modulation techniques in urea photocatalytic degradation. *Water*. **2019**, *11*, 1642.

49) J. Mahajan and P. Jeevanandam, Novel thermal decomposition approach for the synthesis of TiO_2@Ag core-shell nanocomposites and their application for catalytic reduction of 4-nitrophenol, *J Nanoparticle Res*. **2019**, *21*, 1-17

CHAPTER-3

Influence of β-CD and Ag deposition over TiO_2 towards photo-catalytic oxidation of urea under solar irradiation

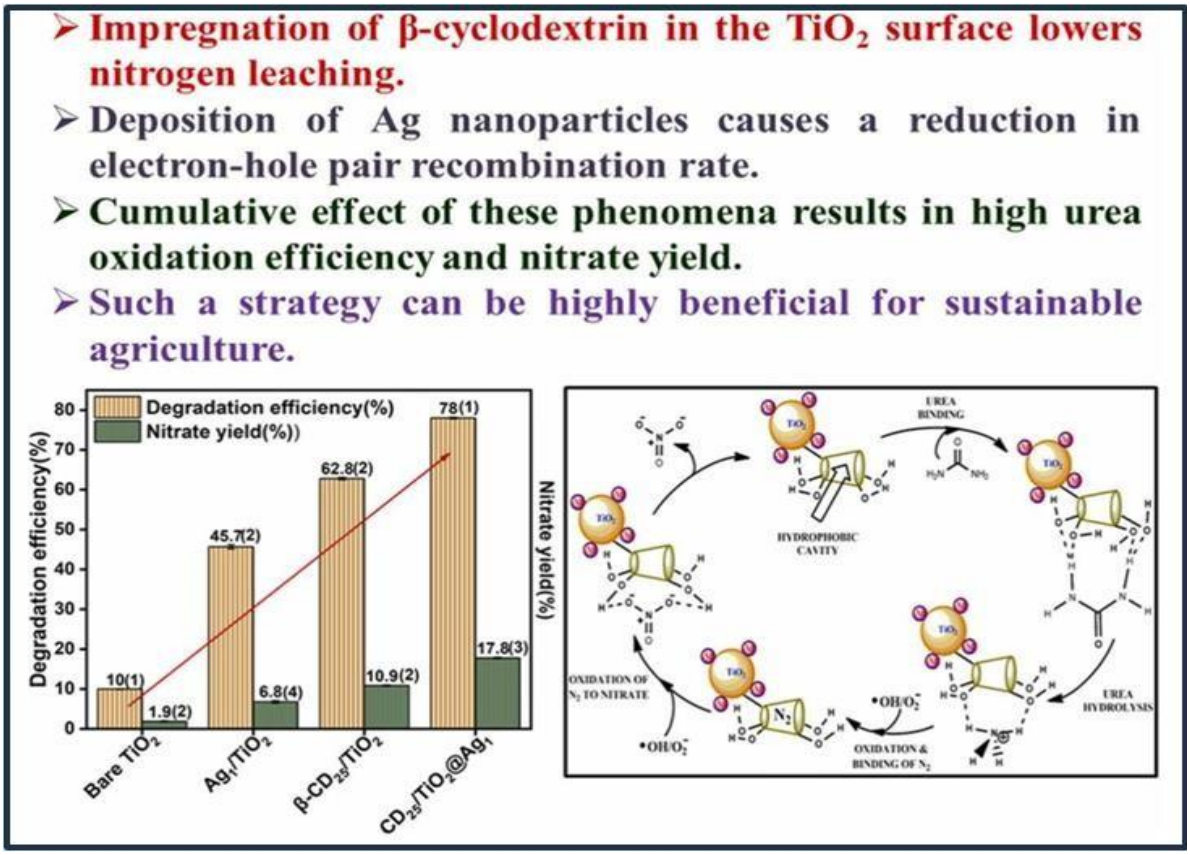

Schematic outline

This study investigates the photocatalytic performance of binary and ternary nanocomposites synthesized with varying weight percentages for urea oxidation under sunlight irradiation. Among the tested composites, β-CD_{25}/TiO_2@Ag_1 (CT3A1) exhibited the highest activity. This enhanced performance is attributed to the synergistic effects of its key components: the high catalytic activity and photostability of TiO_2, the efficient urea and nitrogen binding properties of β-cyclodextrin, and the localized surface plasmon resonance (LSPR) properties of Ag, which enhance charge transfer efficiency. These combined effects result in superior photocatalytic degradation and an increased nitrate yield.

3.1 Introduction

The traditional method of improving the soil's fertility with natural and chemical-based fertilizers such as urea, calcium ammonium nitrate, anhydrous ammonia, etc., is beneficial for escalating agricultural growth (1,2). Urea is an abundantly used fertilizer because it is inexpensive, has a 46% nitrogen content, is easily transported, and is the simplest assimilated form of nitrogen directly involved in the mineralization process(3]). The plants assimilate NO_3^- and NH_4^+ ions instead of urea nitrogen directly. So, urea undergoes hydrolysis to form NH_3 and further protonation results in the formation of NH_4^+ ions (4,5). During nitrification, these NH_4^+ ions undergo oxidation to form NO_3^- ions and simultaneously release protons(6]). During NO_3^- assimilation, OH^- ions liberate, neutralizing the excess protons released during nitrification and making the entire process viable[(7). However, the primary issue related to it is that half of the urea supplied to the soil gets released into nature due to N_2 emissions, NO_3^- leaching, and NH_3 loss brought up by temperature change, soil pH, and soil management practices(8]). As a result, urea is often over-applied to enhance crop production. The presence of unreacted drastically deteriorates soil and groundwater quality, causing various environmental hazards[(9–12).

Moreover, this nitrogen loss directly or indirectly disturbs human life and the ecosystem(13) It is necessary to enhance the production of NO_3^- on urea oxidation, which is desirable in agronomics(14). The existing methodologies involve the modification of fertilizers with urease and nitrogenase inhibitors to control nitrogen loss(15,16). However, the high cost and low stability of these inhibitors under ambient conditions limit their practical applications. As a result, photocatalysis is emerging as a new methodology to increase the NO_3^- efficiency from urea oxidation(17). Photocatalytic urea oxidation involves hydrolysis of urea to ammonium ion (equation 1) followed by oxidation of ammonium ion to afford nitrate (equation 2). The second step involves an 8-electron transfer process. Therefore, it is quite kinetically sluggish. Often, it affords the formation of molecular nitrogen (N_2) as the major product due to incomplete oxidation. The high stability and chemical inertness of N_2 prevent the subsequent oxidation to afford nitrate. Hence, the fabrication of an efficient photocatalyst with a strong oxidizing ability, as well as having a substantial affinity towards N_2, is needed to avoid its leaching and escalate the overall NO_3^- efficiency. Such methodology is highly desirable as it will enhance crop production and reduce the ecotoxic effect of unreacted urea.

$$CO(NH_2)_2 + H_2O + 4H^+ \longrightarrow CO_2 + 2NH_4^+ \quad \text{(1)}$$

$$NH_4^+ + 3H_2O - 8e^- \longrightarrow NO_3^- + 10H^+ \quad \text{(2)}$$

Among all the semiconductors, P25-TiO_2 has distinctive properties like powerful oxidizing ability (•OH. O_2^-), photostable in nature, cheap, structurally stable as well as, environment-friendly(18). However, limited light response towards visible light due to a large band gap (Eg~3.12 eV) and rapid recombination of the photogenerated e-/h+ hinder its application towards urea oxidation(19,20). Therefore, fabricating efficient broad-spectrum sunlight-active and highly adsorbent material is fundamental for enhancing its photoactivity.

Comprehensively, it is considered that the overall photocatalytic activity can further be enriched by doping plasmonic metals like Ag, Au, Cu, etc., on the semiconductor-based binary composites(21). Remarkably, these coinage metals persuade concurrent oscillations of conduction electrons with a resonant frequency called the localized surface plasmon resonance (LSPR) effect, which induces a noteworthy enhancement in the absorption of visible light(22–24). The LSPR transitions permit these nanoparticles to absorb the solar energy to produce a strong electromagnetic field and high-energy electron hole-pairs, which can disperse through the lattice vibrational modes of the nanoparticles to afford high lattice temperature(25–29). The electromagnetic field, hot charge carriers, and high temperature can enhance the efficiency of the photocatalytic reactions quite significantly(30,31). Notably, Ag offers a strong LSPR effect and high electric conductivity, so metallic silver has been identified as a better plasmonic metal for designing this photocatalyst(32,33)

β-cyclodextrin (β-CD) is a novel supramolecular functional system designed by joining seven glucose units (34). Embracing to its engrossing features and structure like innocuous, hole scavenger, stabilizer, cyclic oligosaccharide, a hollow-truncated cone-like structure having hydrophobic inner cavity can encapsulate the nonpolar guests, and hydrophilic outer part accommodates –OH functional groups that can exhibit hydrogen bonding, used widely in biological and photocatalytic applications. Due to its unique structure, β-CD incorporated composite offers various interactions, and adsorbing sites and allows the composite to suppress the charge carrier recombination rate and extend its light absorbance(35–37). β-CD can bind with urea via noncovalent interactions(38) as well as with molecular N_2 quite efficiently through the hydrophobic effect (39–41). Such a dual effect will result in stronger interaction of the catalyst with the reactants as well as a reduction in nitrogen leaching that can lead to higher nitrate yield. β-CD can act as a capping agent to stabilize metal NPs and prevent aggregation on its surface.

To date, there are few reports demonstrating the photocatalytic oxidation of urea to yield nitrate(42,43). Among these, the TiO_2/RGO composite shows the highest nitrate yield

of 9.8(1) % in the presence of NaF under neutral pH(42). Although, the addition of fluoride can lead to the degradation of soil as well as groundwater pollution which is not desirable for sustainable agriculture(44). As a result, it is essential to design an alternative photocatalyst that can promote urea oxidation in the absence of any additive. To this regard, the binary and ternary NCs with different mass ratios of β-CD (15-25wt%) and metallic Ag(1-3wt%) were fabricated by a hydrothermal and photo-deposition method, respectively. This ingenious ternary nanocomposite with immense potential offers better charge separation, plenty of surface-active sites, an enhancement of optical response towards the visible range, and integrated charge transfer between all the components for oxidation of urea to nitrate due to complementary physicochemical properties of each individual constituent (TiO_2, Ag and β-CD). As a result, the ternary composites, i.e.β-CD/TiO_2@Ag, can be promising for various applications like photocatalytic oxidation of urea(17,42,43).

3.2. Experimental section

3.2.1. Chemicals and reagents

Titanium dioxide nano powder (P25-TiO_2; [70% anatase + 30% rutile form]; avg. particle size 35nm) was supplied by Evonik, Degussa Corporation, Germany (photocatalyst). β-cyclodextrin (β-CD; 98.00%)) was purchased from GLR innovations. Silver nitrate ($AgNO_3$; ≥ 99%) was procured from Sigma Aldrich. Isopropanol (IPA; C_3H_8O; 99.5%), ethanol (C_2H_5OH; 99.9%), and urea ($CO(NH_2)_2$, 99% extra pure) were procured from Loba Chemie Pvt. Ltd., India. Deionized water (DI) was obtained from Organo Biotech Laboratories Pvt. Ltd., which was employed during all the experimental studies. All the chemicals were of analytical grade and used without any further purification

3.2.2. Preparation of β-CD/TiO_2 binary composite

β-CD/TiO_2 was synthesized using the hydrothermal method **(Scheme 3.1).** In a beaker, the solution was prepared by dissolving β-CD (0.25 g) and P25-TiO_2 (1 g) in a water-ethanol (2:1 v/v) mixture and kept under an ultrasonication bath for an hour. This dispersion was magnetically stirred for 4 hours, poured the solution to a Teflon-lined autoclave, and kept in a muffle furnace at 160 °C for 14 hours. After the natural cooling process, the precipitates were collected, centrifuged, washed, and dried at 50 °C for 6 hours to obtain a light brown colored powder. The different wt.% β-CD (15, 20,25) loaded P25-TiO_2 are denoted as β-CD_{15}/TiO_2 (**CT1**), β-CD_{20}/TiO_2 (**CT2**) and, β-CD_{25}/TiO_2 (**CT3**) respectively throughout this manuscript.

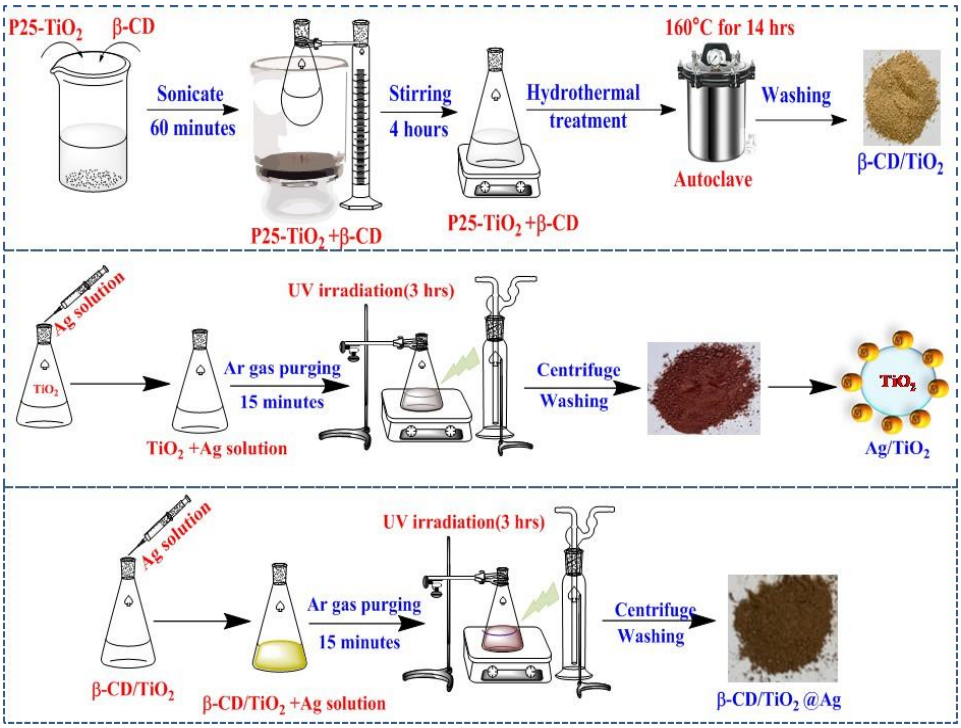

Scheme 3.1 Illustrative representation of the preparation of β-CD/TiO_2, Ag/TiO_2 (binary), and β-CD/TiO_2@Ag ternary nanocomposites.

3.2.3. Preparation of Ag/TiO_2 nanocomposite

Ag-loaded TiO_2 was synthesized by the photo-deposition method(45) **(Scheme 3.1).** In a test tube, 100mg of P25-TiO_2 was taken along with 10 ml of 50% IPA and 934 µl of Ag solution for 1wt% photo deposition. The as-prepared solution was purged with argon gas for 15-20 minutes and irradiated under a UV lamp (125 W Hg arc, 10.4 MW/cm^2, 300-390 nm) with constant stirring for 2 hours. The collected suspension was centrifuged, washed, and dried at 55 °C to afford 1wt% Ag/TiO_2, denoted as **TA1** throughout this manuscript.

3.2.4. Preparation of β-CD_{25}/TiO_2@Ag ternary nanocomposite

The hydrothermal treatment and photo deposition methods were used to fabricate β-CD_{25}/TiO_2@Agternary nanocomposites **(Scheme 3.1).** The preparation of β-CD_{25}/TiO_2 was discussed above in section 3.2.2, and the loading of Ag over β-CD_{25}/TiO_2nanocomposite was also done as Ag/TiO_2 (section 3.2.9). Different wt.% of Ag (1, 2, and 3) loaded β-CD_{25}/TiO_2 NC will be abbreviated as β-CD_{25}/TiO_2@Ag_1 (**CT3A1**). β-CD_{25}/TiO_2@Ag_2 (**CT3A2**), β-CD_{25}/TiO_2@Ag_3 (**CT3A3**) respectively.

3.2.5 Characterization and photocatalytic activity

The characterizations of as prepared photocatalysts by different techniques have already been described on Chapter-1 and Chapter-2.

Urea was chosen as a model molecule to examine the photocatalytic performance of the as-prepared various binary and ternary nanocomposites. The photocatalytic degradation experiments were conducted in separate test tubes carrying 10 mg of catalysts in 10 ml of (1.8 mM) urea solution. These photocatalytic experiments were performed under solar light in Patiala, India (1st-30th September, 2022; 11:00 am-3:00 pm) with average sun radiations of ~785 W/m^2 and ~35 °C temperature. Before the solar irradiations, prepared suspensions were stirred for 30 minutes in the dark to maintain adsorption-desorption equilibrium. Thereafter, the test tubes were irradiated with solar light for 180 minutes to conduct degradation studies. Further, the concentration of urea was determined using a p-Dimethylaminobenzaldehyde (DMAB) assay (46,47). The nitrate (NO_3^-) yield was determined through the ultraviolet spectrophotometer screening method (VARIAN-UV0910M156).

3.3 Results and discussion

To monitor the optical properties, the diffuse reflectance spectra (DRS) were recorded for the as-prepared β-CD loaded binary, Ag_1/TiO_2 (**TA1**), and Ag-loaded ternary nanocomposites **(Fig. .3.1).** The peaks observed at wavelength 329 nm were responsible for the charge trans- fer process from VB of O^{2-}(2p) to the CB of Ti^{3+} (3d). Bare TiO_2 shows an absorption peak at 329 nm in the UV region with no visible light response **(Fig. 3.1(a))**. Noteworthy, the loading of β-CD exhibits broadband at 400-500 nm usually ascribed to ligand to metal charge transfer (LMCT) from β-CD to Ti^{IV} (49,50])and shifts the absorption spectra towards visible region **(Fig.3.1(a)).**

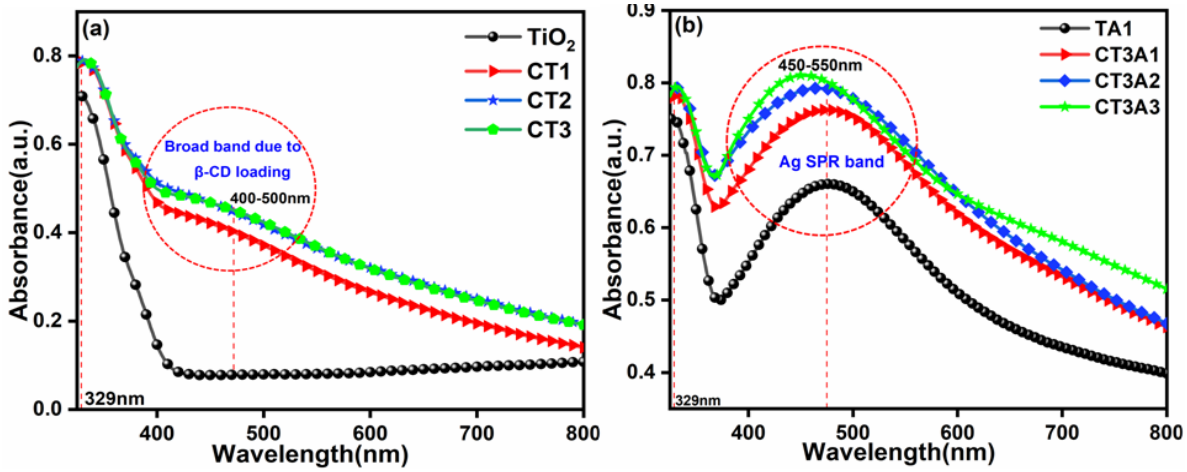

Fig. 3.1. DRS spectra of (a) TiO_2 and different wt.% (15, 20, 25) β-CD loaded TiO_2: **β-CD_{15}/TiO_2 (CT1), β-CD_{20}/TiO_2 (CT2) and, β-CD_{25}/TiO_2 (CT3) (b)** Ag_1/TiO_2 **(AT1)** and different wt.% (1, 2, 3) Ag loaded β-CD/TiO_2 ternary nanocomposites: **β-CD_{25}/TiO_2@Ag_1 (CT3A1). β-CD_{25}/TiO_2@Ag_2 (CT3A2), β-CD_{25}/TiO_2@Ag_3 (CT3A3).**

A new strong plasmonic band at 400-500 nm was observed in Ag loaded TiO_2 and ternary NCs i.e., accredited to the clear red shift in the visible region deriving from the LSPR effect of Ag nanoparticles and conceptually –OH groups of β-CD and TiO_2 form covalent bond suppresses the charge carrier separation. It shifts the adsorption edge towards visible light(51)**(Fig. 1b)**. Further intensification of plasmonic bands was noticed as the Ag wt.% increased from 1wt% to 3wt%. It concludes that plasmonic bands with higher intensities are proportional to the extent of silver loading resulting in higher optical response.

The optical band gap values of the synthesized nanocomposites were calculated from the UV-DRS plot by using the Tauc equation (equation 5):

$$\boldsymbol{\alpha h\nu = A(h\nu - E_g)^n} \qquad (\mathbf{5})$$

Herein, α=adsorption coefficient, h=Planck's constant, ν=frequency of the light, Eg=Band gap value of the sample, n=exponential coefficient (n=2 (indirect band gap). The optical band gaps were calculated by plotting a graph between √αhν v/s hν **(Fig. 3.2**)(52) The band gap (Eg) of bare TiO_2, **CT1**, **CT2**, and **CT3** were found to be 3.31, 3.09, 3.07, and 3.05 eV respectively **(Fig. 3.2(a))**. It is evident that the band gap values decrease from 3.31 to 3.05 eV upon loading of β-CD onto the surface of TiO_2 **(Fig. 3.2(a))** but the differences in band gaps of various β-CD loaded composites are not much significant. As a result, the extent of β-CD loading was not increased further. The loading of the Ag leads to even further decrease in the band gaps **(Fig. 2(b)).** Among all the materials the ternary composite **CT3A1** possess the lowest bang gap of 2.56 eV. Such observation confirms that the loading of Ag shifts the optical response towards the visible region.

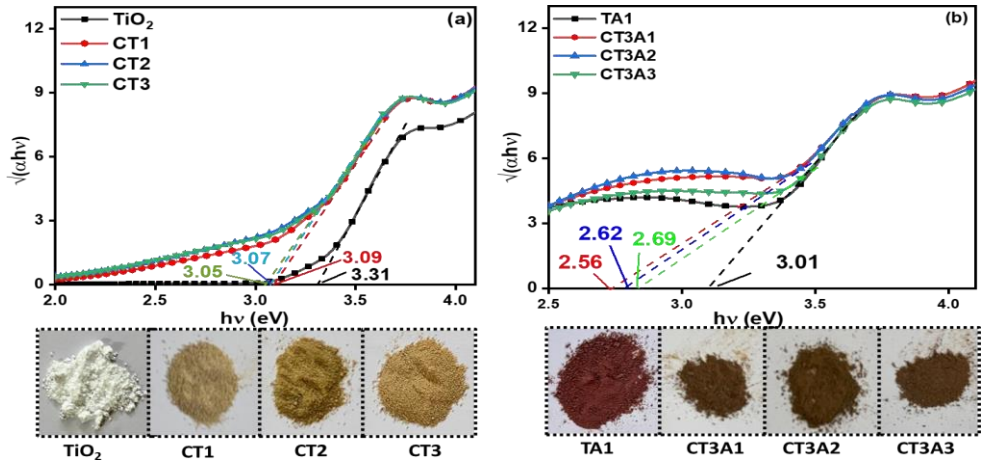

Fig. 3.2. Tauc plots (corresponding band gap values) of (a) TiO_2 and different wt.% (15, 20, 25) β-CD loaded TiO_2: **CT1, CT2** and, **CT3** (b) **AT1** and different wt.% (1, 2, 3) Ag loaded β-CD/TiO_2 ternary nanocomposites: CT3A1, CT3A2 **and** CT3A3.

Photoluminescence (PL) studies of the prepared dispersion at 340nm excitation wavelength were carried out to understand the effect of β-CD and Ag loading on the electron-hole pair recombination process. PL spectra of binary and ternary NCs shown in **(Fig. 3.3)** indicate the quenching of emission bands at 382, 433, and 536 nm. The quenching of emission bands at- tributed to suppression in charge carrier recombination. The broad emission bands could result from surface and intrinsic defects such as surface traps (hydroxyl defects, oxygen vacancies) and surface states of β-CD and Ag(53). Such observation suggests that the rate of electron-hole pair recombination decreases in the order of **CT3**> **CT2**>**CT1**>Bare TiO_2 in binary composites and **CT3A1**>**CT3A2**>**CT3A3**>**TA1** in ternary composites. Higher quenching of PL peaks happens on loading of Ag signifies the depletion in recombination rate and higher charge carrier separation.

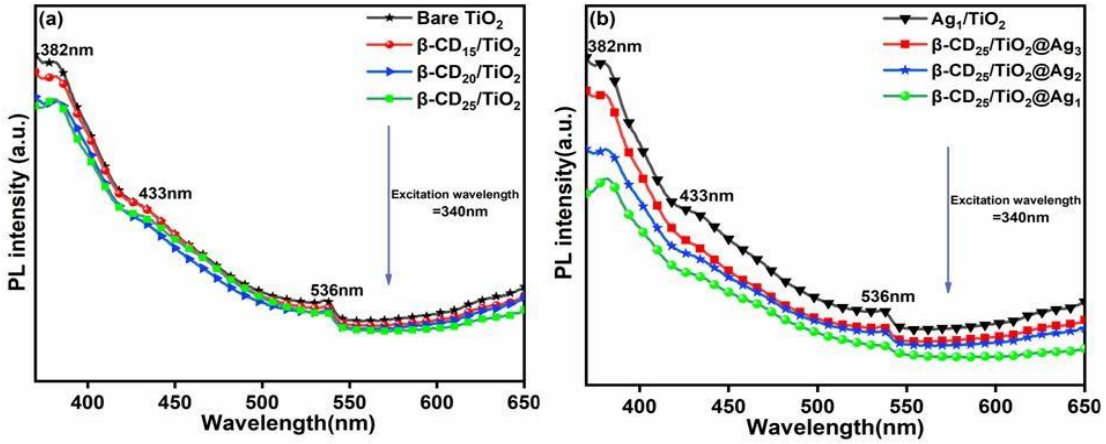

Fig.3.3. PL spectra of (a) TiO_2 and different wt.% (15, 20, 25) β-CD loaded TiO_2: β-CD_{15}/TiO_2 **(CT1)**, β-CD_{20}/TiO_2 **(CT2)** and, β-CD_{25}/TiO_2 **(CT3)** (b) Ag_1/TiO_2 **(AT1)** and different wt.% (1, 2, 3) Ag loaded β-CD/TiO_2 ternary nanocomposites: **β-CD_{25}/TiO_2@Ag_1** (CT3A1)**, β-CD_{25}/TiO_2@Ag_2** (CT3A2) **and β-CD_{25}/TiO_2@Ag_3** (CT3A3).

In **Fig. 3.4**, X-Ray diffraction (XRD) patterns were recorded to study the crystal planes of as-prepared NCs All the patterns exhibited several diffraction peaks of both the phases of bare TiO_2 at 2θ=25.5, 37.8, 48.2, 53.9, 55.3, 68.8, 70.3, 75.2, and 82.9º can be indexed as (101), (004), (200), (105), (211), (115), (220), (215), (301) lattice planes of anatase phase(ICDD card-21-1272)(54) Whereas the other prominent peaks at 2θ=27.4, 36.3, and 62.9º can be attributed to the (110), (103), (204) lattice planes of rutile phase (ICDD card-21-1276)[54]. The XRD pattern of the **CT3** sample was similar to its bare analog **(Fig. 3.4(b))**. Such observation is consistent with the fact that carbon and oxygen possess a smaller x-ray scattering coefficient than Ti and Ag. Furthermore, the **TA1** and the other three ternary plasmonic NCs have identical diffraction patterns with three additional peaks at 2θ=38.1º, 44.2º,

64º correspond to the (111), (200), (220) lattice planes with metallic Ag having face-centered cubic symmetry(54,55). The loading of β-CD and metallic Ag does not cause any change in the peak positions of the signals due to pristine TiO_2 suggesting that there is no change in its structure and crystallinity.

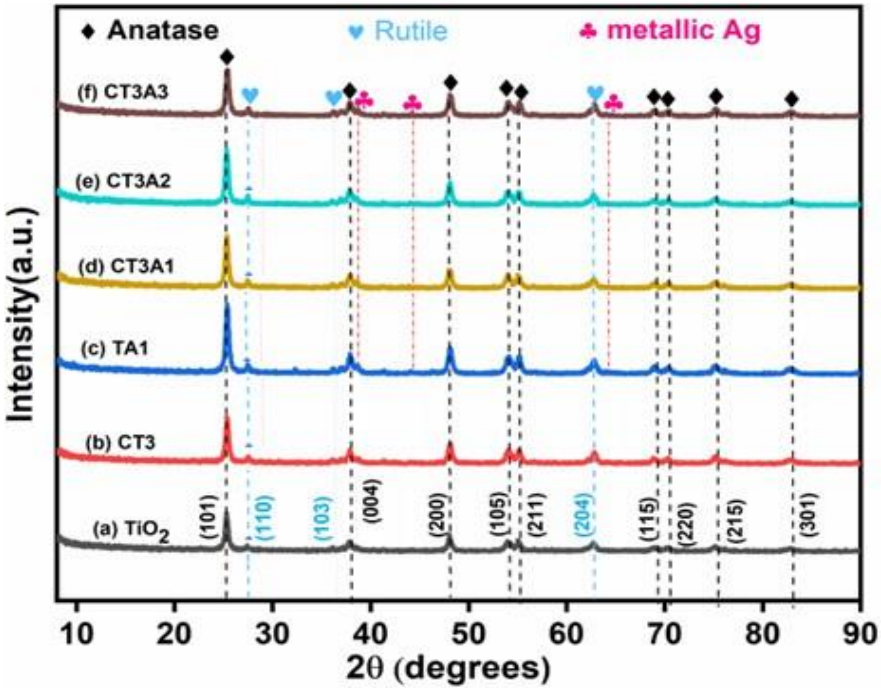

Fig. 3.4. XRD diffractogram of **(a) TiO_2, (b) β-CD_{25}/TiO_2** (CT3)**, (c) Ag_1/TiO_2 (**AT1**) and(d)** different wt.% (1, 2, 3%) Ag loaded **β-CD_{25}/TiO_2** ternary nanocomposites:**β-CD_{25}/TiO_2@Ag_1** (CT3A1). **β-CD_{25}/TiO_2@Ag_2** (CT3A2), **β-CD_{25}/TiO_2@Ag_3** (CT3A3)**.**

FT-IR spectra of nanocomposites are shown in **Fig. 3.5**. All the samples exhibited peaks at 3270-3381 cm^{-1} and 1644 cm^{-1} due to –OH stretching and bending vibrations of C-OH groups. Fig. 3.5(c) shows the spectra of only β-CD exhibiting O–H stretching (3279 cm^{-1}), C-H stretching (2922 cm-^{1}), H–O–H bending (1632 cm^{-1}), C–H bending (1420 cm^{-1}), C–O, C–C stretching (1014 cm^{-1}) vibrations. The absorption signals of O–H stretching vibrations of β-CD incorporated binary and ternary composites (3323 cm^{-1} and 3345 cm^{-1}) are shifted towards higher energy as the binding of TiO_2 results enhances the structural rigidity of β-CD thereby increasing the vibrational frequencies. The broad peak at 536 cm^{-1} and 527 cm^{-1} was the absorption signal of TiO_2 corresponding to the Ti–O–Ti vibrations (56). The shifting of this peak **(Fig. 3.5)** from 536 cm^{-1} and 527 cm^{-1} is probably due to the Ag loading. The absorption signal centered at 1159.1 cm^{-1} and 1031.4 cm^{-1} ascribed to the O–C–O and C–O stretching vibrations of β-CD, and the intensity of peaks gets more intense with the increasing amount of β-CD loading as shown in **(Fig. 3.5(a))**(57) these β-CD peaks disappeared in ternary composites **(Fig. 3.5(b))**, and a new absorption signal appeared at 1395 cm^{-1} due to

the oxidation of β-CD by TiO_2. This absorption peak was related to the –CCH, – OCH, and – COH groups, confirming the presence of β-CD in the ternary composites.

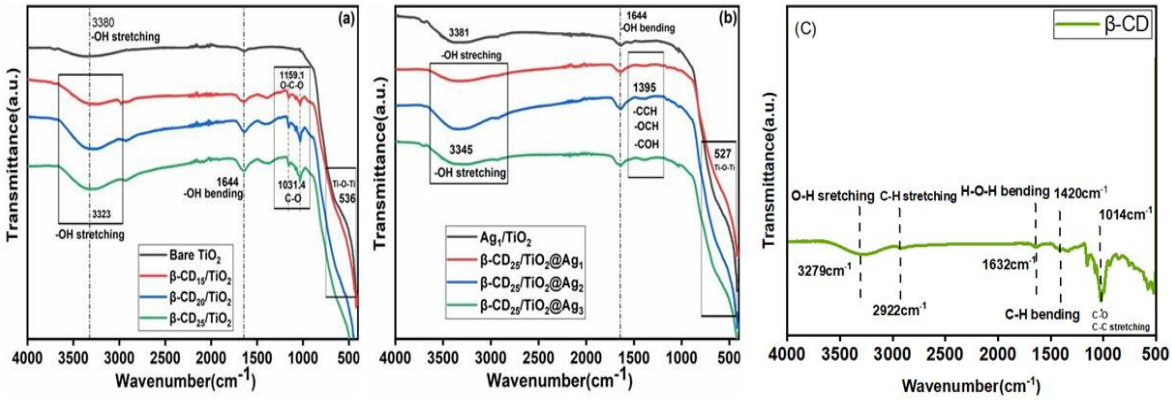

Fig. 3.5. Fourier transform infrared spectra**(a) TiO_2, β-CD_{25}/TiO_2** (CT3)**, Ag_1/TiO_2 (**AT1**) and** different wt.% (1, 2, 3%) Ag loaded **β-CD_{25}/TiO_2** ternary nanocomposites (b) **β-CD_{25}/TiO_2@Ag_1** (CT3A1). **β-CD_{25}/TiO_2@Ag_2** (CT3A2), **β-CD_{25}/TiO_2@Ag_3** (CT3A3) and (c) **β-CD only.**

SEM images in **Fig.3.6 (a,b)** show agglomerated clustered spherical assembly(58), and **Fig.3.6(c/d)** depict the Ag nanoparticles (black spots) that were uniformly attached to the surface of TiO_2.The formation of a white shell around the spherical structure could be due to β-CD which is further confirmed by the HRTEM images.

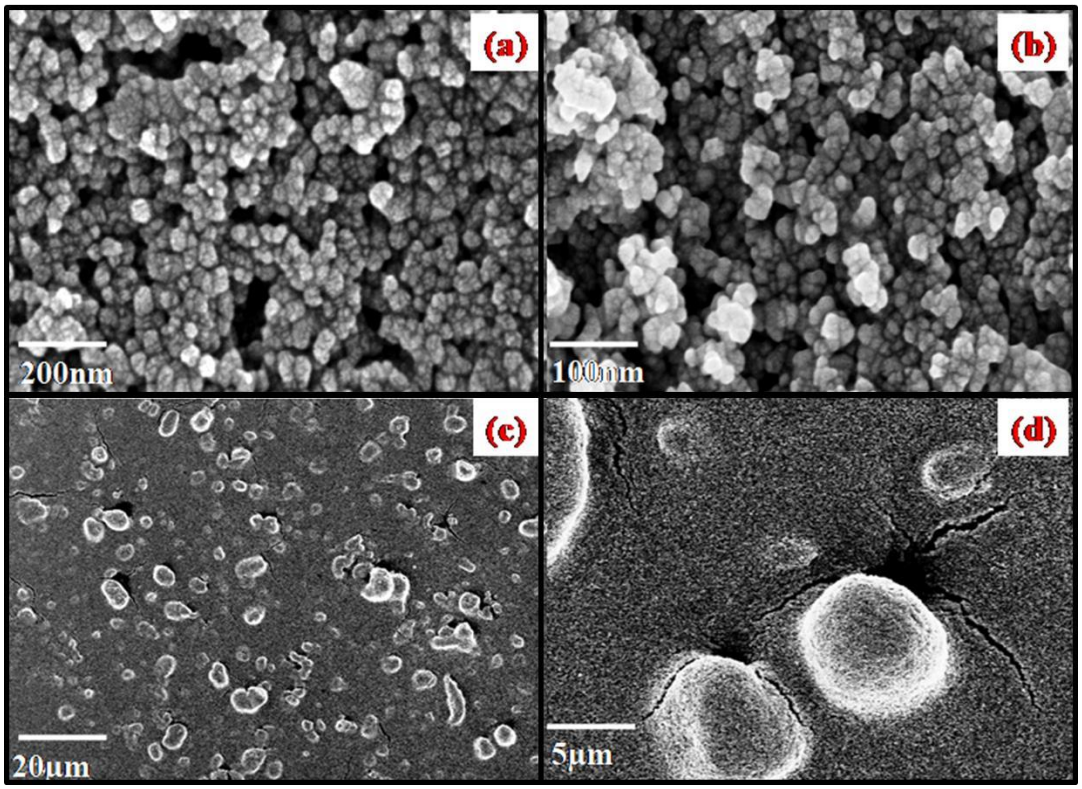

Fig. 3.6. FESEM images (a-d) of β-CD_{25}/TiO_2@Ag_1 (CT3A1) nanocomposite.

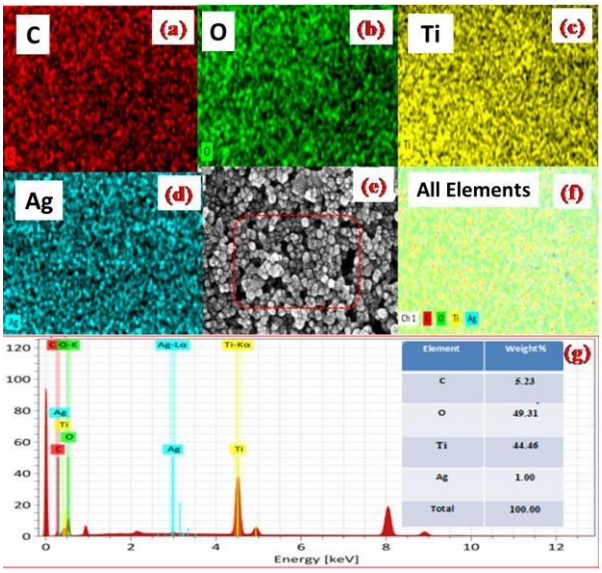

Fig. 3.7. Elemental analysis (a-f) of different elements (C, O, Ti, Ag) shown in different color distributions and EDX Spectra (g) of ternary NC β-CD_{25}/TiO_2@Ag_1 (CT3A1).

The elemental analysis in **Fig. 3.7(a-f)** and EDX spectra **(Fig. 3.7(g))** depicts the presence of C(red), O(green), Ti(yellow), and Ag(blue) elements, respectively. The EDX profiles in **Fig. 3.7(a-f)** support the presence and homogeneous distribution of C, O, Ti, and Ag in the nano-composite

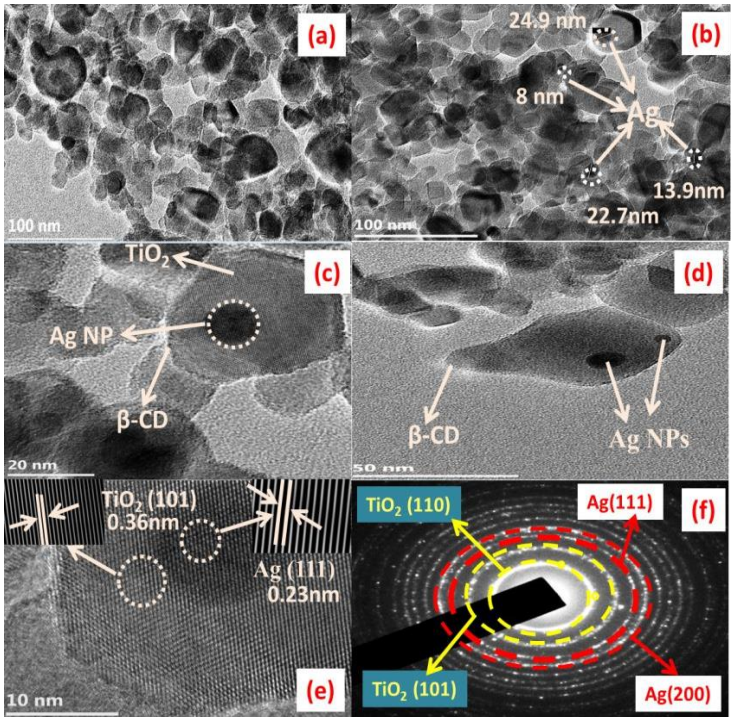

Fig. 3.8. HRTEM images (a-d), corresponding lattice fringes(e) and (f) SAED pattern for β-CD_{25}/TiO_2@Ag_1 (CT3A1) ternary NC.

Fig. 3.8 presents HRTEM images to examine further the morphology and the

synergistic interaction between β-CD, TiO_2, and Ag in the ternary nanocomposite. **Fig. 3.8(a, b)** re- veals the spherical, clustered, and agglomerated-like morphology where metallic Ag NPs of size range 5-25 nm are firmly attached with the TiO_2 particles that appeared as black spots that are consistent with the FESEM results. **Fig. 3.8(c, d)** indicates the core-shell type struc- ture where the white shell around the TiO_2 particles depicts the β-CD, grey colored particle designates the TiO_2, and the red-colored outlined black spot of metallic Ag NP(59).

β-CD is composed of a hydrophilic exterior with –OH groups which participate in co-ordinate bond formation with the oxygen of TiO_2, resulting in the monolayer formation of β-CD around TiO_2. This effective integration of β-CD, TiO_2, and Ag provides multiple electron transfer pathways. Furthermore, **Fig. 3.8(e)** shows the lattice fringes with two different sets. The lattice fringes of TiO_2 with a d value of 0.36 nm correspond to the (101) diffraction plane, and the lattice fringes of metallic Ag with a d value of 0.23 nm belong to the (111) crystal plane. The SAED pattern shown in **Fig. 3.8(f)** presents the bright spots and some distinct coordinated rings which were correlated to the metallic Ag (111), (200), and TiO_2 (110), (101) diffraction planes of β-CD/TiO_2@Ag nanocomposite (60).

The hydrodynamic size of bare TiO_2, **TA1**, **CT3**, and **CT3A1** NCs were determined through a dynamic light scattering experiment. DLS was performed by dispersing 2mg of catalyst in 5 ml of DI water. In Fig. S3, the results revealed that the hydrodynamic size of bare TiO_2 was 170 nm which is further increased to 210, 393, and 908 nm for **TA1**, **CT3**, and **CT3A1** hybrid composites, respectively. The increase in particle size on loading of β-CD and metallic Ag ensures the successful preparation of binary and ternary NCs.

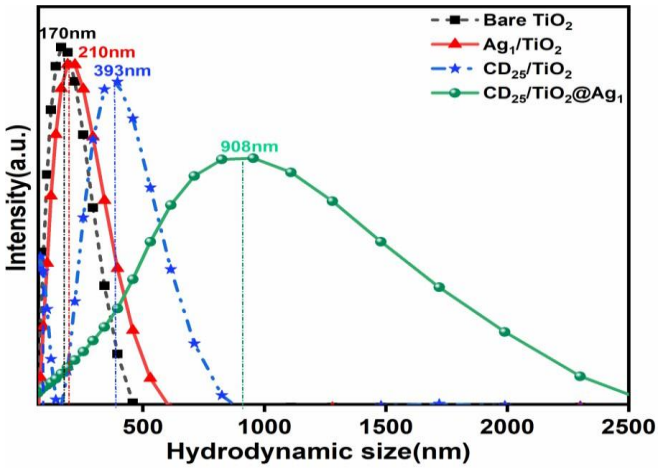

Fig. 3.9. Average hydrodynamic particles size of Bare TiO_2, Ag_1/TiO_2, β-CD_{25}/TiO_2, and β-CD_{25}/TiO_2@Ag_1.

XPS analysis was performed to determine the elemental nature and oxidation state of **CT3A1** ternary NC as shown in **Fig.3.10**. The overall survey spectrum **(Fig. 3.10(a))** verifies the presence of C, O, Ti, and Ag elements as found in EDX elemental mapping **(Fig. 3.7)**. **Fig. 3.10(b)** shows the C1s spectrum having three peaks at 284.7, 286.0, and 288.6 eV that are assigned to the binding energy (BE) of C–C, C–O, and C=O bonds, respectively (61). In the O 1s spectra **(Fig. 3.10(c))** BE of 529.8 and 532.1 eV corresponds to the Ti–O and C–O bonds. The high-resolution spectrum of Ti2p **(Fig. 3.10(d))** fitted in two peaks at 458.6 and 464.3 eV matching with the Ti $2p_{3/2}$ and Ti $2p_{1/2}$ with a BE difference of 5.7 eV evidencing the presence of Ti^{IV} valence state(62). **Fig. 3.10(e)** shows the Ag 3d spectrum resolved in two peaks of Ag $3d_{5/2}$ and Ag $3d_{3/2}$centered at 367.9 and 373.9 eV, respectively, with a BE difference of 6.0 eV confirming the presence of metallic Ag in $CD_{25}/TiO_2@Ag_1$ ternary NC(63) along with two satellite peaks at 368.5 and 375.2 eV(64).

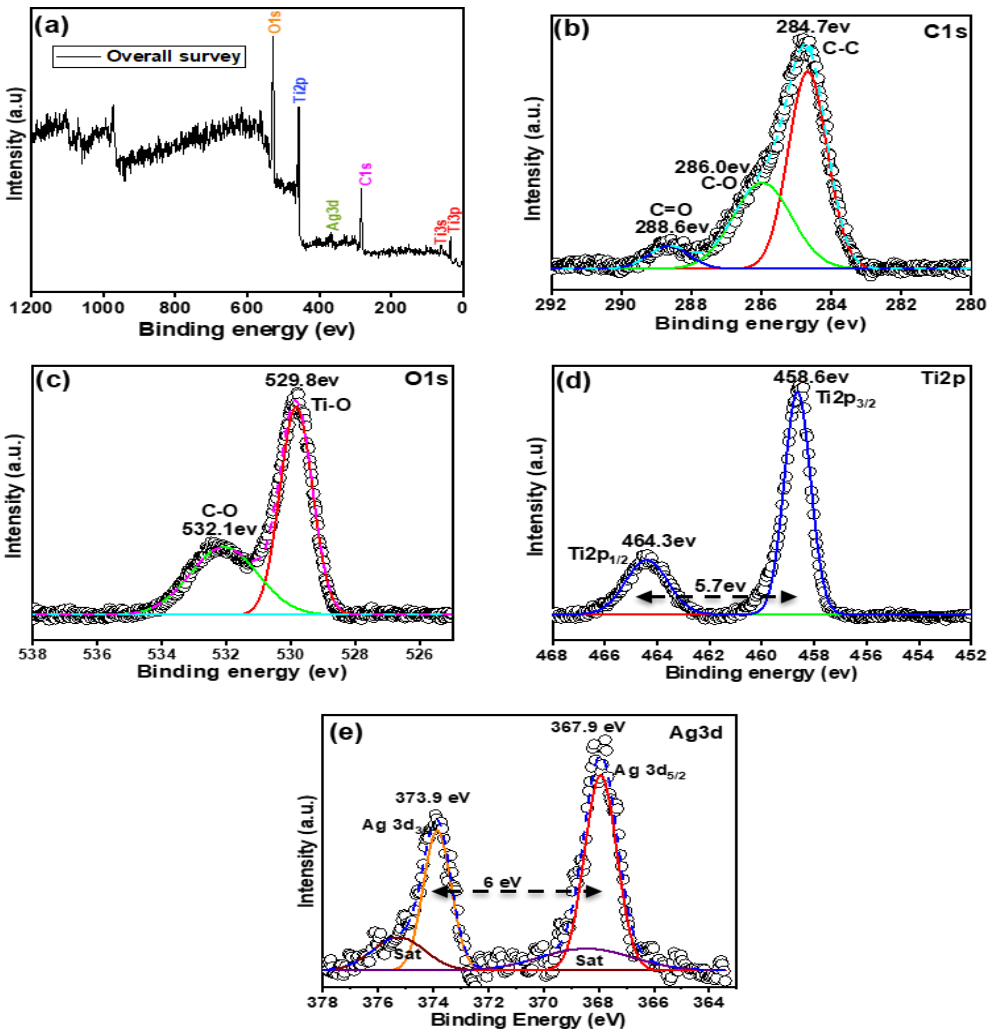

Fig. 3.10. XPS spectra of β-$CD_{25}/TiO_2@Ag_1$ (CT3A1) ternary NC:(a) overall survey; (b)C1s; (c)O1s; (d)Ti2p; (e)Ag 3d.

3.4 Photocatalytic oxidation of urea

The photocatalytic activities of all the binary and ternary nanocomposites were evaluated for urea oxidation **(Figs. 3.11, 3.12 and 3.13)**. **Figs. 3.11(a) and 3.12** show the adsorption rate for various composites after 180 minutes under dark. The **CT3** composite (14.3%) shows higher adsorption of urea than bare TiO_2 and other composites. It has been observed that there are less significant changes in the urea concentration under dark **(Fig. 3.11(a))**. After attaining equilibrium, the catalyst's photoactivity was assessed for 180 minutes under solar irradiation **(Figs. 3.11(b) and 3.13)**. It is apparent that the peak intensity of urea (λ_{max}=420 nm) declines with during photodegradation. Upon increasing the CD loading the photocatalytic activity gradually increases due to enhanced urea binding and lower nitrogen leaching. On modification with different wt.% of β-CD decreases its band gap and enriches its photoactivity in the following order **CT3** (62.8(2) %) > **CT2** (51(1) %) > **CT1** (39.6(3) %) shown in **(Fig. 3.11(c)**).

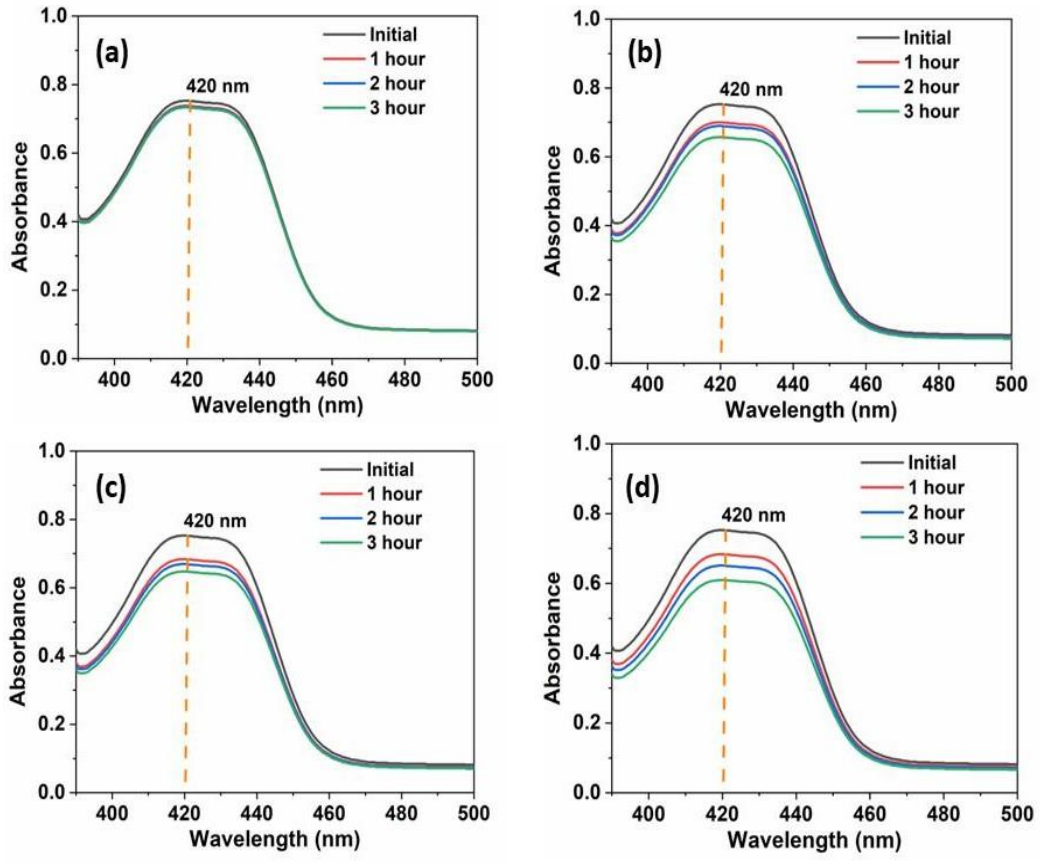

Fig. 3.11. Variation of UV-visible spectra in the presence of (a) TiO_2, (b) β-CD_{15}/TiO_2 (CT1)(c) β-CD_{20}/TiO_2 (CT2), and (d) β-CD_{25}/TiO_2 (CT3) under dark.

Furthermore, a pseudo-first-order kinetic equation (equation 6) was fitted to deter-

mine the rate constants of the urea oxidation process.

$$ln\frac{C_o}{C_t} = kt - - - - - - - - - - - (6)$$

Where C_o=Initial concentration of urea solution before sunlight exposure, C_t = con- centration of urea solution at a different time (t) after sunlight exposure, k=pseudo first order rate constant(min^{-1}), t=time for the experiment (min).

Every photocatalytic oxidation reaction follows a pseudo-first-order kinetic model. The **CT3** composite exhibits the highest rate constant of 0.0054 min^{-1} **(Fig.3.11(d))** among all photocatalysts. Such observation suggests that the loading of β-CD enhances the binding of urea with the photocatalyst through non-covalent interactions [38,65] It also reduces the extent of nitrogen leaching through the supramolecular encapsulation phenomenon[40,41].

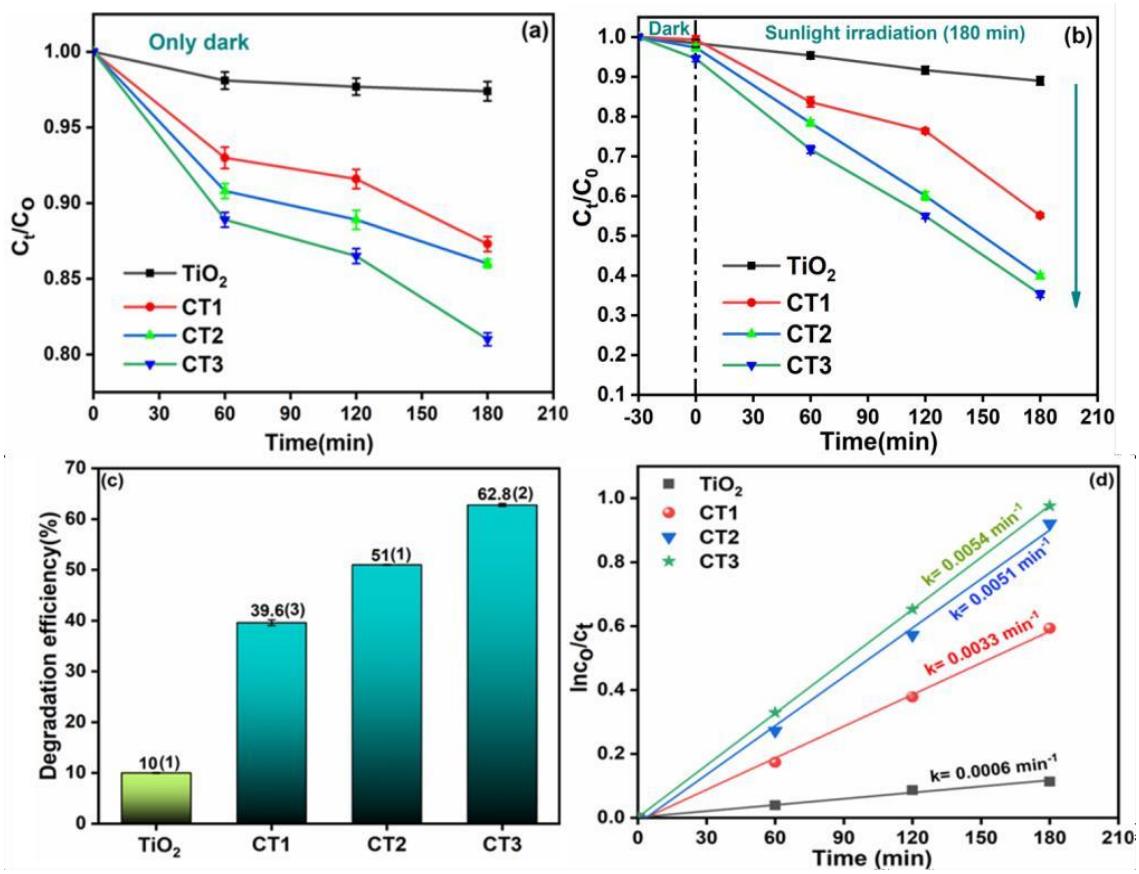

Fig 3.12: (a) Adsorption(dark) curves, (b) comparative absorption change in UV-VIS spectra w.r.t time, (c) Histogram of their photodegradation efficiencies, and (d) the corresponding reaction kinetics of degradation of urea under 180 minutes sunlight irradiation using TiO_2 and β-CD (15, 20, 25) loaded TiO_2 binary NCs: β-CD_{15}/TiO_2 **(CT1)**, β-CD_{20}/TiO_2 **(CT2)**, and β-CD_{25}/TiO_2 **(CT3).**

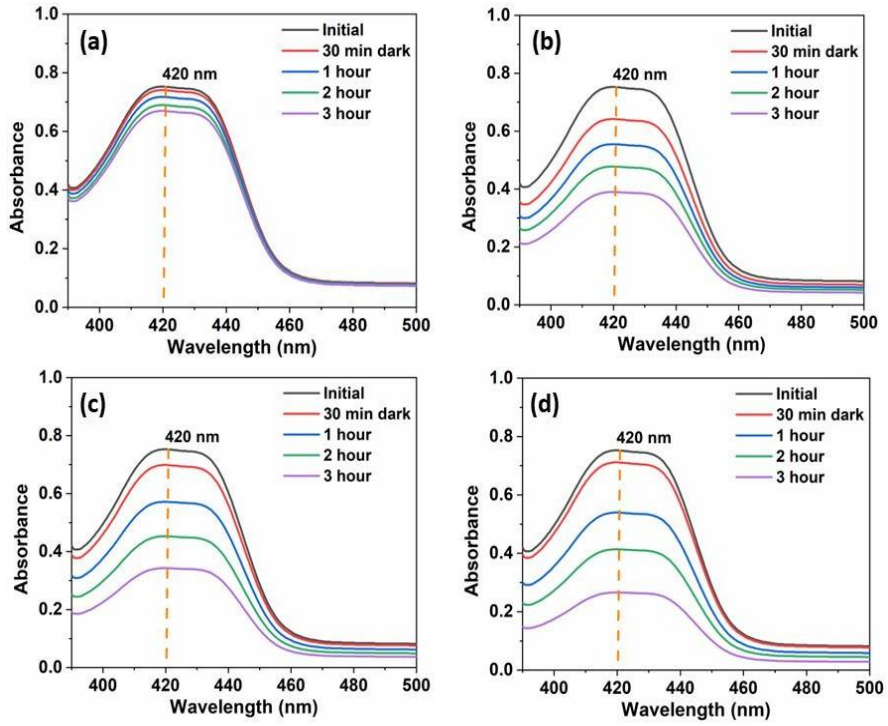

Fig 3.13: Variation of UV-visible spectra in the presence of (a) TiO_2, (b) β-CD_{15}/TiO_2 **(CT1)** (c) β-CD_{20}/TiO_2 **(CT2),** and (d) β-CD_{25}/TiO_2 **(CT3)** under solar light irradiation.

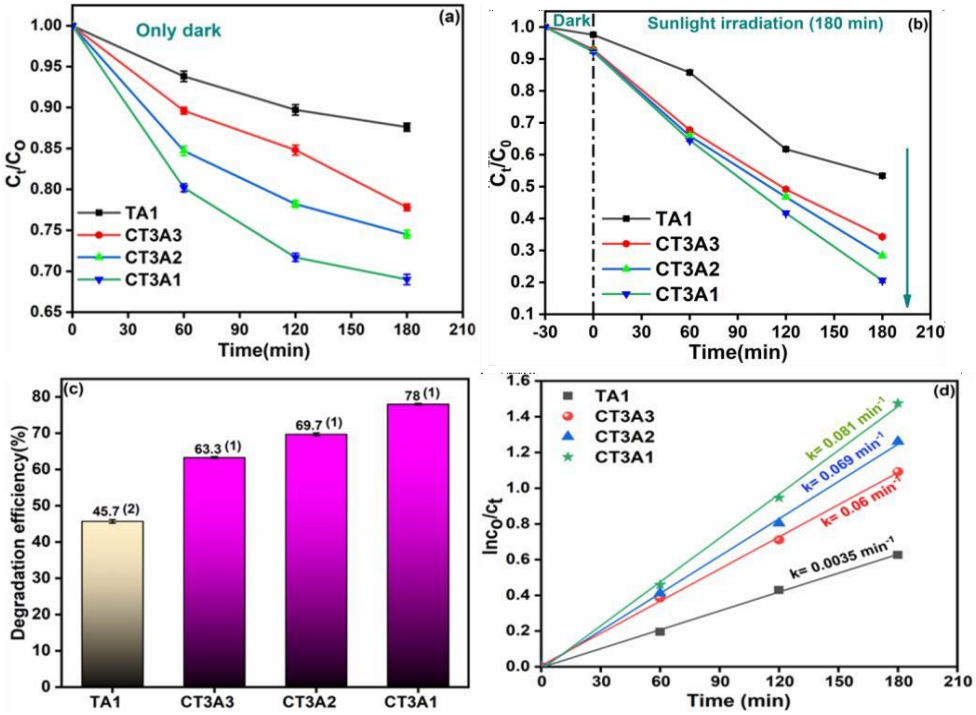

Fig. 3.14. (a) Adsorption(dark) curves, 9b) comparative absorption change in UV-VIS spectra w.r.t time, (c) Histogram of their photodegradation efficiencies, and (d) the corresponding reaction kinetics of degradation of urea under 180 minutes sunlight irradiation using Ag_1/TiO_2 (**TA1**) and Ag (1, 2, 3) loaded β-CD/TiO_2 ternary NCs: β-CD_{25}/TiO_2@Ag_1 **(CT3A1)**, β-CD_{25}/TiO_2@Ag_2 **(CT3A2)**, β-CD_{25}/TiO_2@Ag_3 **(CT3A3).**

To investigate the effect of Ag loading on photooxidation efficiency, different amounts of Ag (1-3%) were loaded over **CT3** and their catalytic efficiencies were monitored **(Figs. 3.14, 3.15 and 3.16)**. Among all the heterostructures **CT3A1** shows maximum photocatalytic efficiency of 78(1) % **(Fig. 3.14(c))**. Such observation suggests that upon loading of Ag, the photooxidation efficiency initially improves due to the enhancement of absorption of visible light resulting from the localized surface plasmon resonance (LSPR) effect and decrease of electron-hole pair recombination rate but upon further loading of Ag suppresses the catalytic efficiency due to agglomeration of Ag particles

All the photodegradation reactions follow the pseudo-first-order kinetics model **(Fig. 3.14(d))**. **CT3A1** exhibits the highest rate constant of 0.081 min^{-1} shown in **Fig. 3.14(d)**. Such findings indicate that the synergism between TiO_2, Ag, β-CD, increases the number of available active sites as well light absorption capacity to enhance the photooxidation of urea.

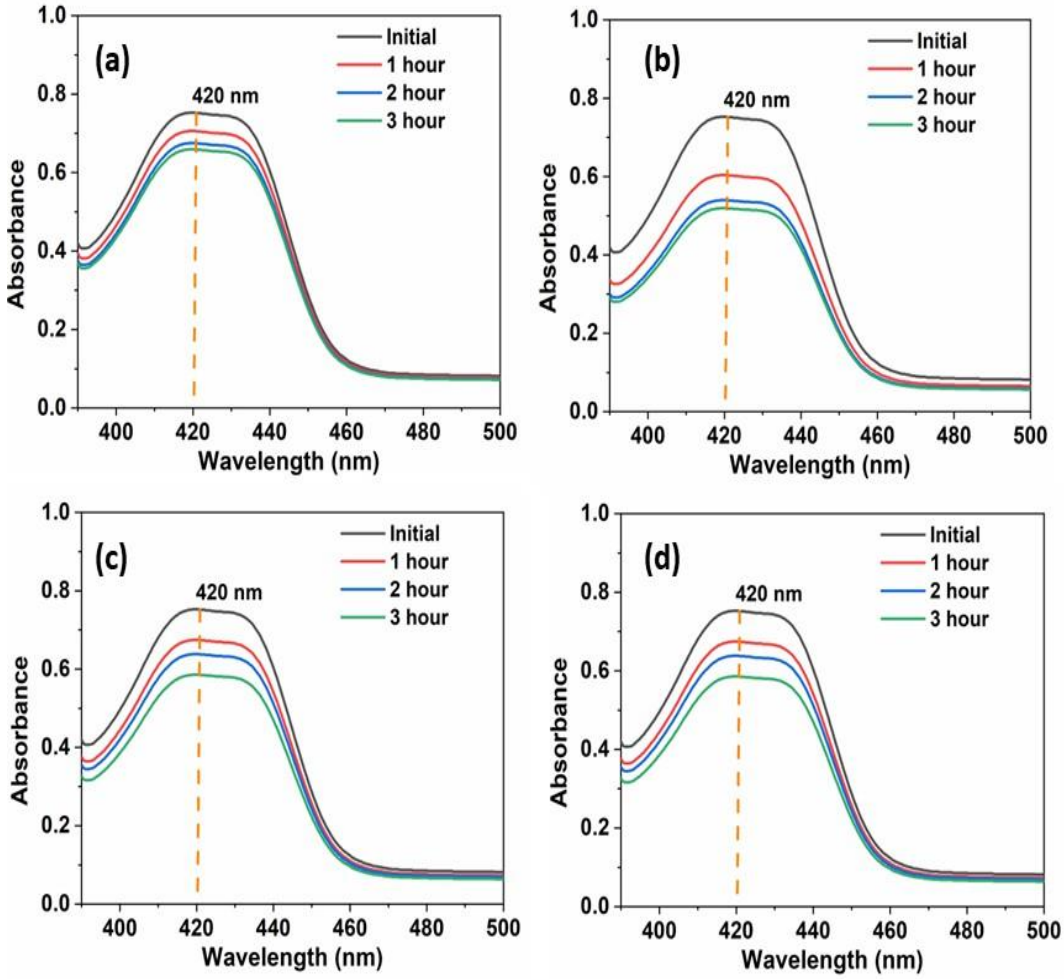

Fig.3.15: Variation of UV-visible spectra in the presence of (a) Ag_1/TiO_2 (**TA1**), (b) β-$CD_{25}/TiO_2@Ag_1$ **(CT3A1)** (c) β-CD25/$TiO_2@Ag_2$ **(CT3A2),** and (d) β-$CD_{25}/TiO_2@Ag_3$ **(CT3A3)** under dark

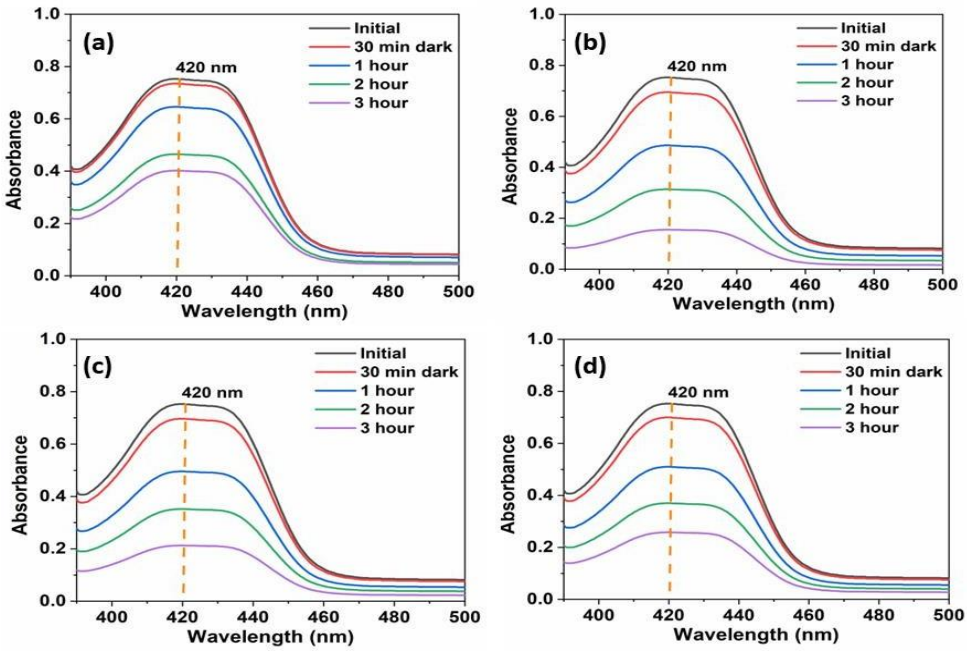

Fig 3.16: Variation of UV-visible spectra in the presence of (a) Ag_1/TiO_2 (**TA1**), (b) β-$CD_{25}/TiO_2@Ag_1$ **(CT3A1)** (c) β-$CD_{25}/TiO_2@Ag_2$ **(CT3A2),** and (d) β-$CD_{25}/TiO_2@Ag_3$**(CT3A3)** under solar light irradiation.

3.5. Demineralization efficiency and nitrate yields

3.5.1. Demineralization efficiency

TOC measurements were carried out to examine the actual demineralization of urea through photooxidation **(Fig. 3.17(a))**. It has been observed that amongst all the composites **CT3A1** possesses the highest demineralization efficiency (equation 2). Remarkably, the demineralization efficiency values were quite close to the photodegradation efficiencies in the presence of **CT3A1** hybrid photocatalyst, suggesting complete urea degradation.

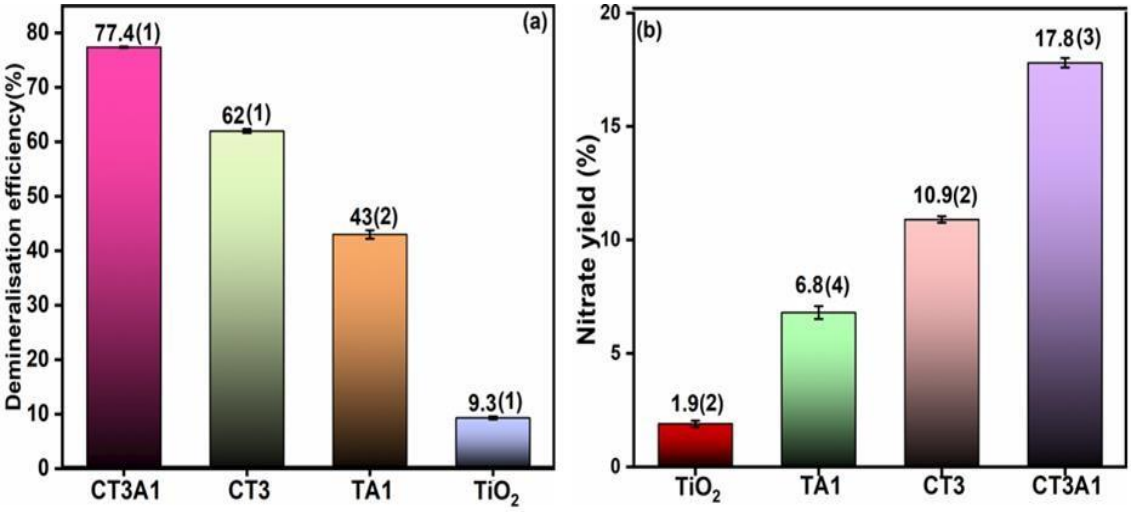

Fig3.17. Variation in (a) demineralization efficiency (%), and (b) nitrate yield (%) for TiO_2, Ag_1/TiO_2 (TA1), β-CD_{25}/TiO_2 (CT3), and β-$CD_{25}/TiO_2@Ag_1$ (CT3A1) nanocomposites.

3.5.2. Nitrate yield (%)

To ascertain, the quantity of urea oxidation as well as the nitrogen leaching, the nitrate (NO_3^-) yields in the presence of different photocatalysts were determined **(Fig. 3.17(b))**. After 3 hours of sunlight irradiation, the bare TiO_2 showed negligible nitrate yield. Upon loading of Ag and β-CD, the nitrate yield values increase to 6.8(4) % and 10.9(2) %, respectively. Remarkably, among all the photocatalysts the ternary hybrid **CT3A1** shows the highest NO_3^- yield of 17.8(3) %. Such observation suggests the cumulative effect of Ag and β-CD loading enhanced absorbance in the visible region, a decrease in electron-hole pair recombination rate, and a lowering in nitrogen loss.

To the best of our knowledge, the β-CD_{25}/TiO_2@Ag_1 (**CT3A1**) ternary hybrid is having highest urea degradation efficiency and nitrate yield compared to earlier reports(42,43).

Table 1: Comparison of photocatalytic urea degradation efficiency and nitrate yield by β-CD_{25}/TiO_2@Ag_1 ternary nanocomposites with reported literature

Photocatalyst	Degradation Efficiency (%)	Nitrate Yield (%)	References
N-doped TiO_2/polystyrene	70	0.37	(43)
RGO/TiO_2	66(1)	9.8(1)	(42)
β-CD_{25}/TiO_2@Ag_1 (**CT3A1**)	78(1)	17.8(3)	This work

3.6. Mechanistic Details

The proposed mechanism includes the formation of electron(e^-) -hole(h^+) pair via adsorption of light by the photocatalyst **(Scheme 3.2**) (34,37,42,66). Then the transfer of high-energy electrons occurs from the TiO_2 conduction band to Ag nanoparticle to suppress the electron-hole pair recombination. The holes oxidize the water molecules to form hydroxide ions whereas the electrons reduce molecular oxygen (O_2) to superoxide ions ($O_2^{\cdot-}$). The hydroxyl radicals and superoxide ions then cause oxidation of urea.

The Ag deposition over TiO_2 plays several important roles. Firstly, it will increase the photoexcited charge separation efficiency by preventing the recombination of electron-hole pairs(24,54). Secondly, it will reduce the overall band gap of the photocatalyst to enhance light absorption in the visible region due to surface plasmon resonance activity. Through

LSPR process, it can also produce hot photoexcited charge carriers which can finally afford formation of high energy reactive oxygen species (hydroxyl radicals and superoxide anions) as well as generation of high lattice temperature(25,30,31,55). Due to such properties Ag nanoparticles loading results significant improvement in the photocatalytic activity of Ag-TiO_2 derived composite.

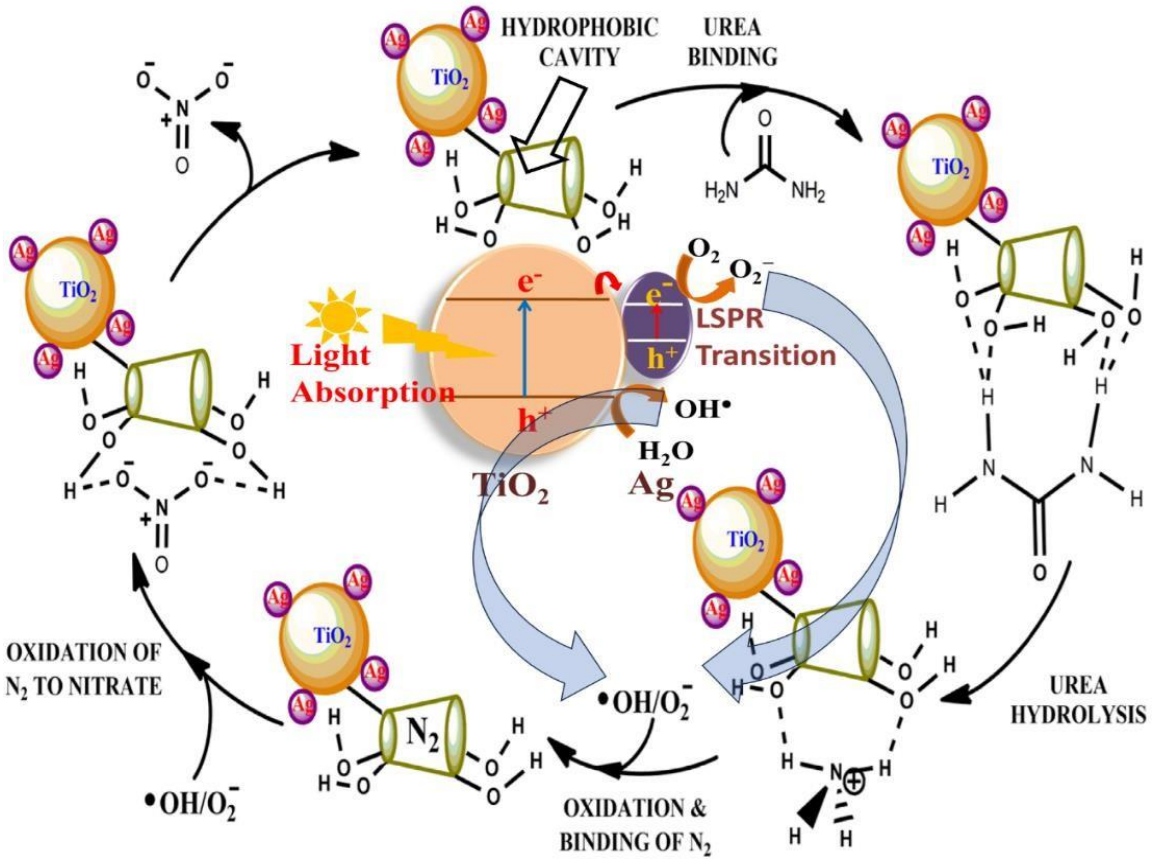

Scheme3.2: Proposed mechanism for the oxidation of urea to nitrate by β-CD_{25}/TiO_2@Ag_1 (CT3A1) composite

The urea molecules undergo binding with the hydroxyl groups of β-CD via noncovalent interactions(38,65) followed by its oxidation to yield molecular nitrogen (N_2). Later, N_2 undergoes binding with the hydrophobic part of β-CD [40,41]to reduce the nitrogen leaching. Thereafter, the β-CD bound N_2 gets oxidized further to form nitrate.

This **CT3A1** nanocomposite possesses several important physicochemical properties such as the high catalytic activity and photostability of TiO_2, efficient urea and nitrogen binding properties of β-cyclodextrin and localized surface plasmon resonance (LSPR) properties, and high charge transfer efficiency of Ag. Such cumulative effect results in high photocatalytic degradation efficiency and nitrate yield.

To investigate the roles of various reactive species, a series of control experiments

were carried out in **Fig. 3.18**. Upon addition of isopropanol (IPA) and Na_2EDTA to the reaction mixture, the photocatalytic degradation efficiency reduces from 78% to 66.3% and 21.5%, respectively. The Na_2EDTA acts as a hole scavenger to inhibit the formatio0n of hydroxyl radicals resulting from oxidation of water by the holes, whereas addition of IPA will result decrease in hydroxyl radical concentration due to its hydroxyl radical scavenging properties. Moreover, upon purging of argon for 15 minutes resulted in a decrease in urea oxidation efficiency to 37.6%. Such observation can be attributed to the removal of oxygen from the reaction mixture thereby preventing the formation of superoxide anions. Such observations suggest that both the superoxide anions and hydroxyl radicals act as the reactive species in the photocatalytic reactions.

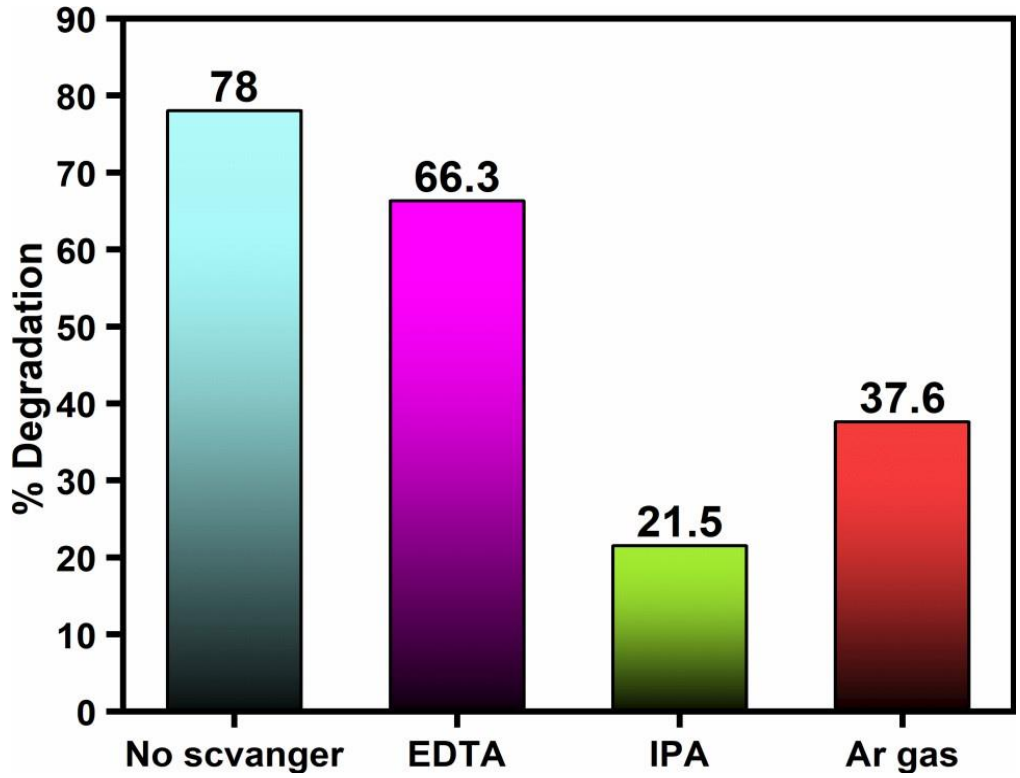

Fig 3.18. The effect of scavengers on the degradation of urea with β-CD_{25}/TiO_2@Ag_1 (CT3A1) nanocomposite.

3.7. Recyclability and stability studies

The reusability and stability studies are essential to explore its future applications. To evaluate the recyclability of **CT3A1** catalyst, the sequential reusable experiments were conducted for four cycles under sunlight with similar reaction conditions **(Fig. 3.19(a))**. It was observed that the degradation efficiency of the **CT3A1** NC dropped only by 12% till the fourth cycle in comparison with 1st cycle, suggesting that **CT3A1** is a highly recyclable catalyst.

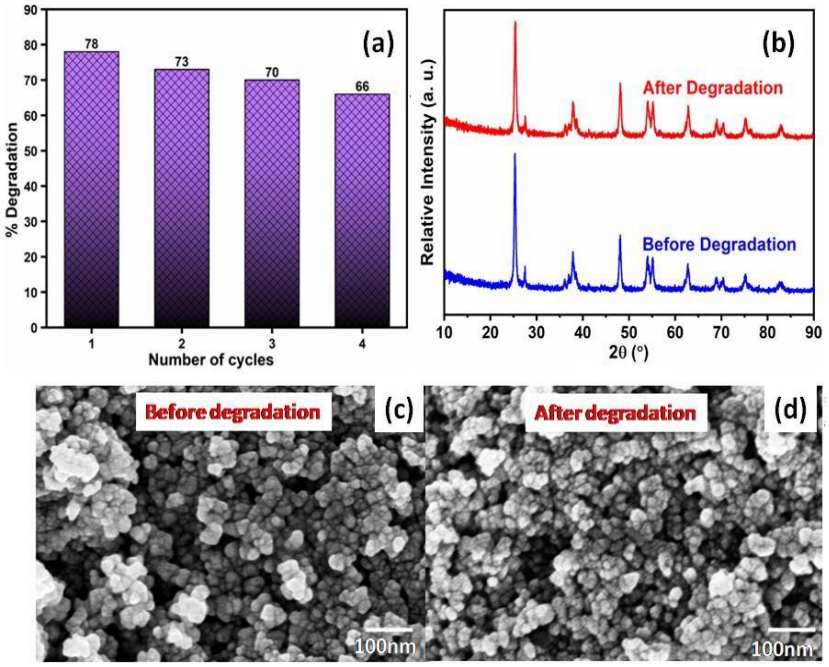

Fig. 3.19. (a)Recyclability studies of β-CD_{25}/TiO_2@Ag_1 (CT3A1) NC for the urea degradation under sunlight for 4 sequential cycles, (b) XRD pattern (c) and (d) FESEM images showing the stability of β-CD_{25}/TiO_2@Ag_1 (CT3A1) NC before and after the urea degradation.

To investigate the stability of the photocatalyst further, the XRD patterns and FESEM images of **CT3A1** catalyst were recorded before and after the photocatalytic reaction (**Fig. 3.19(c-d)).** Importantly, there is no significant difference in the XRD patterns suggesting there is no substantial change in structure as well as crystallinity before and after photocatalytic reactions **(Fig. 3.19(b))**. Also, the FESEM images **(Fig. 3.19(c-d))** also remains practically identical, thereby precluding any change in the surface morphology of the photocatalyst during the photodegradation reactions. Such observations confirm the high stability and recyclability of **CT3A1** photocatalysts.

References

1) L. Ye, X. Zhao, E. Bao, J. Li, Z. Zou, K. Cao, Bio-organic fertilizer with reduced rates of chemical fertilization improves soil fertility and enhances tomato yield and quality, *Sci Rep*, **2020**, *10* , 1–11.
2) A. Akter, M.R. Islam, M.R. Islam, Md.A. Islam, S.L. Hasan, S. Uddin, M.M. Rahman, Methods of Urea Fertilizer Application Influence Growth, Yield, and Nitrogen Use Efficiency of Transplanted Aman Rice, *Water*. **2022**, *14*, 1-12.
3) P. Shetty, C. Acharya, N. Veeresh, Effect of Urea Fertilizer on the Biochemical Characteristics of Soil, *Int J Appl Sci Biotechnol*. **2019**, *7*, 414–420.

4) P. Jadon, R. Selladurai, S.S. Yadav, M.V. Coumar, M.L. Dotaniya, A.K. Singh, J. Bhadouriya, S. Kundu, Volatilization and leaching losses of nitrogen from different coated urea fertilizers, *J Soil Sci Plant Nutr*. **2018**,*18*,1036–1047.
5) K.L. Marsh, G.K. Sims, R.L. Mulvaney, Availability of urea to autotrophic ammonia-oxidizing bacteria as related to the fate of 14C- and 15N-labeled urea added to soil, *Biol Fertil Soils*. **2005**, *42*, 137–145.
6) A.E. Ghaly, V. V. Ramakrishnan, Nitrification of urea and assimilation of nitrate in saturated soils under aerobic conditions, *Am J Agric Biol Sci*. **2013**, *18*, 330–342.
7) J. Gotosa, J. Kodzwa, W. Gwenzi, J. Nyamangara, Maize nitrogen uptake and productivity under reduced and conventional tillage, *Nutr Cycl Agroecosyst*. **2021**, *119*, 23–36.
8) Z. Ma, Y. Yue, M. Feng, Y. Li, X. Ma, X. Zhao, S. Wang, Mitigation of ammonia volatilization and nitrate leaching via loss control urea triggered H-bond forces, *Sci Rep*. **2019**, *9*, 1–9.
9) D. Weerakoon, B. Bansal, L.P. Padhye, A. Rachmani, L. James Wright, G. Silyn Roberts, S. Baroutian, A critical review on current urea removal technologies from water: An approach for pollution prevention and resource recovery, *Sep Purif Technol*. **2023**, *314*, 123652.
10) V.M. Bhandari, L.G. Sorokhaibam, V. V Ranade, Industrial wastewater treatment for fertilizer industry—A case study, *Desalination Water Treat*. **2016**, *57*, 27934–27944.
11) L.E. Scherger, V. Zanello, C. Lexow, Impact of Urea and Ammoniacal Nitrogen Wastewaters on Soil: Field Study in a Fertilizer Industry (Bahía Blanca, Argentina), *Bull Environ Contam Toxicol*. **2021**, *107*, 565–573.
12) S. Farid, M.K. Baloch, A. Razaque, S.A. Ahmad, Water Pollution Threat to the Environment by a Urea Plant, *J Chin Chem Soc*. **2005**, *52*, 283–285.
13) R. Hashimi, M.H. Hashimi, Effect of Losing Nitrogen Fertilizers on Living Organism and Ecosystem, and Prevention Approaches of their Harmful Effect, *Asian Soil Res J*. **2020**,10–20.
14) C.W. Liu, Y. Sung, B.C. Chen, H.Y. Lai, Effects of nitrogen fertilizers on the growth and nitrate content of lettuce (Lactuca sativa L.), *Int J Environ Res Public Health*. **2014**, *11*, 4427–4440.
15) M. Klimczyk, A. Siczek, L. Schimmelpfennig, Improving the efficiency of urea-based fertilization leading to reduction in ammonia emission, *Sci Total Environ*. **2021**, *771*, 1-13.
16) H. Wang, S. Köbke, K. Dittert, Use of urease and nitrification inhibitors to reduce gaseous nitrogen emissions from fertilizers containing ammonium nitrate and urea, *Glob Ecol Conserv*. **2020**, *22*, 1-11.
17) S. Park, J.T. Lee, J. Kim, Photocatalytic oxidation of urea on TiO_2 in water and urine: mech-

anism, product distribution, and effect of surface platinization, *Environ Sci Pollut Res.* **2019**, *26*, 1044–1053.

18) H. il Kim, K. Kim, S. Park, W. Kim, S. Kim, J. Kim, Titanium dioxide surface modified with both palladium and fluoride as an efficient photocatalyst for the degradation of urea, *Sep Purif Technol*. **2019**, *209*, 580–587.

19) L. Madriz, M. Parra, F. S. García Einschlag, O. Núñez, F. M. Cabrerizo, R. Vargas, Photocatalytic Oxidation of Urea on Surface-Modified Bi_2WO_6 with trans-4- Stilbene carboxaldehyde, *J Phys Chem C*. **2021**, *152*, 12682–12689.

20) A.D. Mani, S. Muthusamy, S. Anandan, C. Subrahmanyam, C and N doped nano-sized TiO_2 for visible light photocatalytic degradation of aqueous pollutants, *J Exp Nanosci*. **2015**,*10*, 115–125.

21) A. Ziashahabi, M. Prato, Z. Dang, R. Poursalehi, N. Naseri, The effect of silver oxidation on the photocatalytic activity of Ag/ZnO hybrid plasmonic/metal-oxide nanostructures under visible light and in the dark, *Sci Rep*. **2019**, *9*, 1–12.

22) J. Zhao, S.C. Nguyen, R. Ye, B. Ye, H. Weller, G.A. Somorjai, A.P. Alivisatos, F. Dean Toste, A Comparison of Photocatalytic Activities of Gold Nanoparticles Following Plasmonic and Interband Excitation and a Strategy for Harnessing Interband Hot Carriers for Solution Phase Photocatalysis, *ACS Cent Sci.* **2017**, 3, 482–488.

23) Y. Che, Q. Liu, B. Lu, J. Zhai, K. Wang, Z. Liu, Plasmonic ternary hybrid photocatalyst based on polymeric g-C_3N_4 towards visible light hydrogen generation, *Sci Rep*, **2020**, 10, 1–12.

24) N.R. Reddy, U. Bharagav, M. V Shankar, P.M. Reddy, K.R. Reddy, N.P. Shetti, F. Alonso-Marroquin, M.M. Kumari, T.M. Aminabhavi, S.W. Joo, Photocatalytic hydrogen production by ternary heterojunction composites of silver nanoparticles doped FCNT-TiO_2, *J Environ Manage*. **2021**, *286*, 112130.

25) Z. Zhang, C. Zhang, H. Zheng, H. Xu, Plasmon-Driven Catalysis on Molecules and Nanomaterials, *Acc Chem Res*. 52. **2019**, 2506–2515.

26) R. Li, X. Wang, M. Chen, Non-Noble Metal and Nonmetallic Plasmonic Nanomaterials with Located Surface Plasmon Resonance Effects: Photocatalytic Performance and Applications, *Catalysts*. **2023**, *13*, 940.

27) M. Sayed, J. Yu, G. Liu, M. Jaroniec, Non-Noble Plasmonic Metal-Based Photocatalysts, *Chem Rev*. **2022**, *12*, 10484–10537.

28) C. Yue, L. Zhu, Y. Qiu, Z. Du, J. Qiu, F. Liu, F. Wang, Recent advances of plasmonic

elemental Bi based photocatalysts in environmental remediation and energy conversion, *J Clean Prod.* **2023**, *392*, 136017.

29) N. Wu, Plasmonic metal–semiconductor photocatalysts and photoelectrochemical cells: a review, *Nanoscale*. **2018**, *10*, 2679–2696.

30) L. Mascaretti, A. Naldoni, Hot electron and thermal effects in plasmonic photocatalysis, *J Appl Phys*. **2020**, *128*, 041101.

31) Z. Zheng, W. Xie, B. Huang, Y. Dai, Plasmon-Enhanced Solar Water Splitting on Metal-Semiconductor Photocatalysts, *Chem Eur J*. **2018**, *24*, 18322–18333.

32) X. Ye, Z. Wang, Q. Wang, D. Chen, Y. Lin, S. Liu, Enhanced photocatalytic activity of ternary multilayered Ag/TiO_2/CNT composites for methylene blue degradation, *Micro Nano Lett.* **2019**, 14,771–776.

33) J. Ren, Y.Z. Wu, J.M. Pan, X.H. Yan, M. Chen, J.J. Wang, D.F. Wang, C. Zhou, Q. Wang, X.N. Cheng, Novel ternary Ag/$CeVO_4$/g-C_3N_4 nanocomposite as a highly efficient visible-light-driven photocatalyst, *J Adv Ceram*. **2018**, *10*, 50–57.

34) A. Mohammadi, S.H. Mousavi, Enhanced Photocatalytic Performance of TiO_2 by β-Cyclodextrin for the Degradation of Organic Dyes, *J Water Environ Nanotechnol*. **2018**, *3*, 254–264.

35) E. García-Díaz, D. Zhang, Y. Li, R. Verduzco, P.J.J. Alvarez, TiO_2 microspheres with cross-linked cyclodextrin coating exhibit improved stability and sustained photocatalytic degradation of bisphenol A in secondary effluent, *Water Res.* **2020**,*183*, 1-25.

36) T.Z. Agócs, I. Puskás, E. Varga, M. Molnár, É. Fenyvesi, Stabilization of nanosized titanium dioxide by cyclodextrin polymers and its photocatalytic effect on the degradation of wastewater pollutants, Beilstein *J Org Chem*. **2016**, *12*, 2873–2882.

37) S. Guo, J. Shang, T. Zhao, D. Hou, Z. Jin, G. Sun, TiO_2/Cyclodextrin Hybrid Structure with Efficient Photocatalytic Water Splitting, *ES Mater Manuf.* **2018**, *2*, 24–27.

38) B. Maity, A. Chatterjee, S.A. Ahmed, D. Seth, Deciphering the perturbation effect of urea on the supramolecular host-guest interaction of biologically active hydrophobic molecule inside the nanocavity of cyclodextrins, *J Lumin*. **2017**, *183*, 238–250.

39) F. Biedermann, W.M. Nau, H.-J. Schneider, The Hydrophobic Effect Revisited—Studies with Supramolecular Complexes Imply High-Energy Water as a Noncovalent Driving Force, Angew *Chem Int Ed*. **2014**, *53*, 11158–11171.

40) X. Dai, L. Tian, Z. Liu, W. Xu, Y.-P. Liu, Y. Liu, Nanoreactor Based on Cyclodextrin for Direct Electrocatalyzed Ammonia Synthesis, *ACS Nano*. **2022**, *16*, 18398–18407.

41) Pospíšil, M. Hromadová, M. Gál, J. Bulíčková, R. Sokolová, N. Fanelli, Electrochemical impedance of nitrogen fixation mediated by fullerene–cyclodextrin complex, *Electrochim Acta*. **2008**, *58*, 7445–7450.

42) P. Soni, B. Pal, R.K. Das, enhanced photocatalytic urea oxidation under neutral medium by reduced graphene oxide coated TiO_2 nanoparticles, *Catal Commun*. **2023**, *179*, 106690.

43) V. Vaiano, O. Sacco, G. Di Capua, N. Femia, D. Sannino, Use of visible light modulation techniques in urea photocatalytic degradation, *Water*. **2019**, *11*, 1642.

44) J. Pelc, M. Śnioszek, J. Wróbel, A. Telesiński, Effect of Fluoride on Germination, Early Growth and Antioxidant Enzymes Activity of Three Winter Wheat (Triticum aestivum L.) *Cultivars, Appl Sci*. **2020,** *10*, 6971.

45) S. Bhardwaj, D. Sharma, P. Kumari, B. Pal, Influence of photodeposition time and loading amount of Ag co-catalyst on growth, distribution and photocatalytic properties of $Ag@TiO_2$ nanocatalysts, *Opt Mater*. **2020,** *106*, 109975.

46) J.D. Giraldo, B.L. Rivas, Determination of urea using p-N, N-dimethylaminobenzaldehyde: Solvent effect and interference of chitosan, *J Chil Chem Soc*. **2017**, *62*, 3538–3542.

47) A. Mohamed, A. Salama, W.S. Nasser, A. Uheida, Photodegradation of Ibuprofen, Cetirizine, and Naproxen by PAN-MWCNT/TiO_2–NH_2 nanofiber membrane under UV light irradiation, *Environ Sci Eur*. **2018**, *30*, 1-9.

48) L. Rimoldi, D. Meroni, E. Falletta, V. Pifferi, L. Falciola, G. Cappelletti, S. Ardizzone, Emerging pollutant mixture mineralization by TiO_2 photocatalysts. The role of the water medium, *Photochem Photobiol Sci*. **2017**, *16*, 60–66.

49) P. Velusamy, S. Pitchaimuthu, S. Rajalakshmi, N. Kannan, Modification of the photocatalytic activity of TiO_2 by β-cyclodextrin in decoloration of ethyl violet dye, *J Adv Res*. **2014**, *5*, 19–25.

50) X. Zhang, F. Wu, N. Deng, Efficient photodegradation of dyes using light-induced self-assembly TiO_2/β-cyclodextrin hybrid nanoparticles under visible light irradiation, *J Hazard Mater*. **2011**, *185*, 117–123.

51) N. Attarchi, M. Montazer, T. Toliyat, Ag/TiO2/β-CD nano composite: Preparation and photo catalytic properties for methylene blue degradation, *Appl Catal A Gen*. **2013**, *467*, 107–116.

52) R. Bajaj, M. Sharma, D. Bahadur, Visible light-driven novel nanocomposite (BiVO4/CuCr 2O4) for efficient degradation of organic dye, *Dalton Trans*. **2013**, *42*, 6736–6744.

53) S. Rhatigan, M. Nolan, Activation of water on MnO_x-nanocluster-modified rutile (110) and anatase (101) TiO_2 and the role of cation reduction, *Front Chem*, **2019**, *7*, 1–12.

54) T. Wang, T. Tang, Y. Gao, Q. Chen, Z. Zhang, H. Bian, Hydrothermal preparation of Ag-TiO_2-reduced graphene oxide ternary microspheres structure composite for enhancing photocatalytic activity, *Physica E Low Dimens Syst Nanostruct*. **2019**, *112*, 128–136.

55) H. Lee, Y. Keun Lee, E. Hwang, J. Young Park, Enhanced Surface Plasmon Effect of Ag/TiO_2 Nanodiodes on Internal Photoemission, *J Phys Chem C*. **2014**, *118*, 5650–5656.

56) V. Sharavath, S. Sarkar, D. Gandla, S. Ghosh, Low Temperature Synthesis of TiO_2 - β - Cyclodextrin – Graphene Nanocomposite for Energy Storage and Photocatalytic Applications, *Electrochim Acta*. **2016**, *210*, 385–394

57) Y. Zhang, Q. Li, Q. Gao, S. Wan, P. Yao, X. Zhu, Preparation of Ag/β-cyclodextrin co-doped TiO_2 floating photocatalytic membrane for dynamic adsorption and photoactivity under visible light, *Appl Catal B.* **2020**, *167*, 1-10.

58) I. Shown, M. Ujihara, T. Imae, Synthesis of β-cyclodextrin-modified water-dispersible Ag-TiO_2 core-shell nanoparticles and their photocatalytic activity, *J Nanosci Nanotech- nol.* **2011**, *11*, 3284–3290.

59) N. Attarchi, M. Montazer, T. Toliyat, Ag/TiO_2/β-CD nano composite: Preparation and photo catalytic properties for methylene blue degradation, *Appl Catal A Gen.* **2013**, *467*, 107–116.

60) X. Ye, Z. Wang, Q. Wang, D. Chen, Y. Lin, S. Liu, Enhanced photocatalytic activity of ternary multilayered Ag/TiO_2/CNT composites for methylene blue degradation, *Micro Nano Lett*. **2019**, *14*, 771–776.

61) J. Wang, G. Zhou, R. He, W. Huang, J. Zhu, C. Mao, C. Wu, G. Lu, Experimental preparation and optical properties of CeO_2/TiO_2 heterostructure, *J Mater Res Tech- nol.* **2020**, *9*, 9920–9928.

62) Y. Zhou, L. Liu, T. Wu, G. Yuan, J. Li, Q. Ding, F. Qi, W. Zhu, X. Ouyang, Y. Wang, Flake-like $InVO_4$ modified TiO_2 nanofibers with longer carrier lifetimes for visible-light photocatalysts, *RSC Adv*. **2018**, *8*, 27073–27079.

63) Y. Zhang, Q. Li, Q. Gao, S. Wan, P. Yao, X. Zhu, Preparation of Ag/β-cyclodextrin co-doped TiO_2 floating photocatalytic membrane for dynamic adsorption and photoactivity under visible light, *Appl Catal B.* **2020**, *267*, 1-5.

64) A. Dolatkhah, P. Jani, L. D. Wilson, Redox-Responsive Polymer Template as an Advanced Multifunctional Catalyst Support for Silver Nanoparticles, *Langmuir*. **2018**, *34*, 10560–10568.

65) N. Sarkar, K. Das, D. Nath, K. Bhattacharyya, Interaction of urea with fluorophores bound to cyclodextrins. Fluorescence of p-toluidino naphthalene sulphonate, *Chem Phys Lett*. **1992**, *196*, 491–496.

66) J. Schneider, M. Matsuoka, M. Takeuchi, J. Zhang, Y. Horiuchi, M. Anpo, D.W. Bahnemann, Understanding TiO_2 Photocatalysis: Mechanisms and Materials, *Chem Rev*. **2014**, *114*, 9919–9986.

CHAPTER-4

β-CD and RGO loaded Ag-TiO_2 composites for enhanced photo-catalytic oxidation of urea under sunlight

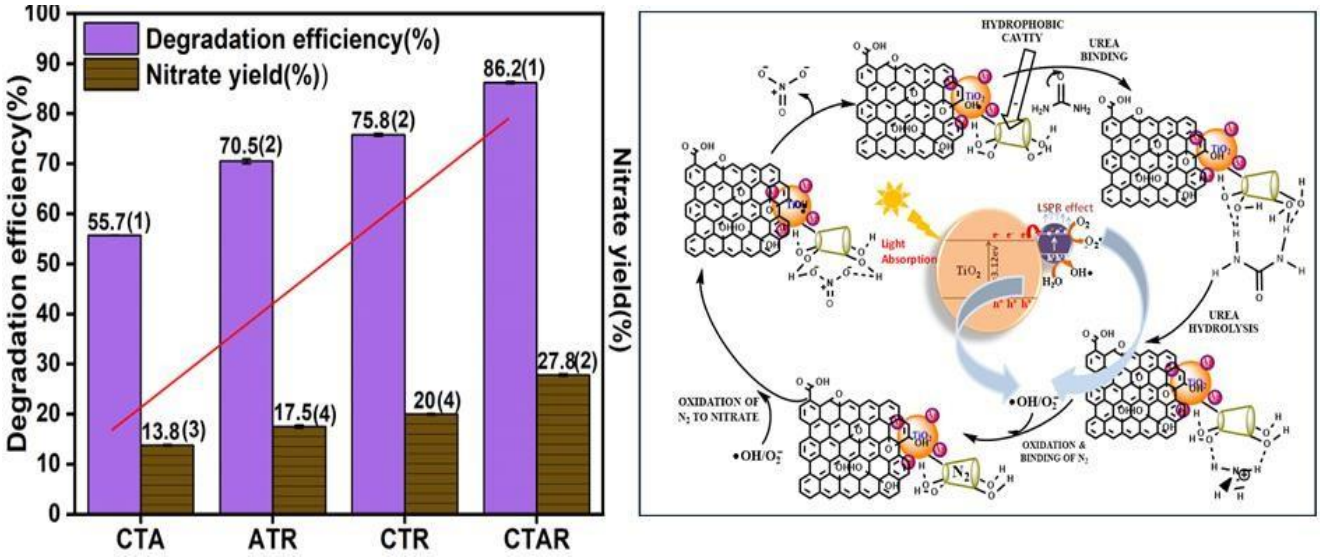

Schematic outline

The study investigates the photocatalytic efficiency of CTA, ATR, CTR, and CTAR nano-composites in urea oxidation under sunlight. Among them, CTAR exhibited the highest performance, showing superior adsorption and photodegradation capabilities due to the combined effects of Ag, RGO, and β-CD. The CTAR composite achieved the highest urea oxidation efficiency (86.2%) and nitrate yield (27.8%), with a rate constant of 0.017 min^{-1}, indicating effective photocatalytic activity. Scavenger experiments identified hydroxide radicals (•OH) and superoxide radicals ($O2^-$) as crucial for the oxidation process. The mechanism involves the transfer of photoexcited electrons from TiO_2 to Ag and RGO, enhancing charge separation and active species formation. CTAR demonstrated excellent reusability with only a 9% efficiency drop after four cycles and maintained structural stability as confirmed by XRD analysis.

4.1 Introduction

With the projected increase in the global population, there's a growing reliance on fertilizers to meet the escalating demand for crops. (1) Nitrogen-rich fertilizers are fundamental for promoting crop growth., remains a cornerstone of agricultural practices. (2) Being an easily assimilable form of nitrogen, Urea is an extensively used fertilizer that accommodates 46% N content engaged in the mineralization process.(3) Plants primarily uptake nitrogen as nitrate (NO_3^-) and ammonium (NH_4^+) ions. Urea, to become assimilable, undergoes hydrolysis and subsequently forms NH_4^+ ions through protonation and a further nitrification process begin where nitrite and nitrate form (4). Plants absorb these ions through specialized transporters that use proton gradients for transportation(5,6). However, urea exhibits significant losses upon contact with soil compared to other fertilizers, leads to ammonia volatilization, denitrification, runoff, leaching, and other pathways, resulting in the accumulation of reactive nitrogen (organic nitrogen and inorganic nitrogen compounds excluding N_2). (7,8)This unintended ammonia emission diminishes crop yields due to nitrogen loss and posing long-term negative health hazards, environmental consequences as agriculture expands. (9,10)Consequently, the oxidation of urea into beneficial products like NO_3^- and N_2 are0 imperative for sustainable agriculture. (11) Hence, there's an urgent need to develop efficient photocatalysts with robust oxidizing capabilities to enhance overall NO_3^- efficiency.

Photocatalysis in the presence of semiconductors is emerging as safe, affordable, and effective method to enhance crop yield. ⸢12) Titanium dioxide (TiO_2) is widely recognized as the most promising semiconductor due to its high photochemical stability, potent oxidizing capability, environmental friendliness, and cost-effectiveness. ⸢13) However, its photocatalytic performance is constrained by limited light responsiveness, limited electrical conductivity, and fast recombination of photogenerated electron-hole pairs. (14) Thus, bare TiO_2 restricts the urea oxidation. (15)

The loading of carbon materials like RGO over TiO_2 could potentially solve these problems.(16) Oxidation of urea to nitrate involves an 8-electron transfer process. RGO is recognized for its exceptional properties, including a high surface-to-volume ratio, chemical stability, surface flexibility, low production cost, and high electron mobility, facilitating efficient electron transfer.(17) However, its effectiveness is hindered by agglomeration and restacking due to π-π stacking and van der Waals forces, that reduces its surface area. (18,19) limiting its practical application.

β-cyclodextrin (β-CD), a well-known supramolecule, is a cyclic oligosaccharide composed of seven glucose units. It is highly adsorbent, non-toxic, and acts as a capping agent to stabilize metal. Urea oxidation frequently results in the formation of N_2 as a primary product due to incomplete oxidation. To further improve the efficiency of photocatalysts, it is necessary to design a hybrid system with a strong affinity for N_2 and significant oxidizing power, which helps to prevent leaching and improves nitrate efficiency (20) β-CD has a toroidal shape with a hydrophilic exterior, exposing –OH groups for hydrogen bonding, and a hydrophobic interior that can encapsulate non-polar guests (21,22). This distinctive structure of β-CD provides numerous adsorption sites and synergistic interactions, extending its absorption spectrum towards the visible region and reducing the recombination rate. (23). This β-CD binds with urea through covalent forces and the hydrophobic interior encapsulates the molecular nitrogen very effectively(24). This mechanistic approach offers stronger interactions, less leaching, and high nitrate yield.

For better charge separation, a photocatalyst should strongly absorb visible light. Adding plasmonic metals such as Ag, Au, or Cu can enhance this ability through localized surface plasmonic resonance (LSPR), which broadens the absorption into the visible spectrum. (25)These transitions enable nanoparticles to absorb sunlight, generating strong electric fields and photogenerated e^-/h^+ pairs. These pairs can disseminate through the phonos, causing a rise in lattice temperatures.(26). High energy charge carriers, electric fields, and elevated temperatures can significantly boost photoactivity (27). Consequently, the deposition of coinage metals is an effective way to elevate the potential of the prepared material.

As far as we know, the literature on photocatalytic oxidation of urea is quite limited. Among the reported studies, β-CD/TiO_2@Ag NC achieves the highest nitrate yield at 17.8(3) %, while TiO_2/RGO yields 9.8(1) % with a NaF additive under neutral pH, which can disrupt ecosystems (28,20). This reaction necessitates high electron mobility to maximize the transfer of electrons for producing nitrate as the main product. Therefore, it is essential to develop a new photocatalyst with high capacitance to facilitate urea oxidation. Inspired by those observations, a highly proficient ternary (β-CD/Ag-TiO_2, Ag-TiO_2@RGO, β-CD/TiO_2/RGO) and quaternary (β-CD/Ag-TiO_2/RGO) heterojunction systems were constructed by photo deposition and hydrothermal method respectively. These innovative nanocomposites, with their promising attributes, offer high electron mobility, increased surface area, enhanced optical response, and improved charge separation, providing a multielectron transfer pathway among all components for urea oxidation. Consequently, the design of the quaternary composite, β-

CD/Ag-TiO_2/RGO can be a better approach for the photocatalytic oxidation of urea.

4.2. Experimental section

4.2.1. Chemical reagents

Graphite powder (98% extra pure); conc. Sulfuric acid (H_2SO_4, 98%); potassium permanganate ($KMnO_4$, 99% extra pure); sodium nitrate ($NaNO_3$,99%); hydrochloride acid (HCl, 35.4%); L-ascorbic acid (L-AA, 99.5%); hydrogen peroxide (H_2O_2/30% w/v extra pure); ammonia (NH_3 ,28%); ethanol (C_2H_5OH, 99.9%); isopropanol (C_2H_5O, 99.5%); urea ($CO(NH_2)_2$, 99% extra pure) were received from Loba Chemie Pvt. Ltd., India. TiO_2 was supplied from Degussa Corporation, Germany. Silver(I) nitrate (AgNO3. ≥ 99%) was procured from Sigma-Aldrich. β-cyclodextrin (β-CD; 98.00%)) was obtained from GLR innovations. Deionized water (DI) was received from Organo Biotech Laboratories Pvt. Ltd. and utilized during all the experimental studies.

4.2.2. Synthesis

Reduced Graphene oxide (RGO) was prepared using a reported procedure (20), while Ag-TiO_2 was prepared using a photo deposition method. (29,30)

4.2.3. Synthesis of Ag/TiO_2@RGO nanostructures

The synthesis of Ag-TiO_2@RGO NC was done hydrothermally. About 200 mg of GO powder was dispersed in a small amount of DI water, and then 1 g of Ag/TiO_2 was added to it (Scheme 4.1). After stirring the mixture for 1 hour, the uniform suspension was transferred to an autoclave for hydrothermal treatment at 180°C for 6 hours. The resulting solid was separated by centrifugation and dried at room temperature to obtain the Ag/ TiO_2@RGO nanocomposite, which will be abbreviated as ATR.

.4.2.4. Synthesis of β-CD/TiO_2/RGO nanostructures

An analogous method was applied for synthesizing β-CD/TiO_2/RGO NC as described in Section 4.2.3 (Scheme 4.1). 120 mg of the β-CD/ TiO_2 composite was added to a 500 mg RGO dispersion under ultrasonication. After stirring the mixture continuously for 1 hour, the homogeneous dispersion was treated hydrothermally at 180°C for 6 hours (29). The final product was then dried overnight at 30°C, and this nanocomposite will be referred to as CTR

4.2.5. Synthesis of β-CD/TiO_2/Ag/RGO quaternary nanohybrid

The β-CD/Ag-TiO_2/RGO quaternary NC was produced using a hydrothermal method. Initially, 1000 mg of β-CD/Ag-TiO_2 was dispersed in a minimal amount of water (Scheme 4.1). Then, 250 mg of GO was added to the prepared uniform dispersion under ultrasonication. After 1 hour of constant stirring, the solution was transferred to an autoclave for further hydrothermal treatment at 180°C for 6 hours(29). The resultant product was dried overnight at room temperature. This prepared quaternary nanocomposite will be referred to as CTAR.

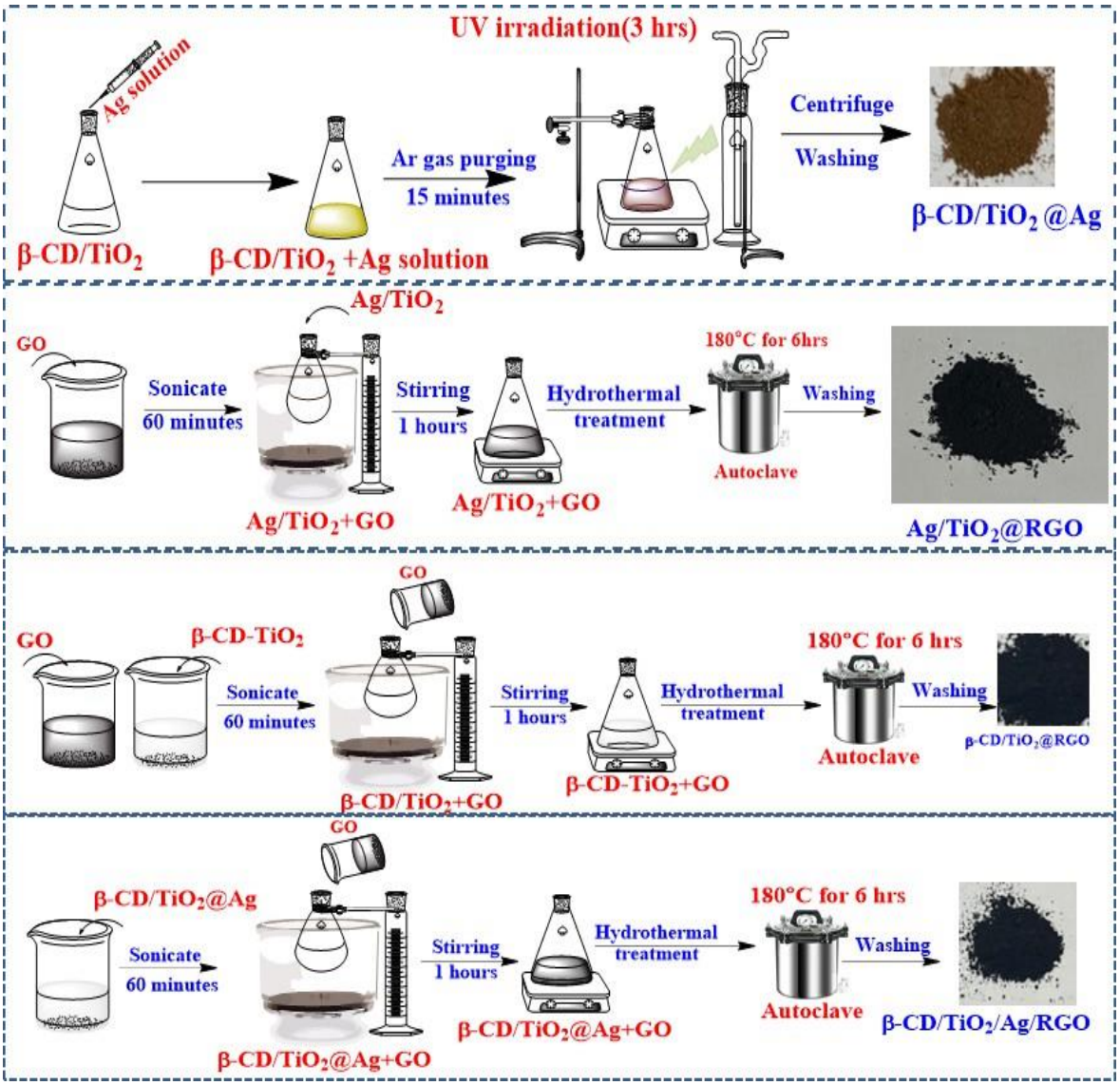

Scheme 4.1 A diagram depicting the fabrication of β-CD/TiO_2@Ag, Ag/TiO_2@RGO, β-CD/TiO_2/RGO, and β-CD/TiO_2/Ag/RGO nanocomposites.

4.2.6 Photodegradation analysis

. The photocatalytic performance of ternary and quaternary nanocomposites (NCs) was investigated using urea as the model molecule at an initial concentration of 1.8 mM. Each test was conducted in separate test tubes, holding 10 mg of catalyst suspended in 10 mL of urea solu-

tion. To attain adsorption-desorption equilibrium, the suspensions were stirred vigorously in the dark for 30 minutes. For urea degradation, the test tubes containing catalysts were kept under sunlight for 150 minutes in Patiala, India (1st-30th May 2023; 12:00 pm - 2:30 pm), with average solar radiation of approximately 785 W/m² and temperatures around 35°C. After 30 minutes of fixed interval, 2 mL of supernatant was collected, and the catalyst was removed by centrifugation at 8000 rpm from the degraded solution. Additionally, urea concentration was estimated using the p-dimethylamino benzaldehyde (DMAB) method (31).

4.3. Results and discussion

UV-DRS spectra shown in Figure 4.1(a) illustrate the optical characteristics of the prepared catalysts. For CTA, a red shift in the visible range (400-500 nm) is observed, accredited to the LSPR effect of Ag nanoparticles (33,34). The inclusion of RGO in ATR NC not only induces a bathochromic shift but also improves light absorption in the visible range. (35). Additionally, a strong and broad band is observed in CTR and CTAR NC due to RGO. In the quaternary composite, the plasmonic band of Ag nanoparticles merges with RGO, owing to the extensive absorption range of RGO. This expanded absorption throughout the visible spectrum increases photon availability, generating a higher number of charge carriers and can thereby enhance photocatalytic performance(36).

The band gap energy of the synthesized ternary and quaternary nanocomposites (NC) was determined using Tauc's plot and the Kubelka-Munk equation.

$$\boldsymbol{\alpha h\nu = A(h\nu - E_g)^n} \qquad (\mathbf{3})$$

where, α =absorption coefficient, hν = energy of the photon, E_g = Band gap, A=constant, n=exponential coefficient (n=1/2 (indirect band gap). The E_g values of CTA, ATR, CTR, and CTAR nanocomposites were found to be 2.57, 2.38, 2.15, and 1.85 eV, respectively, as shown in fig4.1(b). (37) Quaternary NC shows a significantly reduced band gap of 1.85 eV. The reduction in Eg is apparent with the concurrent addition of RGO, Ag and β-CD to the TiO_2 surface, causing a shift in the optical response towards the visible spectrum. Consequently, this enhancement could improve the photocatalytic performance of the fabricated quaternary NC.

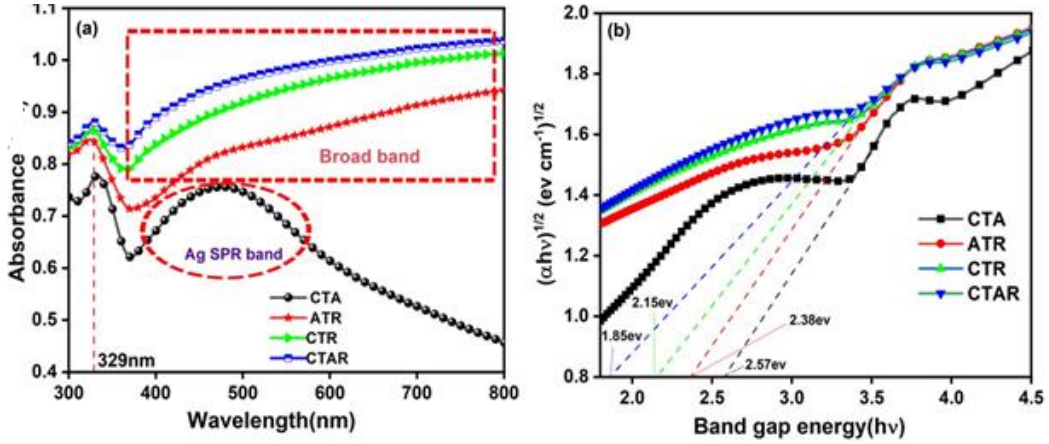

Fig. 4.1. (a)DRS spectra and (b) Tauc's plots CTA, ATR, CTR, CTAR nanocomposites.

To determine the impact of Ag, RGO, and β-CD on charge carrier separation, the PL analysis was carried out using an excitation wavelength of 340 nm. The spectra for the CTA, ATR, CTR, and CTAR nanocomposites exhibited emission bands at 380 nm and 538 nm. The PL results suggest that the lifespan of photoinduced charge carriers in the photocatalysts follows the decreasing order: CTAR > CTR > ATR > CTA. Among all the samples shown in Fig 4.2, CTA displayed the highest emission intensity, which suggests a greater rate of recombination and less effective photoinduced charge separation. In contrast, the emission intensity significantly decreases with the addition of Ag, RGO, and β-CD in the nanocomposite. The quenching of PL signals is attributed to the electron transfer from TiO_2 to the surfaces of metallic Ag and RGO. Moreover, RGO's high electrical conductivity facilitates the transfer of electrons, leading to a lower recombination rate (38,39). Furthermore, β-CD provides a favorable environment for prolonging the lifetime of photogene rated charge carriers. (40) The maximum quenching occurred in the quaternary composite, indicating that the synergistic interaction between Ag, RGO, and β-CD creates multiple electron transfer pathways, thus enhances charge carrier separation and reduces PL peak intensity.

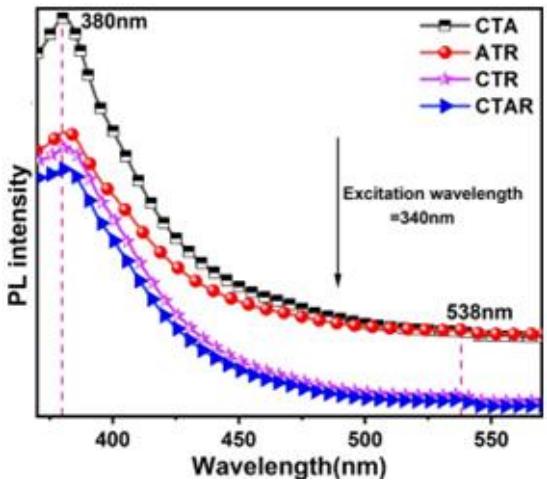

Fig 4.2, Photoluminescence spectra of CTA, ATR, CTR, CTAR nanocomposite

Fig.4.3 illustrates the Raman spectra for CTA, ATR, CTR, and CTAR nanocomposites. The spectra reveal distinct Raman bands for anatase TiO_2 at 145, 390, 518, and 640 cm^{-1}, which are assigned to the Eg(1), B1g(1), A1g + B1g(2), and Eg(2) optical Raman modes, respectively. In CTA nanocomposite, β-CD and Ag exhibited no additional active bands. In contrast, the CTR, ATR, and CTAR nanocomposites containing RGO, exhibit D and G bands centered at 1348 and 1598 cm^{-1}. The D band, associated with sp^3-C atom vibrations, indicates defects and asymmetry, while the G band, linked to sp^2-C atom vibrations, signifies crystallization and uniformity. (41). The CTAR nanocomposite shows similar Raman bands corresponding to anatase TiO_2 and the G and D bands associated with RGO, confirming the successful formation of CTAR NC. The peak intensities in ATR, CTR, and CTAR are noticeably decreased due to the surface coverage by β-CD and RGO.

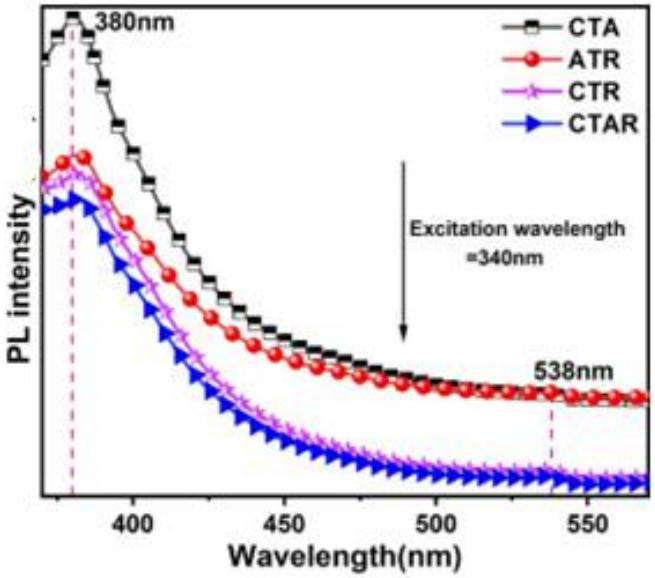

Fig4.3. Raman spectra of CTA, ATR, CTR, CTAR nanocomposites

3.1.4. X-Ray diffraction analysis

XRD diffraction (Fig. 4.4) peaks of TiO_2, common across all samples, are located at 2θ = 25.4, 37.7, 48, 53.8, 55, 68.7, 70.2, 75.2, and 82.9º, corresponding to the (101), (004), (200), (105), (211), (115), (220), (215), and (301) lattice planes of the anatase phase (ICDD card-21-1272). The characteristic peaks observed at 2θ = 27.4, 35.8, and 62.8º are assigned to the (110), (103), and (204) planes of the rutile phase. (42). The CTR sample exhibited similar diffraction peaks to bare TiO_2. Notably, the XRD patterns did not show peaks for β-CD and RGO, likely because C and O have lower X-ray scattering coefficients as compared to silver and titanium. The CTA, ATR, and CTAR nanocomposites displayed the signals at 2θ = 38.2, 44.3, and 64.1º, correlated to the (111), (200), and (220) lattice planes of Ag with face-

centered cubic symmetry (43). The deposition of metallic Ag and β-CD in NCs does not alter any diffraction pattern, proposing the purity and crystallinity of the prepared hybrid photo-catalysts.

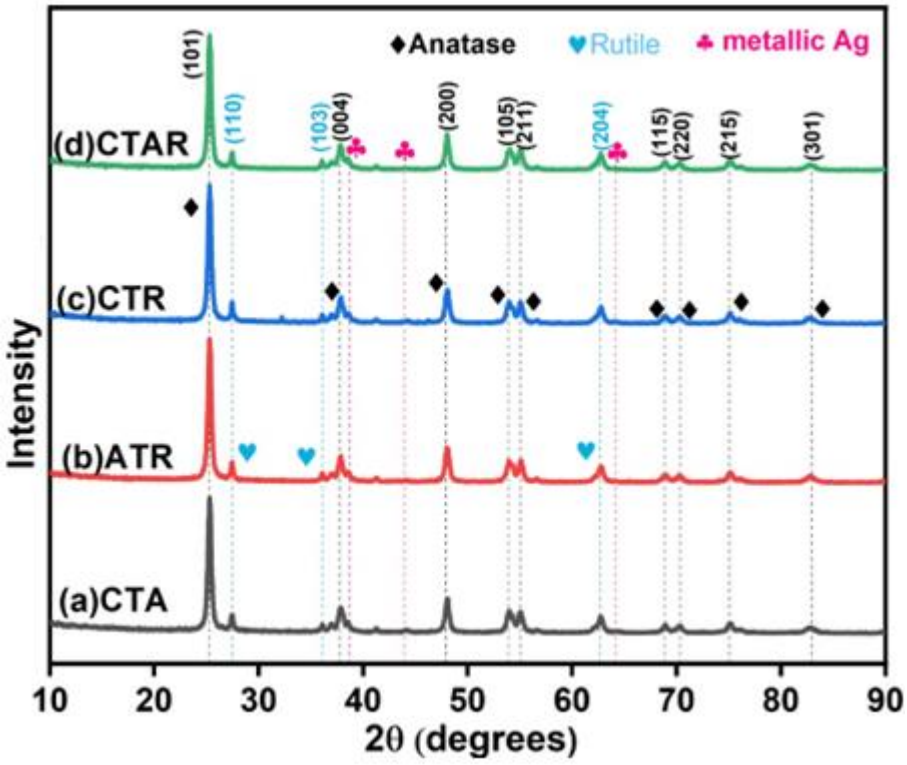

Fig4.4. XRD diffractogram of CTA, ATR, CTR, CTAR nanocomposites.

The structural and morphological characteristics of CTA, ATR, CTR, and CTAR NCs were analysed using the FESEM technique. In Fig. 4.5(a-b), CTA shows a clustered, agglomerated, and spherical structure with Ag nanoparticles embedded on the TiO_2 surface. The presence of a white shell could be attributed to β-CD. The ATR images display a ruffled and crumpled layered structure. Fig. 4.5 (c-d) suggest that TiO_2 particles are evenly distributed across the RGO sheets, with spherical Ag nanoparticles (appearing as bright spots) uniformly embedded on the entire RGO surface (44). In figure 4.5(e-f), CTR is seen to have a sheet-like, RGO-based sandwiched structure with TiO_2 particles evenly attached to the RGO layers, and the white lining around the sheet edges may be due to β-CD loading. The FESEM images in Fig. 4.5(g-h) showed an aggregated, interconnected structure with TiO_2 particles clearly affixed to the RGO surface, and a white lining around the sheets, likely due to β-CD. The Ag nanoparti-cles are not distinctly visible, which is further corroborated by HRTEM images. The ele-mental analysis and EDX spectra (Fig 4.6) depict the presence of C(red), O(green), Ti(yellow), and Ag(purple) elements, respectively. The EDX profiles in Fig. S1(a-f) support the presence and homogeneous distribution of C, O, Ti, and Ag in the nanocomposite.

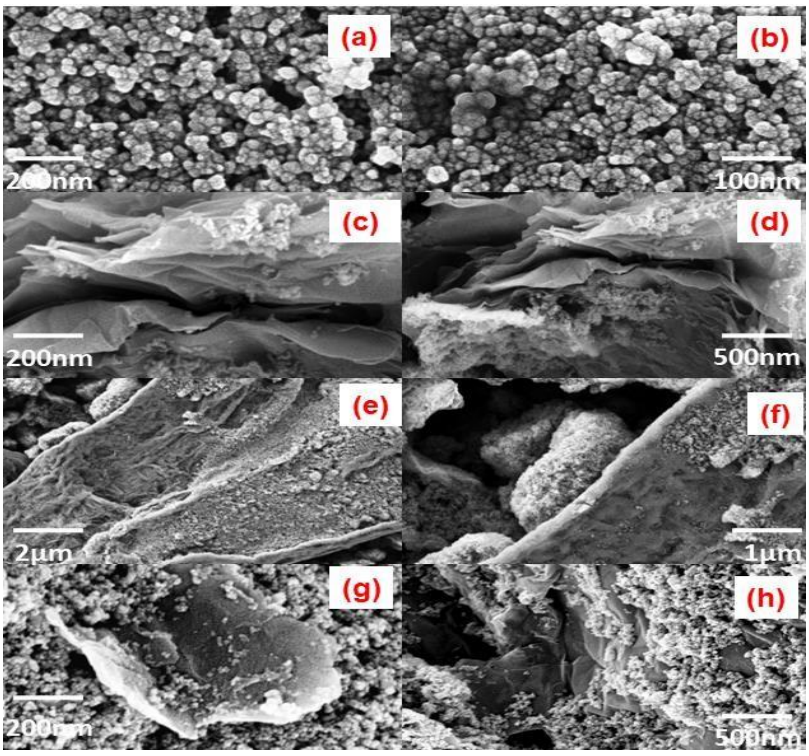

.

Fig.4.5. FESEM images (a-h) of CTA, ATR, CTR, CTAR nanocomposites at different scales.

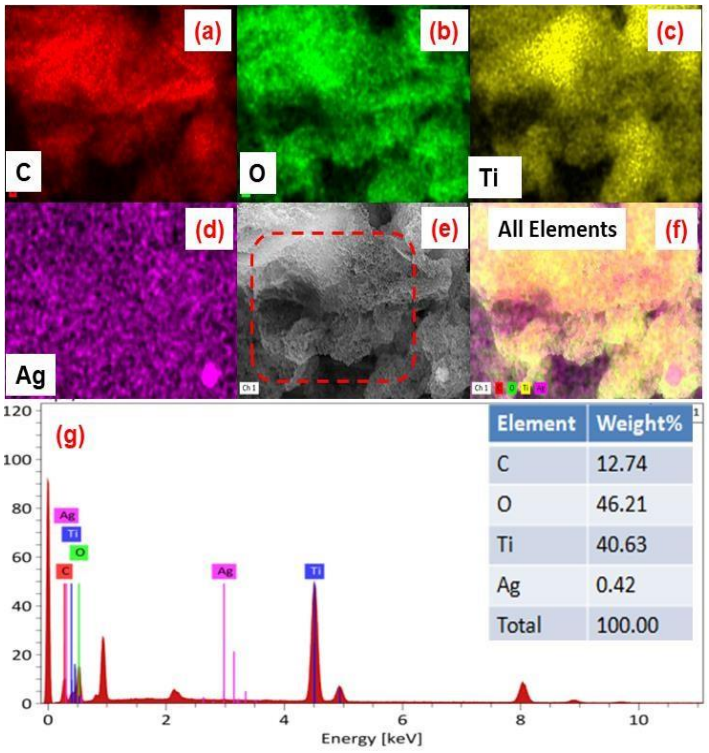

Fig.4.6 Elemental analysis (a-f) shows the color-coded distribution of C, O, Ti, and Ag, and EDX analysis (g) details the composition of the quaternary nanocomposite.

HRTEM analysis was conducted to investigate the shape, size, and interactions between the components of quaternary NCs. Fig. 4.7(a) provides evidence of the layered morphology of RGO sheets. Fig. 4.7(b) shows the accumulation of clustered, spherical, and agglomerated

metallic Ag deposited on TiO_2 over the RGO layers. The dark spots of metallic Ag, which appear black, range in size from 7 to 21 nm. Fig. 4.7(c-d) clearly depicts the white lining of β-CD around the TiO_2 particles and the black spots of metallic Ag firmly attached to the TiO_2 surface (34). The RGO sheets serve as a substrate for the integrated photo-deposited Ag on the TiO_2 nanoparticles(45). Fig. 4.7(e) shows two sets of lattice fringes: one at 0.36 nm for the (101) plane of TiO_2 and another at 0.23 nm for the (111) plane of Ag (0). Fig. 4.7(f) presents the SAED pattern, displaying concurrent rings with bright spots analogous with the TiO_2 (110), (101), and metallic Ag (111), (200) diffraction planes of the CTAR nanocomposites.

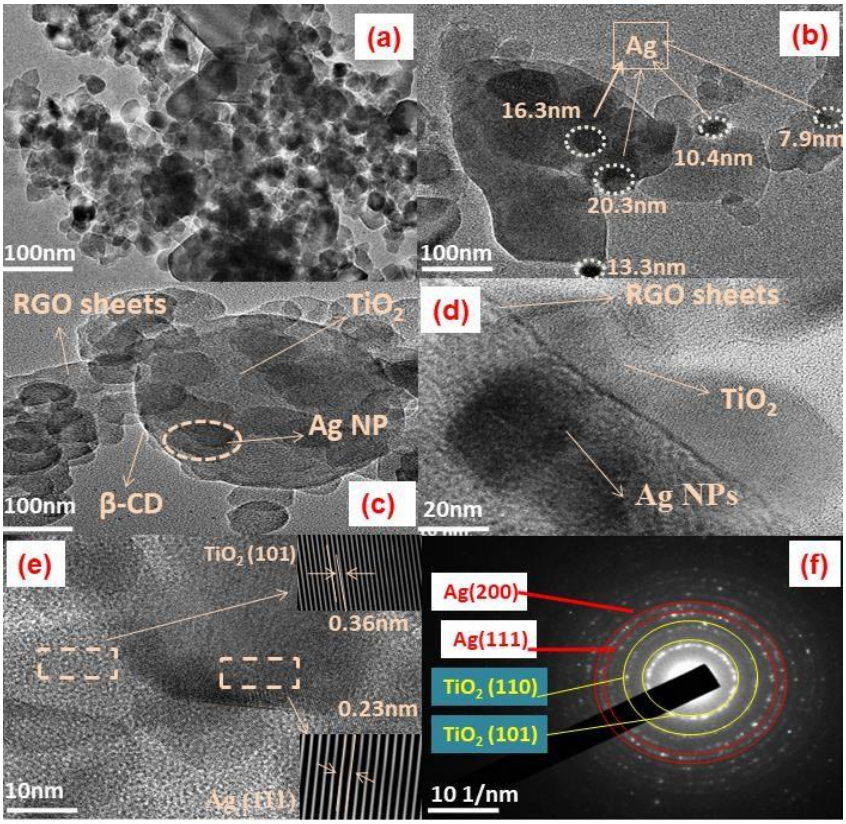

Fig.4.7. HRTEM images (a-f), lattice fringes (e), and SAED pattern (f) of the CTAR nanocomposite.

XPS analysis (Fig. 4.8) confirms the presence of C, O, Ti, and Ag in the CTAR hybrid composite. The C1s spectrum (Fig. 4.8)) contains the characteristic peaks at 284.7, 286.0, and 288.6 eV for the C–C, C–O, and C=O, respectively. The O1s spectrum (Fig. 4.8(c)) shows peaks at 529.8 and 532.1 eV, corresponding to Ti–O and C–O linkages. The Ti2p spectrum (Fig. 4.8(d)) displays peaks at 458.6 eV and 464.3 eV, indicating Ti (IV) with a difference in binding energy of 5.7 eV. The Ag 3d spectrum shows peaks at 367.9 eV and 373.9 eV, with a splitting of 6.0 eV, confirming the presence of zerovalent Ag in CTAR nanocomposite.

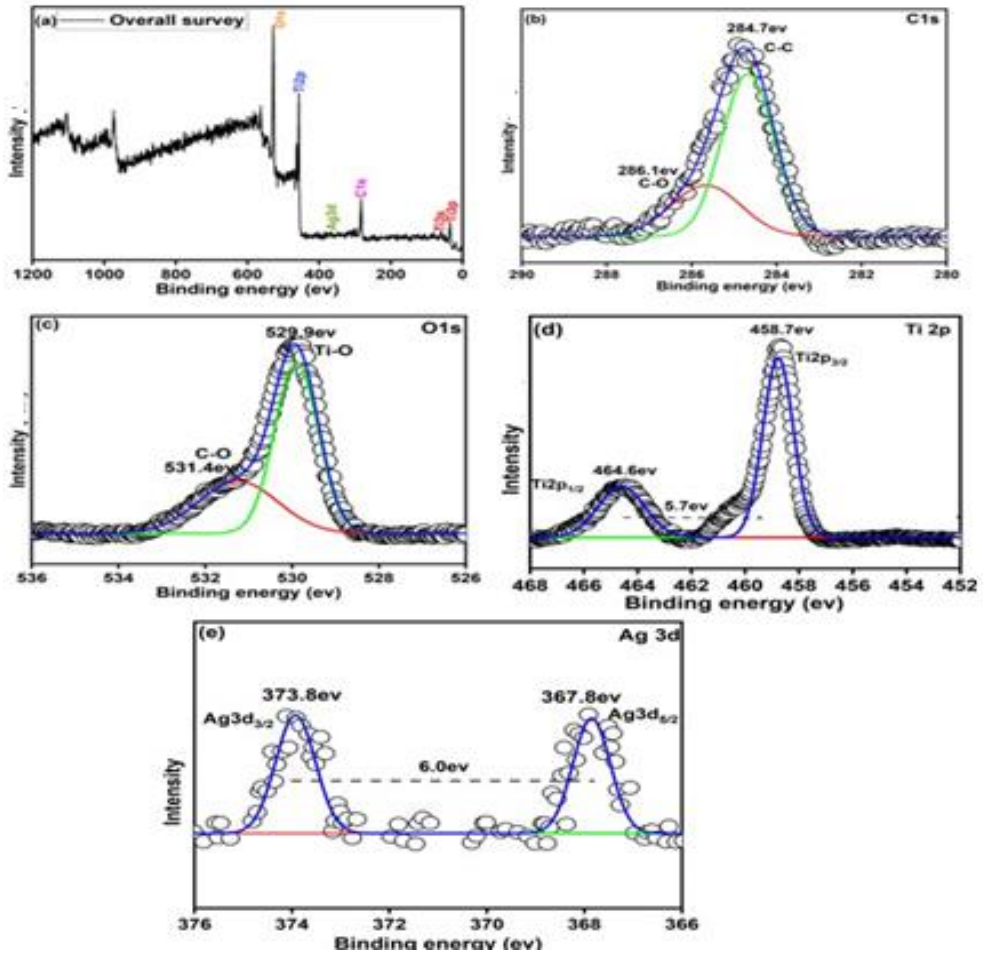

Fig4.8.XPS spectra showing(a) overall survey spectrum; (b)C1s; (c)O1s; (d)Ti2p; (e)Ag 3d of CTAR quaternary NC

4.4. Photooxidation of urea

The efficiencies of CTA, ATR, CTR, and CTAR NCs were assessed in photocatalytic urea oxidation. Fig. 4.9 shows the adsorption and photodegradation curves with the various nanocomposites after 150 minutes of reaction time. The adsorption capacity of the catalysts showed a progressive increase in the following sequence: CTA < ATR < CTR < CTAR. This improvement is likely due to the incorporation of new guest binding sites arising from the deposition of β-CD, RGO, and Ag nanoparticles (Figs. 4.10 and 4.9a). Once equilibrium was achieved, the catalytic activity was examined under sunlight. (Figs. 4.11 and 4.9b). Sunlight exposure enhanced the photoactivity of all the catalysts where the quaternary composite (CTAR) exhibiting the highest adsorption after 150 minutes of sunlight exposure.

The oxidation of urea involves the transfer of 8 electrons to form nitrate (20). The composite incorporates RGO, which has high electron mobility, facilitating electron transfer and enhancing photoinduced charge separation. β-CD provides a large number of sites for urea

binding, which helps to reduce nitrogen leaching. Moreover, the deposition of Ag nanoparticles enhances light absorption due to the LSPR effect (46 ,28).

The modification with different components in all the catalysts altered the oxidation trend, as shown in Fig. 8c, following the order: CTAR (86.2%) > CTR (75.8%) > ATR (70.5%) > CTA (55.7%). The experimental data were fitted to a first-order kinetic equation to investigate the kinetics of urea oxidation with the prepared samples (47).

$$ln \frac{C_0}{C_t} = kt \quad (4)$$

Where C_0 = the initial concentration of urea, C_t = is the concentration at time t, k= is the pseudo-first-order rate constant (min^{-1}), and t is the time.

The rate constant for the urea oxidation followed the order: CTA (0.0069 min^{-1}) <ATR (0.0092 min^{-1}) < CTR (0.0133 min^{-1}) < CTAR (0.017 min^{-1}). Among all nanocomposites, CTAR possesses the higher rate of photocatalytic reaction. The combined components in the CTAR nanocomposite contributed to the improved photocatalytic activity (Fig 4.9d).

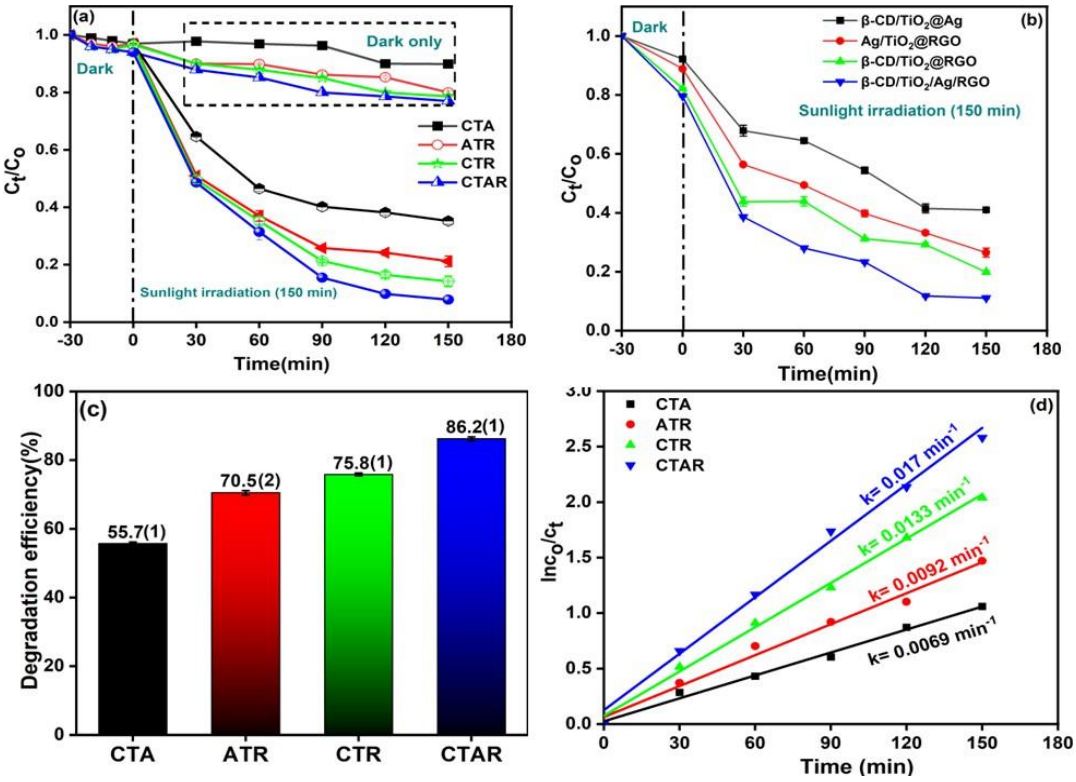

Fig 4.9.(a) Adsorption curves (dark), (b) UV-VIS absorption changes over time, (c) Photodegradation efficiency histogram and (d) Reaction kinetics for urea degradation using CTA, ATR, CTR, and CTAR nanocomposites.

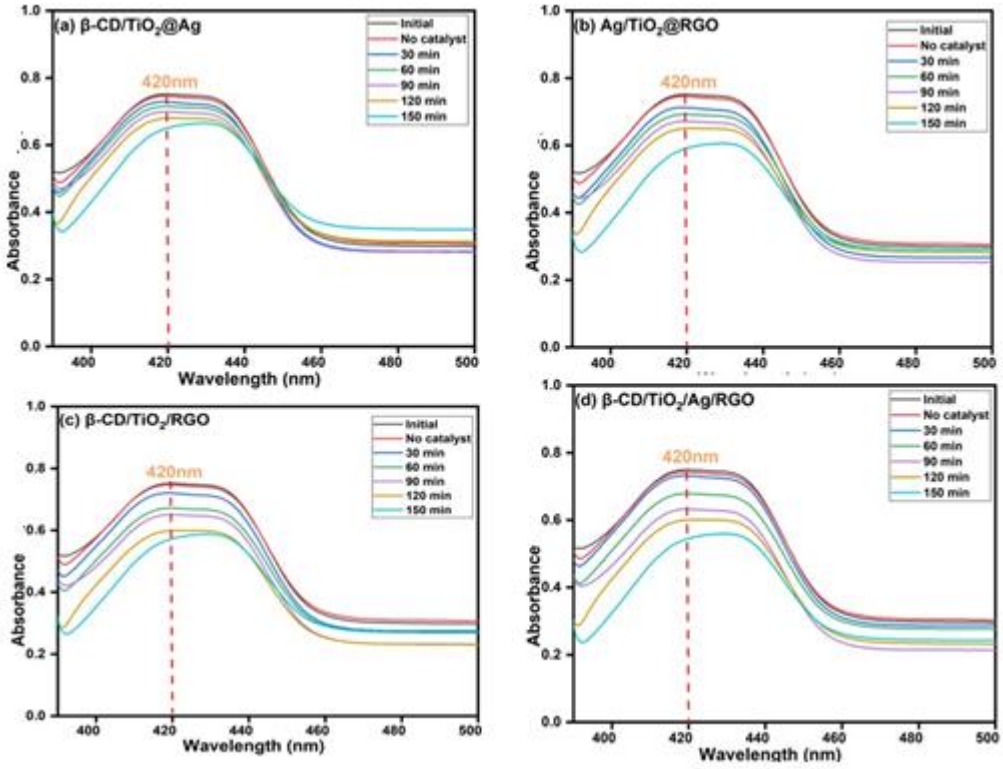

Fig.4.10. Variation of UV-visible spectra in the presence of (a) β-CD/TiO_2@Ag, (b) Ag/TiO_2@RGO, (c) β-CD/TiO_2/RGO, and (d) β-CD/TiO_2/Ag/RGO under dark conditions.

.

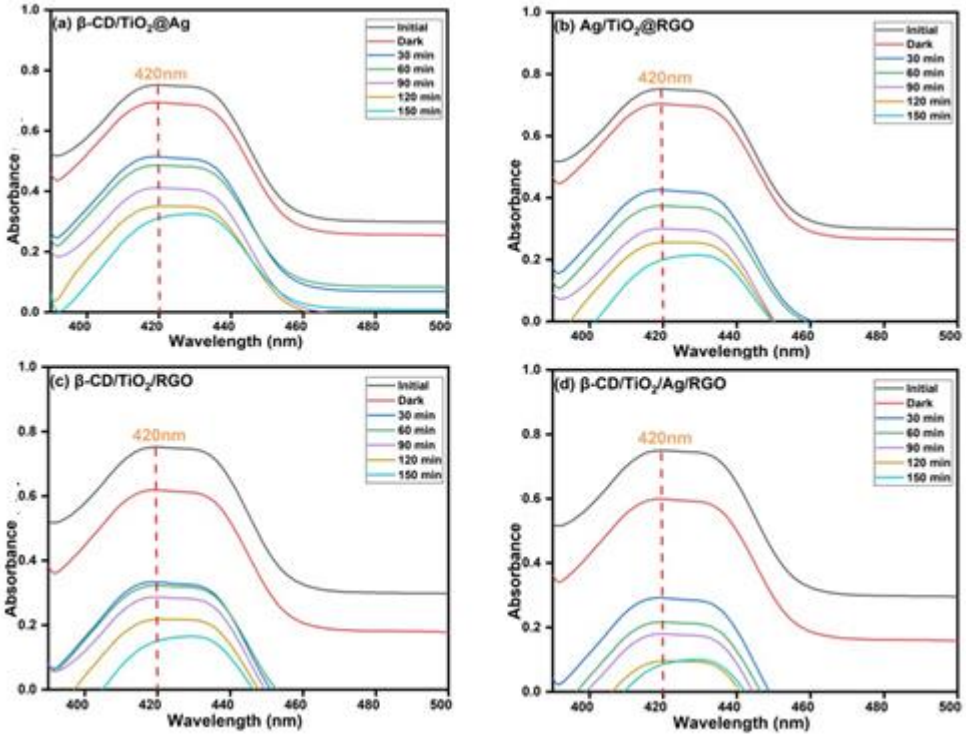

Fig.4.11 Variation of UV-visible spectra in the presence of (a) β-CD/TiO_2@Ag, (b) Ag/TiO_2@RGO, (c) β-CD/TiO_2/RGO, and (d) β-CD/TiO_2/Ag/RGO under solar light irradiation.

4.5. Demineralization efficiency and nitrate yields

4.5.1. Demineralization efficiency (Total Organic Carbon)

It is clear that the oxidation of urea does not necessarily lead to complete mineralization into CO_2 and H_2O. Therefore, it is crucial to assess the demineralization efficiency(48,49) (equation 2). Fig. 4.12a presents the results of urea oxidation using bare CTA (54%), ATR (69.7%), CTR (75%), and CTAR (85%) over 150 minutes under sunlight irradiation. The CTAR nanocomposite demonstrates the highest demineralization efficiency (85%) of urea which aligns closely with its complete photodegradation.

4.5.2. Nitrate yield (%)

The objective of this study is to enhance the overall yield of NO_3^- using potential photocatalysts. The oxidation of urea was conducted using CTA, ATR, CTR, and CTAR under 150 min sunlight to determine the NO_3^- yield. The results depicted in Fig. 4.12b illustrates the NO_3^- yield achieved by these photocatalysts. Remarkably, the CTAR nanocomposite exhibits the highest NO_3^- yield at 27.8%. This synergistic effect of Ag, RGO and β-CD loading demonstrates the enhanced visible light absorption, reduces electron-hole pair recombination, and minimizes nitrogen loss. (50)

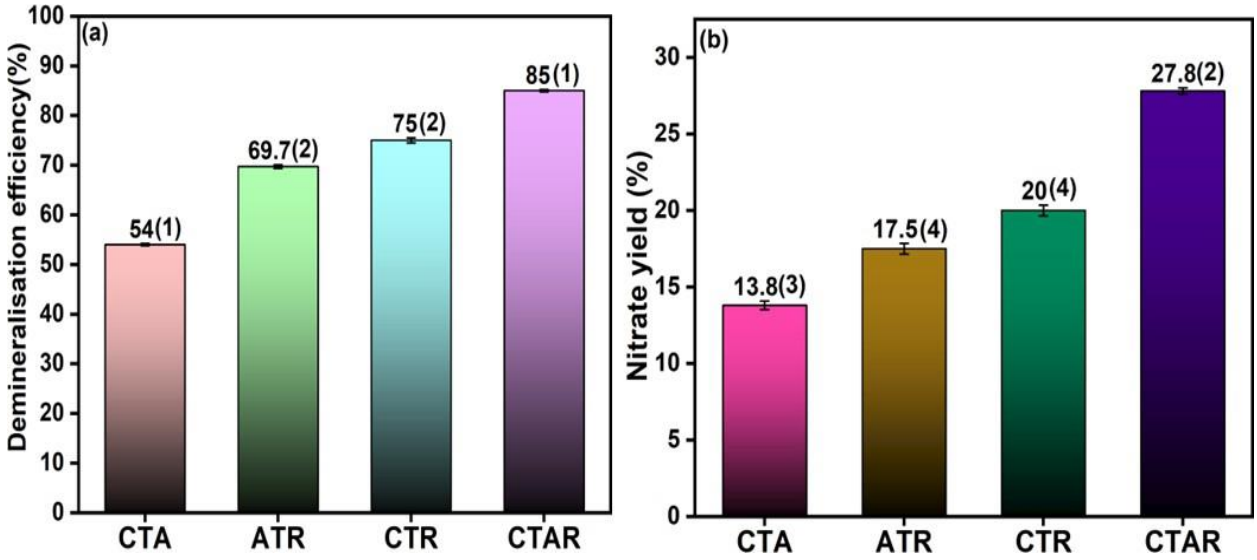

Fig4.12. (a)Trends of demineralization efficiency (%) and (b) nitrate yield (%) for the CTAR nanocomposite, highlighting the TOC and nitrate formation.

It found that the CTAR quaternary hybrid possesses the highest urea oxidation and nitrate yield (%) compared to previous reports(Table 1) .

Table 1: Comparison of urea degradation and nitrate yield for CTAR quaternary nanocomposites with reported literature values.

Photocatalyst	Degradation Efficiency (%)	Nitrate Yield (%)	References
N-doped TiO_2/polystyrene	70	0.37	(51)
RGO/TiO_2	66(1)	9.8(1)	(20)
β-CD_{25}/TiO_2@Ag_1	78(1)	17.8(3)	(28)
CTAR	85(1)	27.8(2)	This work

Various scavengers such as EDTA, IPA, and argon gas were selected to discern the roles of photogenerated holes (h^+), hydroxide radicals (•OH), and superoxide radicals (O_2^-) in the photocatalytic oxidation of urea, respectively(52). Scavenging experiments were performed during the urea oxidation over the CTAR photocatalyst under similar conditions (Fig. 4.13). As depicted in Figure 10, the degradation rate significantly decreased in the presence of IPA and argon gas, indicating that •OH and O_2^- act as the essential active species in the oxidation of urea. Conversely, the rate of degradation also decreased with the EDTA scavenger, although the reduction was comparable to the control experiment (no scavenger), suggesting that the holes (h^+) have minor participation in the oxidation process.

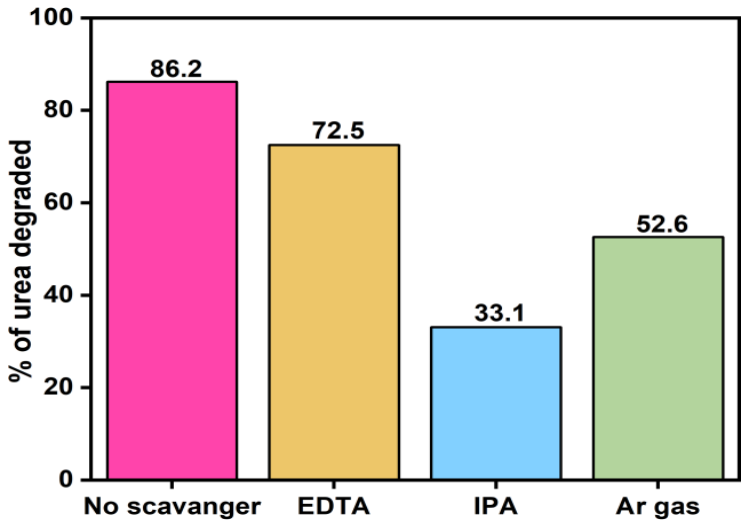

Fig4.13. The influence of scavengers on urea degradation with the CTAR nanocomposite.

4.6. Mechanistic details

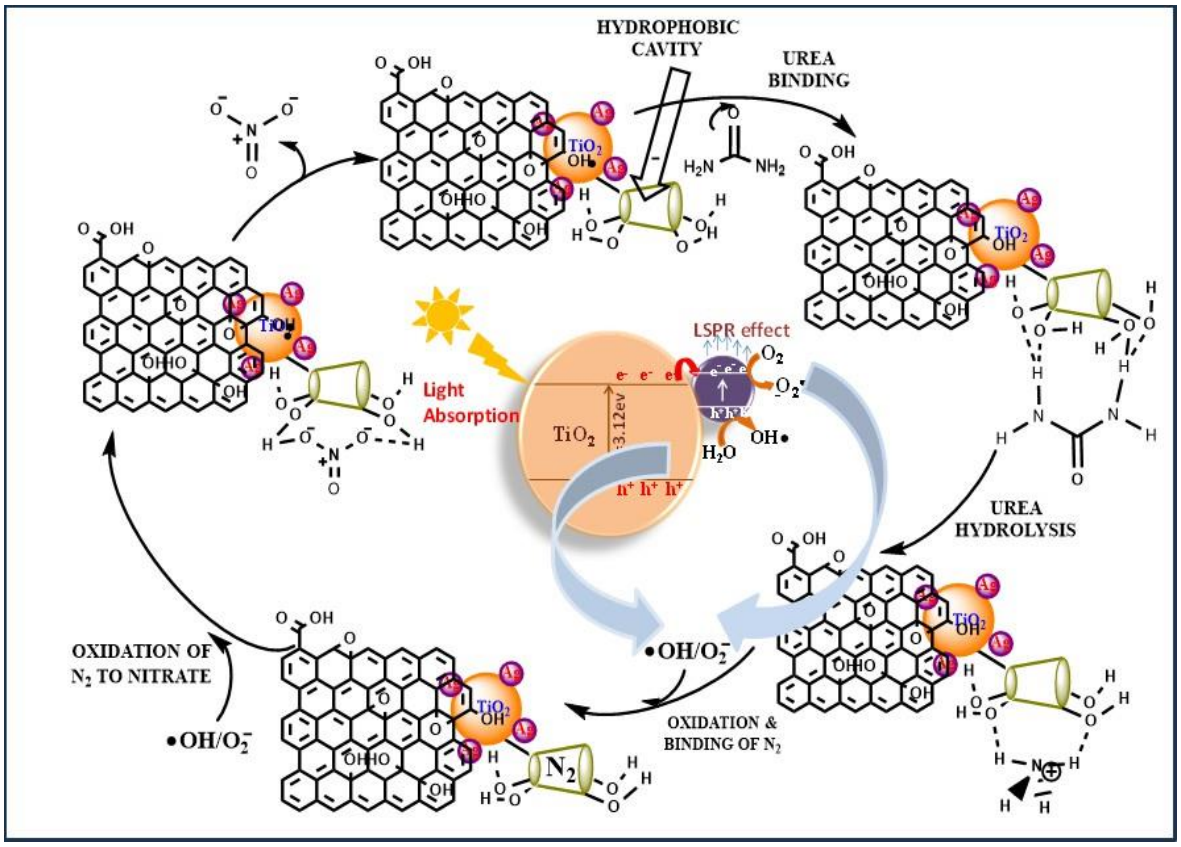

Scheme4.2 Detailed mechanism for the urea oxidation by β-CD/TiO_2/Ag/RGO (CTAR) quaternary composite.

The mechanism involves the synergistic interaction between Ag, Ti, and RGO as shown in (Scheme 4.2). Photoexcited electrons from the TiO_2 conduction band swiftly migrated to Ag nanoparticles and the RGO sheet, preventing photoelectron pair recombination and increasing charge carriers to form active species ($O_2^{\cdot-}$, •OH), thus boosting photocatalytic performance. The two-dimensional RGO structure provides excellent conductivity, facilitating rapid charge transport and separation. Ag nanoparticles generate high-energy electrons LSPR effect, which are quickly transferred to the RGO surface. These electrons react with surface-absorbed oxygen to form superoxide ions (O_2^-), while excited holes interact with H_2O and hydroxyl ($^-$OH) on TiO_2, producing hydroxyl radicals (•OH). Both species are important for urea degradation(44),(53).Urea molecules first interact noncovalently with the hydroxyl groups of β-CD and are oxidized to produce molecular nitrogen (N_2). This nitrogen binds to the hydrophobic region of β-CD, which helps minimize nitrogen leaching. Following this, the nitrogen bound to β-CD undergoes further oxidation, resulting in the formation of nitrate.

4.7. Reusability and stability studies

The practical applicability of a catalyst is often assessed based on its reusability and stability. In this study, the recyclability of the CTAR catalyst was evaluated over 4 cycles under sunlight. As shown in Fig. 4.14a, the CTAR NC's degradation efficiency dropped by only 9% after four cycles, highlighting its potential as a reusable catalyst. The slight decline in photocatalytic performance could be attributed to the loss of catalyst mass during continuous experiments (54).

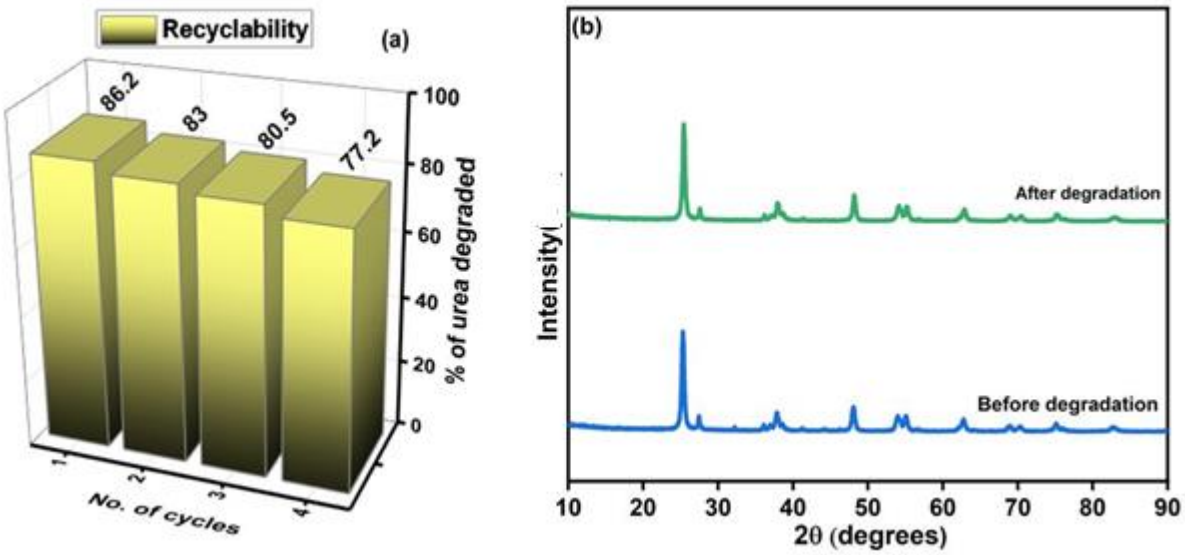

Fig. 4.14(a) Recyclability of the CTAR NC for urea degradation under sunlight over four consecutive cycles. (b) XRD pattern showing the stability of CTAR NC before and after degradation.

Furthermore, the structural stability of the catalyst was also evaluated to support this assertion. Figure 4.14(b) displays the XRD patterns of CTAR nanocomposite before and after degradation. No shifts in peak positions or changes in peak intensities indicative of crystalline nature were observed. Therefore, CTAR NC is considered an excellent material for the photocatalytic oxidation of urea.

References

1) J. Penuelas, F. Coello and J. Sardans, A better use of fertilizers is needed for global food security and environmental sustainability, *Ag Food Sec.* **2023**, *12*, 1–9.
2) S. J. Leghari, N. A. Wahocho, G. M. Laghari, A. H. Laghari, G. M. Bhabhan, K.H.Talpur, Lashari. and A.A., Role of nitrogen for plant growth and development: A review. *AEB*.

2016, *10*, 209–218.

3) P. Shetty, C. Acharya and N. Veeresh, Effect of Urea Fertilizer on the Biochemical Characteristics of Soil, *IJASBT*. **2019**, *7*, 414– 420.
4) C. Masclaux-Daubresse, F. Daniel-Vedele, J. Dechorgnat, F. Chardon, L. Gaufichon and A. Suzuki, Nitrogen uptake, assimilation and remobilization in plants: Challenges for sustainable and productive agriculture, *Ann. Bot.* **2010**, *105*, 1141–1157.
5) Y. S. Ku, S. S. Cheng, M. S. Ng, G. Chung and H. M. Lam, The Tiny Companion Matters: The Important Role of Protons in Active Transports in Plants, *Int. J. Mol. Sci.* **2022**, *23*, 2824.
6) T. Ketehouli, K. F. I. Carther, M. Noman, F. W. Wang, X. W. Li and H. Y. Li, Adaptation of plants to salt stress: Characterization of Na+ and K+ transporters and role of Cbl gene family in regulating salt stress response, *J. Agron.* **2019**, *9*, 687.
7) M. Skorupka and A. Nosalewicz, Ammonia volatilization from fertilizer urea—A new challenge for agriculture and industry in view of growing global demand for food and energy crops, *Agric. Res. J.* **2021**, *11*, 822.
8) Z. Ma, Y. Yue, M. Feng, Y. Li, X. Ma, X. Zhao and S. Wang, Mitigation of ammonia volatilization and nitrate leaching via loss control urea triggered H-bond forces, *Sci Rep*. **2019**, *9*, 1–9.
9) Y. Liu, Y. Ge, J. Tan, H. Wang and Y. Ding, Research on ammonia emissions characteristics from light-duty gasoline vehicles, *J. Environ. Sci. Stud.* **2021**, *106*, 182–193.
10) M. Anas, F. Liao, K. K. Verma, M. A. Sarwar, A. Mahmood, Z. L. Chen, Q. Li, X. P. Zeng, Y. Liu and Y. R. Li, Fate of nitrogen in agriculture and environment: agronomic, eco-physiological and molecular approaches to improve nitrogen use efficiency, *Biol. Res.* **2020**, *53*, 1–20.
11) Y. Jiang, Y. Zhu, W. Lin and J. Luo, Urea Fertilization Significantly Promotes Nitrous Oxide Emissions from Agricultural Soils and Is Attributed to the Short-Term Suppression of Nitrite-Oxidizing Bacteria during Urea Hydrolysis, *Microorganisms*. **2024**, *12*, 685.
12) F. Zhang, X. Wang, H. Liu, C. Liu, Y. Wan, Y. Long and Z. Cai, Recent advances and applications of semiconductor photocatalytic technology, *Appl. Sci.* **2019**,*9*,2489
13) S. A. Mousa, H. Abdallah and S. A. Khairy, Low-cost photocatalytic membrane modified with green heterojunction TiO_2/ZnO nanoparticles prepared from waste, *Sci. Rep.* **2023**, *13*, 1–19.

14) L. Lu, G. Wang, Z. Xiong, Z. Hu, Y. Liao, J. Wang and J. Li, Enhanced photocatalytic activity under visible light by the synergistic effects of plasmonics and Ti^{3+} -doping at the Ag/TiO_{2-x} heterojunction, *Ceram. Int.* **2020**, *46*, 10667–10677.

15) G. Shao, Y. Zang and B. J. Hinds, TiO_2 Nanowires Based System for Urea Photodecomposition and Dialysate Regeneration, *ACS Appl. Nano Mater.* **2019,** *2*, 6116–6123.

16) H. Liu, P. Li, H. Bai, C. Du, D. Wei, Y. Su, Y. Wang and L. Yang, Incorporation of reduced graphene oxide into faceted flower-like f001g TiO_2 for enhanced photocatalytic activity, *R. Soc. Open Sci.* **2018**, *5*, 180613.

17) W. Liu and G. Speranza, Tuning the Oxygen Content of Reduced Graphene Oxide and Effects on Its Properties, *ACS Omega*. **2021**, *6*, 6195–6205.

18) R. Geetha Bai, K. Muthoosamy, F. N. Shipton and S. Manickam, Acoustic cavitation induced generation of stabilizer-free, extremely stable reduced graphene oxide nano dispersion for efficient delivery of paclitaxel in cancer cells, *Ultrason. Sonochem*. **2017**, *36*, 129– 138.

19) K. I. Nargatti, S. S. Ahankari, J. R. C. Dizon and R. T. Subramaniam, Environmentally Friendly Water-Based Reduced Graphene Oxide/Cellulose Nanofiber Ink for Supercapacitor Electrode Applications, *ACS Omega*. **2024**, 9, 11730–11737.

20) P. Soni, B. Pal and R. K. Das, Enhanced photocatalytic urea oxidation under neutral medium by reduced graphene oxide coated TiO_2 nanoparticles, *Catal. Commun.* **2023**, *179*, 106690.

21) M. Chen, Y. Meng, W. Zhang, J. Zhou, J. Xie and G. Diao, β-Cyclodextrin polymer functionalized reduced-graphene oxide: Application for electrochemical determination imidacloprid, *Electrochim. Acta*. **2013**, *108*, 1–9.

22) X. Tu, F. Gao, X. Ma, J. Zou, Y. Yu, M. Li, F. Qu, X. Huang and L. Lu, Mxene/carbon nanohorn/β-cyclodextrin-Metal-organic frameworks as high-performance electrochemical sensing platform for sensitive detection of carbendazim pesticide, *J. Hazard. Mater.* **2020**, *396*, 122776.

23) P. Sakthivel and P. Velusamy, Modification of the photocatalytic performance of various metal oxides by the addition of β-cyclodextrin under visible light irradiation, *JWPE*. **2017**, *16*, 329–337.

24) A. Szwajca and H. Koroniak, Encapsulation of fluoroaromatics by β-cyclodextrin and their derivatives theoretical studies, *J. Fluor. Chem.* **2014**, *167*, 122–127.

25) I. Ibrahim Zamkoye, B. Lucas and S. Vedraine, Synergistic Effects of Localized Surface Plasmon Resonance, Surface Plasmon Polariton, and Waveguide Plasmonic Resonance on

the Same Material: A Promising Hypothesis to Enhance Organic Solar Cell Efficiency, *J. Nanomater.* **2023**, *13*, 2209.

26) I. Ahmed, L. Shi, H. Pasanen, P. Vivo, P. Maity, M. Hatamvand and Y. Zhan, There is plenty of room at the top: generation of hot charge carriers and their applications in perovskite and other semiconductor-based optoelectronic devices, *Light: Sci. Appl. J.* **2021**, *10*, 1-7.

27) Y. Hattori, J. Meng, K. Zheng, A. Meier De Andrade, J. Kullgren, P. Broqvist, P. Nordlander and J. Sá, Phonon-Assisted Hot Carrier Generation in Plasmonic Semiconductor Systems, *Nano Lett.* **2021**, *21*, 1083–1089.

28) P. Soni, B. Pal and R. K. Das, Influence of β-CD and Ag deposition over TiO_2 towards photocatalytic oxidation of urea under solar irradiation. *Environ. Chem. Eng.* **2024**, *12*, 112150.

29) K. H. Leong, L. C. Sim, D. Bahnemann, M. Jang, S. Ibrahim and P. Saravanan, Reduced graphene oxide and Ag wrapped TiO_2 photocatalyst for enhanced visible light photocatalysis, *APL Mater*. **2015**, *3*, 104503.

30) S. Bhardwaj, D. Sharma, P. Kumari and B. Pal, Influence of photodeposition time and loading amount of Ag co-catalyst on growth, distribution and photocatalytic properties of Ag@TiO_2 nanocatalysts, *Opt. Mater.* **2020**, *106*, 109975.

31) J. D. Giraldo and B. L. Rivas, Determination of urea using p-N, N-dimethylaminobenzaldehyde: Solvent effect and interference of chitosan, *J. Chil. Chem. Soc.* **2017,** *62*, 3538–3542.

32) L. Rimoldi, D. Meroni, E. Falletta, V. Pifferi, L. Falciola, G. Cappelletti and S. Ardizzone, Emerging pollutant mixture mineralization by TiO_2 photocatalysts. The role of the water medium, *Photochem. Photobiol. Sci.* **2017**, *16*, 60–66.

33) W. Cao, T. Huang, X. H. N. Xu and H. E. Elsayed-Ali, Localized surface plasmon resonance of single silver nanoparticles studied by dark-field optical microscopy and spectroscopy, *J. Appl. Phys.* **2011**, *109*, 34310.

34) N. Attarchi, M. Montazer and T. Toliyat, Ag/TiO_2/β-CD nano composite: Preparation and photo catalytic properties for methylene blue degradation, *Appl. Catal. A Gen.* **2013**, *467*, 107–116.

35) H. N. Tien, V. H. Luan, L. T. Hoa, N. T. Khoa, S. H. Hahn, J. S. Chung, E. W. Shin and S. H. Hur, One-pot synthesis of a reduced graphene oxide-zinc oxide sphere composite and its

use as a visible light photocatalyst, *Chem. Eng. J.* **2013**, *229*, 126–133.

36) J. T. Abdalla, J. Wang and D. Wang, Effect of Ag/rGO on the Optical Properties of Plasmon-Modified SnO_2 Composite and Its Application in Self-Powered UV Photodetector, *Crystals*. **2019**, *9*, 648.

37) S. Nayak, L. Mohapatra and K. Parida, Visible light-driven novel g-C_3N_4/NiFe-LDH composite photocatalyst with enhanced photocatalytic activity towards water oxidation and reduction reaction, *J. Mater. Chem. A.* **2015**, *3*, 18622–18635.

38) N. A. M. Barakat and H. Y. Kim, Effect of silver-doping on the crystal structure, morphology and photocatalytic activity of TiO_2 nanofibers, *IOP Conference Series: Mater. Sci. Eng.* **2012**, *40*, 012003.

39) H. Tian, C. Wan, X. Xue, X. Hu and X. Wang, Effective electron transfer pathway of the ternary TiO_2/RGO/Ag nanocomposite with enhanced photocatalytic activity under visible light, *Catalysts*. **2017**, ***7***, 156.

40) W. Sun, Q. Meng, L. Jing, L. He and X. Fu, Synthesis of long-lived photogenerated charge carriers of Si-modified α-Fe_2O_3 and its enhanced visible photocatalytic activity, *Mater. Res. Bull.* **2014**, *49*, 331–337.

41) G. T. S. How, A. Pandikumar, H. N. Ming and L. H. Ngee, Highly exposed {001} facets of titanium dioxide modified with reduced graphene oxide for dopamine sensing, *Sci. Rep.* **2014**, *4*, 2–9.

42) S. Dai, Y. Wu, T. Sakai, Z. Du, H. Sakai and M. Abe, Preparation of highly crystalline TiO_2 nanostructures by acid-assisted hydrothermal treatment of hexagonal-structured nanocrystalline titania/cetyltrimethyammonium bromide nanoskeleton, *Nanoscale Res. Lett.* **2010**, *5*, 1829–1835.

43) R. Geng, J. Yin, J. Zhou, T. Jiao, Y. Feng, L. Zhang, Y. Chen, Z. Bai and Q. Peng, In situ construction of Ag/TiO_2/g-C_3N_4 heterojunction nanocomposite based on hierarchical co-assembly with sustainable hydrogen evolution, *Nanomaterials*. **2020**, *10*, 1-10.

44) S. Athithya, V. S. Manikandan, S. K. Harish, K. Silambarasan, S. Gopalakrishnan, H. Ikeda, M. Navaneethan and J. Archana, Plasmon Effect of Ag Nanoparticles on TiO_2/rGO Nanostructures for Enhanced Energy Harvesting and Environmental Remediation, *Nanomaterials*. **2023**, *13*, 1–16.

45) A. Bokare, S. Chinnusamy and F. Erogbogbo, TiO_2–graphene quantum dots nanocomposites for photocatalysis in energy and biomedical applications, *Catalysts*. **2021**, *11*, 1–51.

46) Y. Zhang, Q. Li, Q. Gao, S. Wan, P. Yao and X. Zhu, Preparation of Ag/β-cyclodextrin co-doped TiO_2 floating photocatalytic membrane for dynamic adsorption and photoactivity under visible light, *Appl. Catal. B-Environ.* **2020**, *267*, 118715.

47) E. Linde, N. H. Giron and M. C. Celina, Diffusion-Limited Hydrolysis in Polymeric Materials, *Polym. Degrad. Stab.* **2022**, *204*, 110095.

48) D. Chatterjee and A. Mahata, Demineralization of organic pollutants on the dye modified TiO_2 semiconductor particulate system using visible light, *Appl. Catal. B-Environ.* **2001**, *33*, 119–125.

49) I. Prabha and S. Lathasree, Effective photocatalytic demineralization of reactive red 198 utilizing nanocomposite particles under UV light irradiation, *JICS*. **2017**, *94*, 269–277.

50) V. Lalan, V. P. Mahadevan Pillai and K. G. Gopchandran, Enhanced electron transfer due to RGO makes Ag–$CaTiO_3$@rGO a promising plasmonic photocatalyst. *J SCI-ADV MATER DEV*, **2022**, *7*, 100468.

51) V. Vaiano, O. Sacco, G. Di Capua, N. Femia and D. Sannino, Use of visible light modulation techniques in urea photocatalytic degradation, *Water*. **2019**, *11*, 1642.

52) X. Xu, Y. Sun, Z. Fan, D. Zhao, S. Xiong, B. Zhang, S. Zhou and G. Liu, Mechanisms for $\cdot O_2^-$ and ·OH production on flowerlike $BiVO_4$ photocatalysis based on electron spin resonance, *Front. Chem.* **2018**, *6*, 1–12.

53) P. Attri, P. Garg, P. Sharma, R. Singh, M. Chauhan, D. K. Lim, S. Kumar, G. R. Chaudhary, Precursor-dependent fabrication of exfoliated graphitic carbon nitride (g-CN) for enhanced photocatalytic and antimicrobial activity under visible light irradiation, *J Clean. Prod.* **2023**, *422*, 0959-6526.

54) Gillingham M, Gomes RL, Ferrari R and West H, 2022. Sorption, separation and recycling of ammonium in agricultural soils: A viable application for magnetic biochar? *Sci. Total Environ.* **2021**, 812, 151440

Conclusions and Future Aspects

Chapter-1 This chapter summarizes the brief introduction about the essential role of nitrogenous fertilizers, particularly urea, in modern agriculture, while addressing the environmental and efficiency challenges posed by nitrogen loss. The study highlighted the urgent need to enhance nitrogen use efficiency (NUE) to mitigate these negative impacts. By investigating advanced solutions such as urease and nitrification inhibitors, photocatalytic oxidation, and nanocomposites, we identified promising strategies to reduce nitrogen losses and improve urea application. Notably, the development of innovative photocatalysts like M-TiO_2 combined with reduced graphene oxide (RGO) and cyclodextrin (CD) was emphasized for their potential to enhance urea conversion to nitrate while minimizing harmful emissions. This research underscores the importance of adopting advanced technologies to achieve sustainable agricultural practices, ensuring high productivity while protecting environmental integrity.

This chapter outlines key research gaps and details the standard procedures for synthesizing binary, ternary, and quaternary nanostructures. It also summarizes various characterization techniques, including UV-Visible spectroscopy, dynamic light scattering, X-ray diffraction, morphological analysis, Fourier transform infrared spectroscopy, Raman spectroscopy, total organic carbon analysis, and nitrate yield analysis, used to evaluate the optical and structural properties of these nanostructures.

Chapter-2 In conclusion, the photocatalytic urea oxidation activities of bare TiO_2 and the RGOT25% composites were scrutinized under solar radiation. It has been observed that the RGOT25% composites possess superior photocatalytic activity as compared to their bare analog, as it has higher absorbance in the visible region, lower electron-hole pair recombination rate, and facile charge transport properties. Notably, in the presence of NaF, the photocatalyst shows the highest urea oxidation efficiency and nitrate yield under a nearly neutral medium owing to a smaller extent of NH_3 leaching and stronger interaction of urea with the photocatalyst surface. Such observation can have a great impact in designing milder reaction conditions to suppress nitrogen loss and maximize nitrate production from urea to afford sustainable agriculture. Such an outcome will attract the attention of a significant portion of the

chemical and agricultural scientific community as well as agricultural industries to discover new and affordable technologies for sustainable agriculture.

Chapter-3 This present report involves the preparation and study of photocatalytic urea oxidation activities of bare TiO_2 as well as different Ag and β-CD loaded binary and ternary nanocomposites. Loading of Ag nanoparticles enhances the visible light sensitivity and lowers the electron-hole pair recombination rate, whereas the β-CD binds with nitrogen due to the hydrophobic effect to lower the nitrogen leaching. As a result, the $\beta\text{-}CD_{25}/TiO_2@Ag_1$ ternary composite shows the highest urea degradation efficiency and nitrate yield. Furthermore, the active species detection experiment suggests that hydroxyl radicals and superoxide ions are responsible for the oxidation of urea. It is interesting to note that all the urea oxidation reactions are performed under ambient conditions in water. The catalyst shows excellent stability and recyclability. Such observation will allure the attraction from a large number of chemists as well as agricultural scientists to design economic and emerging methodologies for sustainable agricultural development

Chapter-4 In summary, novel ternary and quaternary nanocomposites incorporating Ag, RGO, and β-CD were synthesized for the first time and extensively studied to enhance the photocatalytic oxidation of urea. Among these, the CTAR quaternary nanocomposite demonstrated exceptional photocatalytic efficiency, achieving 86.2% degradation within 150 minutes under solar light, surpassing other ternary nanocomposites. The incorporation of Ag extended the visible light sensitivity of TiO_2, β-CD facilitated nitrogen binding through hydrophobic interactions to minimize nitrogen leaching, and RGO provided high capacitance and electron mobility while preventing rapid recombination of photogenerated charge carriers. The synergistic interactions among TiO_2, Ag, β-CD, and RGO contributed to the superior photocatalytic performance of the quaternary nanocomposite. Furthermore, the catalyst exhibited remarkable stability and recyclability. This study underscores the potential of the CTAR composite as a green, solar light-activated catalyst for enhancing the photocatalytic oxidation of urea.

Future Aspects

The present study has demonstrated significant advancements in enhancing the photocatalytic efficiency of TiO_2 for urea oxidation by combining it with noble metals, reduced graphene oxide (RGO), and cyclodextrins. However, there remain several areas for further exploration to optimize these systems for practical applications A key area for future exploration is material optimization. The current composites (RGO-TiO_2, β-CD_{25}/TiO_2@Ag, β-CD/TiO_2/Ag/RGO) have shown improved efficiency, but further enhancement could be achieved by incorporating other materials, such as different 2D materials, α, γ cyclodextrins, different metals or novel dopants. These modifications could tune the bandgap, improve charge carrier separation, or enhance light absorption properties. Understanding how these materials perform under extended photocatalytic cycles and in real-world environments will be critical for practical applications. Preventing issues such as nanoparticle aggregation or material degradation through protective coatings or stabilizers could lead to more robust and reliable systems.

Another area worth investigating is mechanistic understanding of the photocatalytic processes involved. Advanced characterization tools, such as in-situ spectroscopic techniques, like LC-MS, EPR and HPLC could offer deeper insights into the electron transfer mechanisms and intermediate reaction species. This would enable precise control over the material properties and photocatalytic processes, improving their efficiency for specific reactions like urea oxidation. Finally, conducting a thorough environmental and economic assessment will be necessary to evaluate the feasibility of these photocatalysts in industrial applications. Factors such as material recyclability, toxicity, and overall lifecycle impact need to be considered. Cost-effective synthesis methods and sustainable material choices will be key to making these systems commercially viable.

These future directions could help further unlock the potential of TiO_2-based photocatalysts, offering sustainable solutions for environmental and industrial challenges.

List of Publications

1. **Palak Soni,** Bonamali Pal, Raj Kumar Das (2023). Enhanced photocatalytic urea oxidation under neutral medium by reduced graphene oxide coated TiO_2 nanoparticles ***Catalysis communications,* 179, 1-10, IF=3.4, ISSN:1566-7367.**
2. **Palak Soni,** Bonamali Pal, Raj Kumar Das (2024). Influence of β-CD and Ag depos- tion over TiO_2 towards photocatalytic oxidation of urea under solar irradiation. ***Jour- nal of Environment Chemical Engineering,* 12, 1.13, IF=7.3, ISSN:2213-3437.**
3. **Palak Soni,** Bonamali Pal, Raj Kumar Das. β-CD and RGO loaded Ag-TiO_2 compo- sites for enhanced photocatalytic oxidation of urea under sunlight**. (submitted in *Nanoscale Advances*).**
4. **Palak Soni,** Bonamali Pal, Raj Kumar Das. Efficient utilization of nitrogenous fertilizers for sustainable agriculture: overall progress and futuristic directions. **(Review paper under preparation).**

Conferences and Workshops

1. **Palak Soni,** Bonamali Pal, Raj Kumar Das. Participated in seven days' workshop on "Particle Characterization Techniques (PCT-2022) organized by Department of Chemistry & International Research Centre, Satyabhama Institute of Science and Technology (Deemed to be University) in association with CSIR-National Metallurgical Laboratory Madras Centre, CSIR Madras Complex during 30th-06th june,2022.
2. **Palak Soni,** Bonamali Pal, Raj Kumar Das. Participated in workshop on "Art of Effective Presentations" organized by Team CAPSL in collaboration with School of Humanities and Social Sciences held on 24.05.22.
3. **Palak Soni,** Bonamali Pal, Raj Kumar Das. Participated in workshop on "Drawing 3D Structures on Jmol Software" organized by GEI, Roorkee, Uttarakhand.
4. **Palak Soni,** Bonamali Pal, Raj Kumar Das. Participated in 6th National Conference on Advanced Materials and Radiation Physics held at Longowal, Sangrur on 18-19th May 2023.
5. **Palak Soni,** Bonamali Pal, Raj Kumar Das. Participated in International conference on Emerging Trends in Science and Technology (ICETST) organized by the Department of Applied Sciences, Punjab engineering college, Chandigarh. 10-11th June, 2022.
6. **Palak Soni,** Bonamali Pal, Raj Kumar Das. Participated in 1st international conference on Recent Advances in Chemistry (CRAC-2023) organized by department of chemistry, Punjabi university, Patiala held on February 23-24,2023 (Poster).

Catalysis Communications 179 (2023) 106690

Contents lists available at ScienceDirect

Catalysis Communications

journal homepage: www.elsevier.com/locate/catcom

Enhanced photocatalytic urea oxidation under neutral medium by reduced graphene oxide coated TiO_2 nanoparticles

Palak Soni, Bonamali Pal *, Raj Kumar Das *

School of Chemistry and Biochemistry, Thapar Institute of Engineering and Technology, Patiala 147004, Punjab, India

ARTICLE INFO

Keywords:
Hybrid composites
Photocatalytic degradation
Urea oxidation
Nitrate production
Sustainable agriculture

ABSTRACT

Nowadays, fertilizers are used to boost crop production. Nitrogenous fertilizers are assimilated as nitrate. Unfortunately, 60–70% of nitrogen is lost due to different leaching processes. Photocatalytic urea oxidation is now emerging as a new methodology. Nitrate conversion is favorable under alkaline pH. However, it can subsequently cause deprotonation of ammonium ions to result ammonia leaching. In this report, efficiencies of bare and RGO loaded TiO_2 were examined. In the presence of NaF, the nanocomposite possesses a 9.8(1)% nitrate yield, significantly greater than the other analogous reactions. Such observation will be helpful in developing new methodologies to afford sustainable agriculture.

1. Introduction

In the last few decades, due to enormous growth in population besides the depreciation of accessibility of land for agriculture, the whole world is facing the risk of food shortage. Consequently, crop production has to be increased manifold. Therefore, fertilizers have been applied to agricultural fields to enhance the growth and yield of crops. Urea is one of the most widely used nitrogenous fertilizers engaged in ammonification, nitrification, denitrification, and mineralization process [1,2]. Urea accommodates 46% of nitrogen content and supplements essential nutriment to the plants, attributed to its effectiveness towards sustainable agriculture [3–5]. Result of the inefficacious availability and easy leaching of nitrogen from the soil, the external supply of nitrogen is foremost essential to enhance crop yield, which has been executed globally for a long back by augmenting nitrogenous fertilizers like $CO(NH_2)_2$, NH_4NO_3, anhydrous NH_3, etc. [6,7] Generally, plants assimilate nitrogen through the soil in the form of nitrate and ammonium ions. Therefore, to absorb nitrogen from the soil, $CO(NH_2)_2$ must be hydrolyzed and the resultant NH_3 needs to be protonated to afford NH_4^+ ions (eq. 1). Subsequently, the ammonium ions undergo a nitrification process to yield nitrate (eq. 2). With the help of nitrate and ammonium transporters, these ions are taken up by plants, and the transport is powered by a proton gradient.

$$CO(NH_2)_2 + H_2O + 4H^+ = CO_2 + 2NH_4^+ \quad (1)$$

$$NH_4^+ + 3H_2O = NO_3^- + 10H^+ + 8e^- \quad (2)$$

A vital concern associated with it is that a significant fraction (60–70%) of urea gets vanished into the atmosphere through nitrate leaching, ammonia volatilization, and N_2O emissions which deteriorate plant growth and the environment through subsurface water acidification and global warming [8]; [9]; [10]. Also, the nitrification process often produces nitrogen gas (N_2) as the major product due to incomplete oxidation, thus resulting in nitrogen leaching. Urea-contaminated water adversely affects not only human beings but also birds, wildlife, and livestock [11]; [12]. Accordingly, it is essential to oxidize urea into beneficial and harmless products like NO_3^-, which is helpful in increasing overall crop production.

Several researchers attempted to oxidize urea in many different methodologies, such as the electrochemical method [13,14], photocatalytic method [15,16], chemical method [17], and biological method [18], to get beneficial products. However, in most cases, the principal issue is the formation of N_2 (gaseous product) due to incomplete oxidation of ammonia, which probably decreases the nitrate efficiency. As a result, more efficient oxidants are required to ensure the complete oxidation of urea.

TiO_2 has been regarded as one of the most widely used photocatalyst as it is non-toxic, economical, eco-friendly, and chemically stable [19].

Abbreviations: XRD, X-ray Diffraction; HR-TEM, High-resolution transmission electron microscopy; SEM, Scanning electron microscopy; DRS, Diffused reflectance spectroscopy; DLS, Dynamic light scattering; XPS, X-Ray photoelectron spectroscopy; RM, reaction mixture; TOC, Total organic carbon.

* Corresponding author.
E-mail addresses: bpal@thapar.edu (B. Pal), rkdas@thapar.edu (R.K. Das).

https://doi.org/10.1016/j.catcom.2023.106690
Received 3 April 2023; Received in revised form 2 May 2023; Accepted 4 May 2023
Available online 6 May 2023

Journal of Environmental Chemical Engineering 12 (2024) 112150

Contents lists available at ScienceDirect

Journal of Environmental Chemical Engineering

journal homepage: www.elsevier.com/locate/jece

Influence of β-CD and Ag deposition over TiO_2 towards photocatalytic oxidation of urea under solar irradiation

Palak Soni [a], Bonamali Pal [a,b,*], Raj Kumar Das [a,b,*]

[a] Department of Chemistry and Biochemistry, Thapar Institute of Engineering & Technology, Patiala 147004, Punjab, India
[b] TIET-Virginia Tech Center of Excellence in Emerging Materials, Thapar Institute of Engineering and Technology, Patiala 147004, India

ARTICLE INFO

Editor: Giovanni PALMISANO

Keywords:
Photocatalytic oxidation of urea
Sustainable agriculture
Composite materials
Nitrate yield

ABSTRACT

Photocatalytic oxidation of urea is an essential area of study for converting urea to nitrate. As crops absorb nitrogen in the form of NO_3^- but due to incomplete oxidation, a substantial fraction of it escapes into the atmosphere as N_2. Hence, an effective photocatalyst is urgently needed to improve nitrate conversion. This study focuses on the influence of β-cyclodextrin and Ag deposition on TiO_2 towards the photocatalytic oxidation of urea. β-cyclodextrin (15–25 wt%) and Ag(1–3 wt%) loaded binary and ternary nanocomposites have been prepared using hydrothermal and photodeposition methods, respectively. The binary and ternary hybrids were characterized using FESEM, EDX, HR-TEM, XRD, XPS, DRS, PL, DLS, and FT-IR analysis. Photocatalytic urea degradation activity was evaluated under solar irradiation. The β-CD_{25}/TiO_2@Ag_1 ternary nanocomposites show 78% degradation efficiency with 17.8% nitrate yield after 180 min reaction time which is the highest. This observation can be ascribed to the higher affinity of β-CD towards N_2 due to the hydrophobic effect and the surface plasmon effect of Ag, which amplifies its visible light response. Such observations will attract much interest from a large section of material and agricultural chemists to design new catalysts for photochemical urea oxidation to afford sustainable agriculture.

1. Introduction

The traditional method of improving the soil's fertility with natural and chemical-based fertilizers such as urea, calcium ammonium nitrate, anhydrous ammonia, etc., is beneficial for escalating agricultural growth[1,2]. Urea is an abundantly used fertilizer because it is inexpensive, has a 46% nitrogen content, is easily transported, and is the simplest assimilated form of nitrogen directly involved in the mineralization process[3]. The plants assimilate NO_3^- and NH_4^+ ions instead of urea nitrogen directly. So, urea undergoes hydrolysis to form NH_3 and further protonation results in the formation of NH_4^+ ions[4,5]. During nitrification, these NH_4^+ ions undergo oxidation to form NO_3^- ions and simultaneously release protons[6]. During NO_3^- assimilation, OH^- ions liberate, neutralizing the excess protons released during nitrification and making the entire process viable[7]. However, the primary issue related to it is that half of the urea supplied to the soil gets released into nature due to N_2 emissions, NO_3^- leaching, and NH_3 loss brought up by temperature change, soil pH, and soil management practices[8]. As a result, urea is often over-applied to enhance crop production. The presence of unreacted urea drastically deteriorates soil and groundwater quality, causing various environmental hazards[9–12].

Moreover, this nitrogen loss directly or indirectly disturbs human life and the ecosystem[13] It is necessary to enhance the production of NO_3^- on urea oxidation, which is desirable in agronomics[14]. The existing methodologies involve the modification of fertilizers with urease and nitrogenase inhibitors to control nitrogen loss[15,16]. However, the high cost and low stability of these inhibitors under ambient conditions limit their practical applications. As a result, photocatalysis is emerging as a new methodology to increase the NO_3^- efficiency from urea oxidation[17]. Photocatalytic urea oxidation involves hydrolysis of urea to ammonium ion (Eq. 1) followed by oxidation of ammonium ion to afford nitrate (Eq. 2). The second step involves an 8-electron transfer process. Therefore, it is quite kinetically sluggish. Often, it affords the formation of molecular nitrogen (N_2) as the major product due to incomplete oxidation. The high stability and chemical inertness of N_2 prevent the subsequent oxidation to afford nitrate. Hence, the fabrication of an efficient photocatalyst with a strong oxidizing ability, as well as having a substantial affinity towards N_2, is needed to avoid its leaching and escalate the overall NO_3^- efficiency. Such methodology is highly desirable as it will enhance crop production and reduce the ecotoxic effect of

* Corresponding authors at: Department of Chemistry and Biochemistry, Thapar Institute of Engineering & Technology, Patiala 147004, Punjab, India.
E-mail addresses: bpal@thapar.edu (B. Pal), rkdas@thapar.edu (R.K. Das).

https://doi.org/10.1016/j.jece.2024.112150
Received 2 December 2023; Received in revised form 24 January 2024; Accepted 3 February 2024
Available online 6 February 2024

Palak Thesis Plagiarism check

ORIGINALITY REPORT

13%	8%	9%	2%
SIMILARITY INDEX	INTERNET SOURCES	PUBLICATIONS	STUDENT PAPERS

PRIMARY SOURCES

1	Wee-Jun Ong, Lling-Lling Tan, Yun Hau Ng, Siek-Ting Yong, Siang-Piao Chai. " Graphitic Carbon Nitride (g-C N)-Based Photocatalysts for Artificial Photosynthesis and Environmental Remediation: Are We a Step Closer To Achieving Sustainability? ", Chemical Reviews, 2016 Publication	1%
2	tudr.thapar.edu:8080 Internet Source	1%
3	Manjusha Passi, Bonamali Pal. "Influence of Ag/Cu photodeposition on CaTiO3 photocatalytic activity for degradation of Rhodamine B dye", Korean Journal of Chemical Engineering, 2022 Publication	1%
4	pubs.rsc.org Internet Source	1%
5	doaj.org Internet Source	1%

Raj Kumar Das